UNIVERSITY OF LATVIA

FACULTY OF PHYSICS, MATHEMATICS AND OPTOMETRY

Aleksejs Zolotarjovs

Optical properties of Plasma Electrolytic Oxidation coatings on aluminium alloy surface

DOCTORAL THESIS

Submitted for the Degree of Doctor of Physics

Subfield of Material Physics

Riga, 2021

Promocijas darbs izstrādāts Latvijas Universitātes Cietvielu fizikas institūtā laika posmā no 10. 2016. līdz 01. 2021.

Darbs sastāv no ievada, četrām nodaļām, aizstāvamām tēzēm un literatūras saraksta.
Darba forma: disertācija fizikas nozarē, Materiālu Fizikas apakšnozarē
Darba vadītājs:

- Dr. Phys. Krišjānis Šmits, vadošais pētnieks, Materiālu morfoloģijas un struktūras pētījumu laboratorijas vadītājs, LU Cietvielu fizikas institūts.

Recenzenti:
1. Dr. Phys. Raivo Jaaniso
2. Dr. Phys. Anatolijs Šarakovskis
3. Dr. Phys. Juris Prikulis

Anotācija

Plazmas elektrolītiskā oksidēšana (PEO) ir process biezu (daži desmiti mikronu), cietu un ķīmiski izturīgu oksīdu pārklājumu veidošanai uz metāla virsmām. Gadu desmitiem šo procesu pēta gan zinātnieki, gan industrijas speciālisti, jo pārklājumu iegūšana ir videi draudzīga, tehnoloģiski ir relatīvi vienkārša ar zemām ekspluatācijas izmaksām. Pārklājumu izgatavošanas tehnoloģiskajā procesā ir daudz maināmo parametru, tādēļ pēdējos pāris gados ātri attīstās jaunas PEO procesā iegūtu pārklājumu izmantošanas iespējas: intensīvi tiek pētīta pārklājumu bioloģiskā saderība, antibakteriālās, fotoelektriskās, fotokatalīzes un citas īpašības.

Šajā darbā pētīti **PEO pārklājumu dažādi luminiscences īpašību aspekti**. Pētītas gan pārklājumu iegūšanas procesa modificēšanas iespējas, gan iegūto pārklājumu praktiskie pielietojumi, īpašu uzmanību pievēršot korelācijai starp sintēzes parametriem un pārklājumu optiskajām īpašībām.

Šajā pētījumā apskatītas trīs galvenās tēmas:

1) PEO pārklājumu aktivēšana ar piejaukumiem to luminiscences īpašību pētīšanai;
2) pārklājumu izgatavošana ar dozimetra īpašībām un to pielietojamības novērtēšana;
3) aktivēta stroncija alumināta kompleksā oksīda sintēze PEO procesā fosforiscentu pārklājumu izveidei.

Apvienojumā ar agrāk plaši pētītajām PEO īpašībām (izcilu cietību, lielisku adhēziju, ķīmisko stabilitāti un ātru ražošanas procesu), pārklājumu luminiscentās īpašības var pavērt plašas šādā PEO procesā iegūtu pārklājumu pielietojuma iespējas dažādās zinātnes nozarēs un jaunajās tehnoloģijās.

Annotation

Plasma Electrolytic Oxidation (PEO) is a process for producing thick (tens of microns), hard and chemically stable oxide coatings on metal surfaces. For decades, the process is under investigation by both scientific and industrial communities due to the low operational cost and ease of production. Due to the flexibility of the process, in the last couple of years, novel possibilities of PEO are quickly emerging: biocompatibility, antibacterial, photovoltaic, photocatalysis and other properties of the coatings are intensively studied.

This work explores the different aspects of **luminescence properties of PEO coatings** which was not studied prior. Both process modification possibilities and practical applications are studied, with the focus on correlation between synthesis parameters and optical properties of the coatings.

Three main topics are covered in this thesis:

1) Doping of the coating oxide structure with additives that alter the luminescence output
2) Production of coatings with dosimeter properties and evaluation of their performance
3) Synthesis of complex oxide structure of doped strontium aluminate thus creating persistent phosphorescent coatings

In combination with inherited PEO properties like outstanding hardness, great adhesion to the surface, chemical stability and quick production, the added luminescence properties can make this coating technology promising for practical applications in various fields of science and technology.

List of abbreviations

1T1C - one trap one center

AAO - Anodic Aluminium Oxide

BSE - Backscattered-Electron

CB - conduction band

CCD - charge coupled device

CMOS - complementary metal–oxide–semiconductor

EDX - energy dispersive X-ray spectrometer

E_k - activation energy

FWHM - full widths at half maximum

GOT – General One Trap

IMRT - intensity modulated radiation therapy

ISO - International Organization for Standardization

k – Boltzmann constant

MAO - Micro-Arc Oxidation,

MCP - LiF:Mg, Cu, P

MTS - LiF:Mg, Ti

OSL - Optically Stimulated Luminescence

OTOR - One Trap One Recombination

PC – personal computer

PED Plasma Electrolytic Deposition

PEN/PEC - Plasma Electrolytic Nitriding/Carburizing

PEO - Plasma Electrolytic Oxidation

PES Plasma Electrolytic Saturation

PL - photoluminescence

PMT - photomultiplier tube

PSU - power supply unit

RE - rare earth elements

RER - relative energy response

S(E) - energy response value

SEM – Scanning Electron Microscopy

SrAl – $SrAl_2O_4:Eu^{2+}, Dy^{3+}$

TEM - Transmission Electron Microscopy

TLD – thermoluminescent dosimeter

TSL – Thermostimulated Luminescence

VC - valence band

XRD - X-ray diffraction

XRL - x-ray luminescence

Z_{eff} - effective nuclear charge

ρ_e - electrolyte resistivity

σ - electrolyte conductivity

Table of contents

1 Introduction

1.1 Motivation

From all the coating techniques Plasma Electrolytic Oxidation (PEO) stands out as one producing the best adhering, hardest, most chemically stable and relatively easily reproducible coatings on valve metals. Thanks to the many desirable characteristics and in combination with acceptable cost and ease of production of the PEO, the process gained large interest in both scientific and industrial communities. In addition, large amount of variable parameters allows the process to be modified to meet specific needs of each individual application. Historically, the process is mainly used to improve mechanical and chemical characteristics of Al, Ti, Mg, Zr metals and their alloys by creating a thick (hundreds of microns) protective oxide coating on the surface. However, **the ability to create crystalline structures and implement dopant atoms in the lattice makes PEO process suitable for production of "functional" coatings** – ones with added benefits of increased luminescence output or the ability to convert one type of energy to another (e.g. X-rays to visible light). Although the process is suitable, **there is a notable lack of studies on the PEO coatings with the focus on their luminescent properties**, thus thorough search for practical applications of the technology should be performed.

1.2 Aim

The aim of this work is to explore the possibilities for PEO coating technology to be used for production of coatings with enhanced luminescent properties.

The following tasks are set:

1) explore the different possibilities to dope the coating oxide structure with additives that alter the luminescence output;

2) produce a PEO coating with dosimetric properties for detection and quantification of ionizing radiation;

3) explore the ways to create a persistent luminophore coating using PEO.

1.3 Contribution of the author and scientific novelty of work

The author of this work participated in the PEO setup development: the development of software for automation of PEO process that allows dynamic pre-defined control of all electrical parameters and registration of measured voltage and current. The software is described in more

detail in section 3.1.3. Additionally, some modifications of PEO setup were performed to improve crucial parameters of the PEO reactor (cooling, ventilation, sample holding).

The author developed the software for thermostimulated luminescence (TSL) setup that was used to evaluate the dosimetric properties of the coatings. In addition, some hardware modifications were performed by the author in this and other luminescence measurement setups.

PEO sample synthesis was performed by the author unless stated otherwise in the corresponding publications. Same goes for the data analysis, luminescence measurements, the electron microscopy and structure measurements. Other contributors in measurements, data analysis and publication of the results in peer reviewed journals are reflected in the author list of respective publications in section 7.1.

The author of this work is a main author of three publications related to the topic of this work and a co-author of 3 PEO-related publications, as well as co-author in 27 other scientific publications in indexable peer-reviewed journals. Full list of publications can be found in section 7.

The author was a scientific advisor of one defended bachelor's thesis connected with the development of PEO luminescent coatings and one bachelor's thesis about the dosimetry of alumina.

2 Literature review

2.1 Electrolytic passivation processes

Since the first applications of metals and alloys it was evident that the corrosion is an important and most often undesirable effect one should consider when designing, storing and using metallic parts. Surface layer of chemically active metals and alloys is prone to corrosion when in contact with the environment. With time, the corrosion can decrease structural rigidity of metallic items thus limiting their usability and lifetime. Naturally, ways to protect the metal from the environment were developed. Simplest approach is the physical coating of the metal using liquid (paint) that upon drying leaves uniform, undisturbed and well-adhering layer preventing the metal contact with the environment – a barrier coating. Although the process is easy to implement, it has a range of drawbacks: high dependency on the initial surface preparation, degradation overtime due to the organic base of most paints, difficulties to uniformly cover parts, low mechanical resistance and others. In attempts to fix the downsides, researchers have developed a wide variety of coating processes with varying characteristics; however, paints are still the most used ways of protecting metals from the environment.

In 1800s, Christian Friedrich Schönbein [1][2] noticed that the reactivity of iron when placed in nitric acid is hindered if the iron was prior placed in a much more concentrated nitric acid. This led to the conclusion that iron forms a protective layer on the surface when placed in acidic environment making the surface “passive” and preventing further corrosion. The passivation of metals thus gained increased interest as it provided another solution to the corrosion of metals and solved some of the drawbacks of barrier coatings. Other metals were found to exhibit passivation properties and are forming thin protective oxide layer on the surface preventing further corrosion. The most prominent example is aluminium and its alloys – it was observed that the aluminium quickly forms a thin (2-3nm [3] [4]) oxide layer when in contact with air. The layer, however, is too thin to withstand even slightest acidic environments, and the thickness is often decreased if any foreign atoms are present in the aluminium [5] – a requirement for improving the mechanical characteristics of metals by creating alloys. Nevertheless, the passivation layer on aluminium is often the most important property of this material for certain applications. With the development of electric circuits and discovery of electrolysis the ability to increase the thickness of naturally occurring oxide layer emerged. The science of anodization investigates the possibilities to use the electric potential to controllably increase oxide layer on the metal surface. The electric circuit for electrolysis is therefore

implied – the part to be coated is the anode (hence the term “anodic alumina oxide” or AAO) with the counter-electrode (often inert metal like platinum, however, other options are possible) as the cathode. The general setup of anodization is shown on fig. 2.1. Due to its widespread use, the parameters of the process are well-established: anodization usually is performed in slightly acidic or neutral electrolytes (pH 5-7) [6] [7] using constant voltage in range of 10-100V. Most of the experimental setups track the current (thus acquiring current density value). The current decays exponentially with process time, and current density correlates with the coating thickness at a particular point in time. The maximum thickness of the coating, however, is proportional to the applied voltage [8] [4].

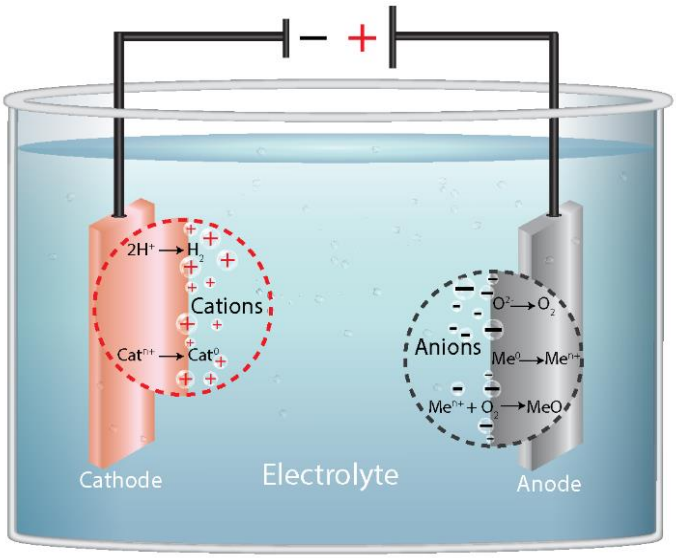

Fig. 2.1 Overview of electrolysis of metals in aqueous solutions

Two distinct directions can be observed in anodization research – production of the barrier-type coatings and porous oxide coatings.

Porous AAO

Historically, AAO was primarily used to increase corrosion resistance of the aluminium with some benefits in mechanical performance of the coated parts. However, with the advancement of nanotechnology, electron microscopy and material science, the focus of electrochemists shifted from the development of coatings for straight-forward practical use as a protective layer to the more specific application of AAO. Main catalyst for the use of AAO in nanoscience was the discovery of porous AAO. Nowadays the amount of publications on porous AAO far surpasses the amount of barrier AAO studies. When meeting a particular set of conditions, it

was discovered that a highly ordered, uniform nanosized porous structure can be easily obtained on the aluminium surface. In combination with other characteristics of alumina (good chemical stability and hardness), the organized nanostructure is proven to be useful not only as the material itself (e.g. in production of colored coatings) but also as a mask for the production of other nanostructures. Naturally, a great amount of research was done on the porous AAO since the first discovery of its usefulness mainly focused on the precise control of size, wall profile, depth of the pores as well as large surface uniformity and porosity of the coating. In-depth review of different parameters for porous AAO synthesis is out of the scope of this work; however, two mechanisms for initial pore formation should be outlined. Core element for the porosity is not the controlled growth of pore walls, but rather careful dissolution of the wells that can be described with the two simultaneously occurring mechanisms – heat-induced and field induced oxide dissolutions. While mechanism for heat-induced oxide dissolution is straight-forward (lattice vibrations expand the chemical bonds on a surface layer of the oxide to a point where bonds break followed by reaction with ions in the electrolyte), the mechanism for field induced oxide dissolution is more complex and was first described by O'Sullivan and Wood [9]. A notable characteristic of production of porous AAO that is used in theoretical models, correlates with the experimental observations and should be considered in commercial environments is the use of acidic electrolytes. The solubility of the anodic oxide in the electrolyte is the deterministic factor in formation of pores. The sulphuric, chromic, oxalic and phosphoric acid electrolytes are often used for porous AAO production. [10] [11]

The most widespread use of porous AAO is corrosion protection with wear improvements [12] [13] [14] [15], decorative coloring by filling the pores with dyes and subsequent "sealing" of pores [16] [17]. However, other properties and applications of porous AAO are explored by many scientific groups due to the simplicity of experimental setups and a wide range of obtainable structures and materials. Some of them are electrical insulation and application in electronics [18], hydrophobic and anti-icing performance [19], various photoluminescence-based applications and use of optical properties [20] [21][22][23] [24] and as a matrices for nanopillar materials (e.g. copper [25], CdS [26], gold [27] [28] , ZnO [29] and others). There are currently 300-400 papers per year with the "AAO" as a keyword (Scopus, last 5 year data) – a clear indication of outstanding performance of this system for various fields of science.

Barrier AAO

Barrier oxide layer is a uniform, non-porous coating on a metal surface usually created to protect the metal from corrosive environments and in addition improve mechanical

characteristics of the surface. Even though compact amorphous layer of barrier AAO exhibits less defects than porous AAO and provides much better stability of the layer at high temperatures, applications of such coatings are limited and mainly applied in protection of vacuum-deposited materials [30], gate insulator materials [31] and general protection of materials from the environment.

2.1.1 Dielectric breakdown of oxide coatings

The oxide layer on the surface of metals exhibits much lower conductivity when compared to the electrolyte or substrate, therefore a phenomena of dielectric breakdown through the coating is often occurring when anodization is performed at high voltages. As mentioned before, some anodization procedures require operation in galvanostatic (constant current density) conditions. While it is required for the production of porous AAO, it also can be applied for the barrier type oxide coatings. That way, the thickness of the oxide increases linearly with time with the subsequent rise of voltage. If the power supply is not current-limited and the oxidation is run long enough, at some point in time the dielectric breakdown will occur – an event usually considered parasitic in anodization - it prevents the uniform growth of the oxide and degrades dielectric properties of the material. The threshold voltage (breakdown potential) is the deterministic parameter for the breakdown and is defined as the electric potential applied to the system for the first breakdown event to occur. In praxis, one can define an easier to understand explanation of the threshold voltage: a critical potential difference between two surfaces of the oxide – oxide/electrolyte and metal/oxide – for the dielectric breakdown to appear. Naturally, oxides of metals used for anodization are dielectric, therefore the first parameter to directly affect the breakdown voltage is the conductivity of the oxide itself. The greater the conductivity – the less voltage is needed to induce electron avalanche effect in it, and conductivity of dielectrics is determined by their bandgap between the valence and conduction bands. The metal from which the oxide is formed has a great influence on the bandgap (e.g. Al_2O_3 has the bandgap of 6.2-8.8eV [32] [33] and ZnO – 3.3-3.4eV [34] [35] [36]) ; however, the bandgap can also be affected by the presence of defects in the amorphous structure of the oxide or the type of crystalline structure, if present. Despite that, for all intents and purposes, all effects outside the base metal are not taken into the account in determination of band gap due to the relatively low amount of the defects in the structure and absence of crystalline structure.

The electric circuit used for anodization also contains a crucial element greatly affecting the breakdown voltage – the electrolyte. It was established previously that the breakdown voltage

correlates with the electric potential difference on both surfaces of the oxide, and while the potential on the metal is fixed by the power supply, the potential on oxide-electrolyte surface can be influenced by the resistivity of the electrolyte. In fact, it is well-established, that the breakdown potential U_B increases linearly with the logarithm of the electrolyte resistivity ρ_e, Moreover, there are other parameters influencing the breakdown: uniformity of the surface before anodization, presence of cracks and other damaged interfaces in the coating, purity of the both electrolyte and metal and other factors affecting the breakdown indirectly (e.g. electrolyte temperature changing its resistivity and affecting anodized coating). Interestingly, current density was proven to affect the breakdown only in a minor way – and this is understandable as only the potential difference is of interest. The movements of the electrolyte, the history of the film and macroscopic surface roughness was reported to have negligible effect. [37]

Prediction of the breakdown voltage is crucial for controlled production of high quality coatings. Some studies on production of porous AAO reported that the best self-ordering of pores required operation in a voltage range very close to the breakdown, therefore prediction and avoidance of the breakdown is of essence. Nevertheless, the breakdown naturally limits the maximum thickness of the oxide produced with anodization technique, and the event itself is generally not desired as breaks the structure of the coating and pronounces localized “burning” of the layer. However, with enough processing time and high enough voltage the breakdown event can be used to even further enhance the mechanical properties of the coating. Operation under “breakdown” conditions require a much higher power from power supply (to reliably hold the voltage above breakdown potential) and will generate substantial amounts of heat. The coatings produced under breakdown conditions will have a wide range of interesting properties and will be drastically different from those produced with anodization, therefore, a completely new field of electrolytic processing of valve metals was formed – plasma electrolytic oxidation (PEO).

2.1.2 Plasma electrolytic oxidation

The PEO is a method to produce ceramic coatings on various metal and alloy surfaces exhibiting outstanding corrosion, thermal, electrical and mechanical properties. The characteristic factor of PEO is the use of high voltage power supply to apply the DC, AC, bipolar or modulated DC electrical power on metal in appropriate electrolyte. The process is of high interest for industrial applications due to the relatively low time of production, wide variety

of metals that can be coated (Zn [38], Mg [39], Ti [40], [41], Ta, Hf, Nb, Zr and others), eco-friendly resource use and ease of scalability; therefore, the technology is already applied in various fields - aviation, automotive, medicine and biology, maritime transport and others. However, some drawbacks for a wider application range are still present, some inherited from the process itself (e.g. porosity and amount of variable parameters described in detail later) and others are financial (high upfront cost, complexity of required infrastructure).

During the early development of the technology, there was no consensus on a proper naming of the process, which led to a confusion and description of essentially the same process using different names. Plasma electrolytic saturation (PES), plasma electrolytic deposition (PED), micro-arc oxidation (MAO), plasma electrolytic nitriding/carburizing (PEN/PEC) and others were often used; however, mostly MAO and PEO are in use today due to the sufficient definition and historical aspects [42]. Fig. 2.2 shows the amount of publications by year for "Plasma Electrolytic Oxidation" or "Micro Arc Oxidation" keywords – as one can see, in 2000s, a rapid development of the technology emerged and the interest in the field exhibits significant growth every year.

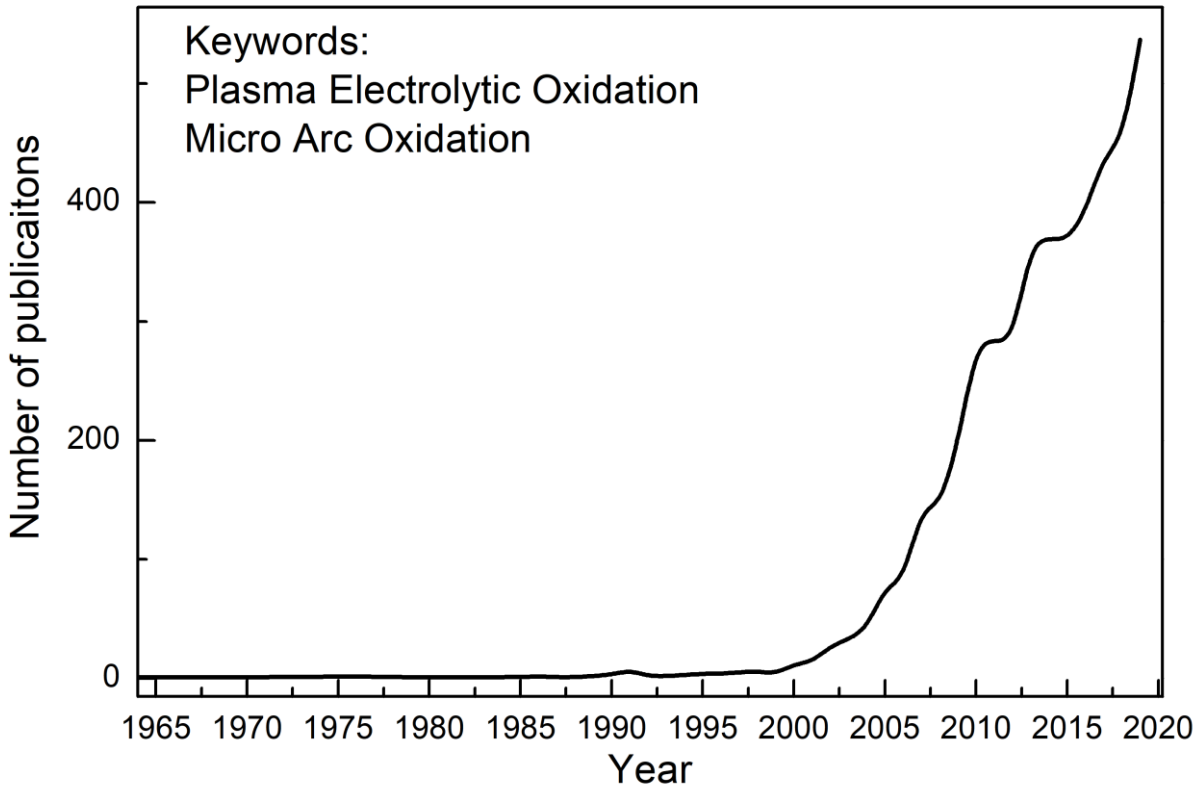

Fig. 2.2 The number of publications with keywords "Plasma Electrolytic Oxidation" or "Micro Arc Oxidation" by year in Scopus database.

Naturally, PEO evolved from conventional anodization by application of substantially higher current and voltage to the part so that the electrical discharge will occur through the anodized oxide layer. First mentions of the PEO process can be traced back 8 decades [42] and over the years scientists and engineers formed concepts of the processes occurring during the oxidation. Step by step representation of the mechanisms is presented in fig. 2.3.

I. The formation of the oxide layer starts with the initial, thin layer of amorphous oxide. This is a crucial step for the whole process as low conductivity of the oxide is deterministic for the increase of potential between the electrodes and, later, formation of electrical discharges through the layer.

II. The growth of the oxide film continues forming porous layer and further increasing the voltage drop, where most of the resistance is now corresponding to the thickness of the coating. Up until this point, the formation of porous oxide film is exactly the same as in anodization described previously; however, if the setup is not voltage-limited by design, the further increase of voltage will enable dielectric breakdown of the coating forming a “micro-arc”.

III. “Arching” or electrical discharge through the coating occurs at least resistance point (inside pores) once the critical value of the electrical gradient is reached and is followed by observable light emission. The oxide layer continues to grow further isolating the substrate from electrolyte. Mainly impact ionization processes are occurring at this stage of the process, like the dielectric breakdown of anodization coatings described previously.

IV. At some critical point the local temperature in the vicinity of micro-arcs reaches critical value and thermal ionization processes take place significantly increasing the power of the discharges. The increased voltage and current lead to the higher temperatures thus allowing crystalline structures to form – with many reports describing the ability to create even the hardest phases of alumina (α-Al_2O_3 with transition temperature of 1150-1200°C)

V. The prolonged discharge processes on the surface will result in the increase of the pore diameter and localization of pores. During micro-arching and sparking, the discharges are mobile and “move” on the surface thus initiating the recrystallisation of oxide in different parts on the surface. The increase of pores and thickness, however, will lead to the presence of a much larger discharge channels with no movement. These discharges have variable impact on the coating - they might form high-temperature

crystalline phases of oxides and may cause excessive cracking of the layer or even cause delamination of the coating.

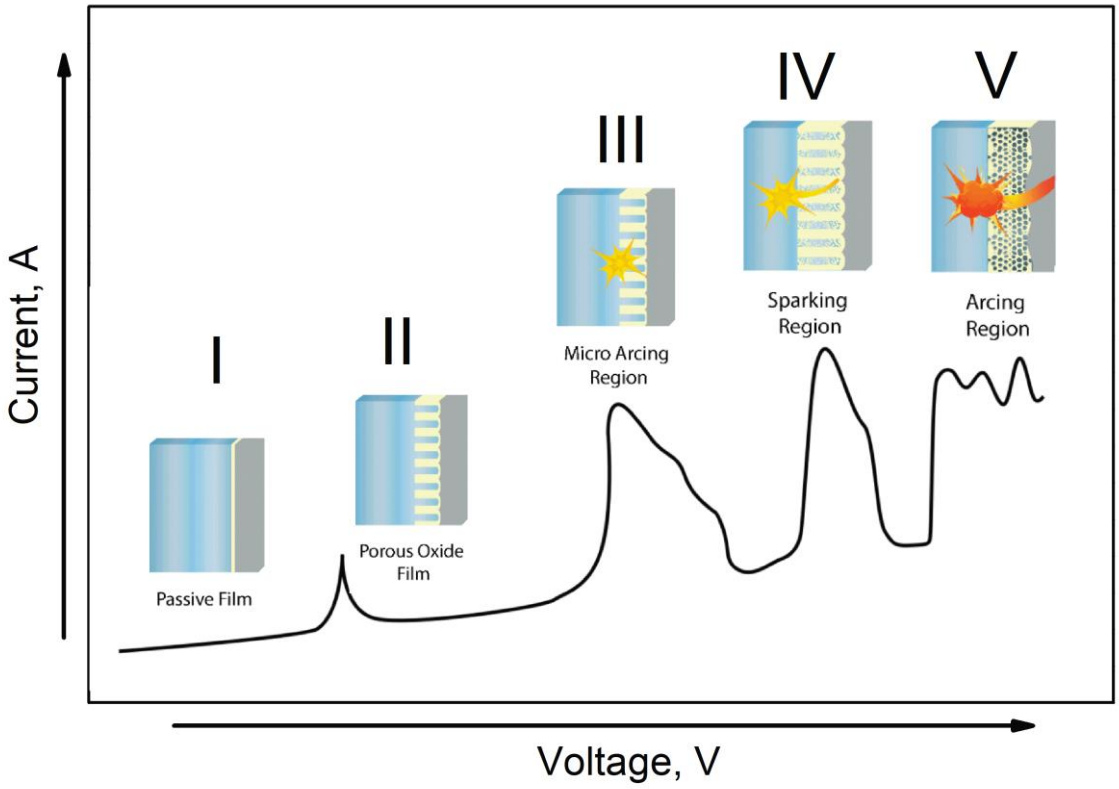

Fig. 2.3 Schematic representation of the evolution of the coating during PEO process and current-voltage graph connected to each step.

It is important to note that, although distinct, the different stages of PEO process can occur at the same time on different regions of the surface, therefore real current-voltage graph will rarely resemble the one presented in fig. 2.3.

2.1.3 Variable parameters of PEO

The successful use of PEO implies precise control of all variable parameters to get desired and reliable results. When compared to anodization where electrodes, electrolyte and voltage should be carefully thought through, PEO includes even more power supply parameters (especially in pulsed bipolar DC mode) and exhibits even greater dependence on quality, composition, and temperature of the electrolyte. Although the amount of variable parameters is overwhelming at first, it offers additional possibilities to control the structure and composition of the coating and adds the ability to include foreign atoms in the crystalline lattice of the oxide - an extremely useful property for modification of luminescence properties of the layer. Here, a list of all variable parameters, their typical values and some key research is listed.

Substrate

Since the first research on oxidation of metals it was evident that the substrate (metal) plays a major role in final composition of the coating, regardless of the type of process (PEO, anodizing). Metal ions, especially when subjected to electrical potential, bond easily with oxygen, thus forming a metal oxide layer, which leads to the assumption that all atoms present in the metal alloy will be present in the coating structure. For practical applications, where any significantly pure metal is rarely used and mostly alloys are applied, this means that the coating will never be truly free of any dopants or contaminations. Engineers and researchers, therefore, are always wary of the ramifications of this property when trying to achieve any particular goal with the coating.

Any impurities present in the structure of crystals and amorphous solids produce defects thus altering the hardness and promote the formation and prolongation of cracks. Therefore, mutually competing factors are present - on the one hand extensive research is done to produce harder, stiffer alloys of metals by implementing different atoms in metal structure and on the other hand those atoms prevent the growth of crystalline structures on the surface. In absolute majority of applications the desire for structural rigidity of part is much more important than the difference in quality of the coating arising from additional atoms.

As PEO process is often used to enhance mechanical properties of the surfaces of metals, one of the main structural differences when compared to other coating technologies is the crystalline structure of obtained oxides. There are reports on synthesis of gamma, eta or even alpha phases [43] [44] [45] of alumina on aluminium surfaces thus increasing the surface hardness. A single pure crystalline phase cannot be achieved, mechanical characteristics are improved with relative increase of harder crystalline alumina phases in a mix with amorphous alumina.

Although incorporation of desired atoms in the coating from the substrate itself is possible, most of the time this type of doping is extremely hard to implement and scale for any kind of practical application as the preparation of specific alloy requires additional expenses and time. Other factors against the use of this method are important too, for example: alloying element that is good for luminescent properties might change mechanical properties significantly. Moreover, alloying of metals is made in bulk whereas atoms participating in the preparation of coatings are located in the surface layer of part; therefore, a waste of material occurs with some of the atoms in bulk of the material remain unused after the coating process is finished. With other much more promising methods of doping developed (doping from electrolyte or pore filling technique), this method is rarely used.

Surface quality

Decades of studies of anodization proved the ability to produce highly-organized porous nanostructures on the surface of valve metals (aluminium, titanium and others). As previously described, structures led to the development of various devices and are used for assistance in synthesis of other nanostructures. One extremely important factor in production of highly-ordered structures is the surface preparation - great amounts of time are spent preparing the surface of aluminium for AAO growth mechanically (polishing) or chemically (etching, chemical cleaning). Fortunately, PEO coatings are on another size scale - tens of microns of thickness with micrometer pores in comparison with AAO, where tens/hundreds of nanometers in thickness with nanoscale pores are typical. Therefore, the surface quality of the part before PEO does not need to meet as strict requirements; however, some key operations should be performed.

Large defects on surface (deep scratches, uneven surface) should be removed before the PEO as sharp edges will exhibit larger current densities than flat surfaces thus incorrectly distributing desired overall current density resulting in uneven structure of the coating. Polishing to 1000 ISO grit sandpaper is usually enough with less care needed for longer PEO processing times/thicker coatings. However, during our studies we found that PEO process can be used to produce ordered structures or highly-porous coatings much larger than anodic AAO (fig. 2.4) and they do require careful consideration of surface quality - polishing with 1-2 micron diamond paste was necessary - but due to the lack of potential applications of such coatings, this is rather an exception.

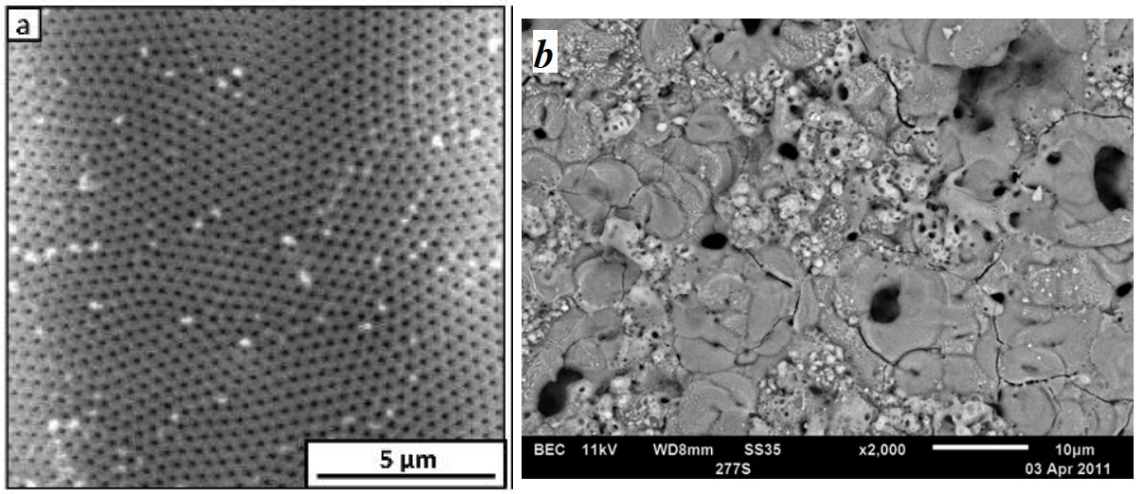

Fig. 2.4 a- a typical SEM image of porous AAO with average pore diameter of 120nm [46] and b – a typical PEO coating on aluminium surface [47]

An interface between the substrate and electrolyte is extremely important, especially during the first stages of the process. Oil and organics on the surface of the part might prevent wetting of the surface by the electrolyte thus preventing the oxide growth in certain parts and increasing current density in others. Therefore, a thorough cleaning and degreasing of part should be performed before the PEO process using acetone, ethanol or other solvents.

As PEO will use some volume of the metal from the surface to create the oxide, not only morphology is important, but also the surface structure of the metal. Some technological processes will inevitably lead to the work-hardening of the metal or the alloy, changing the grain size of the metal. It was reported that the corrosion resistance of anodized coatings is affected by the grain size [48][49] .

Electrolyte

The electrolyte is one of the most important variables in the PEO process. The electrical characteristics of it will mainly govern the parameters of power supply, while chemical composition of electrolyte will influence the structure of the coating. With many variations and types of electrolytes consisting of a range components and each component behaving differently it is easy to get lost in selection of the needed electrolyte; however, over the years some general rules were noted.

The most important role of the electrolyte is to allow the flow of charge in a circuit, therefore free charge carriers should be present in the electrolyte. Contrary to anodization where mostly acidic electrolytes were used, in PEO mainly alkaline electrolytes are used with pH values in the range of 9-13, thus providing negatively charged OH- ions as a charge carriers; however, less commonly (e.g. coatings on titanium [50] [51] [52]) the acidic electrolytes are used. Usually, KOH and Na_2SiO_3 is added to deionized water in order to adjust the pH vale. Typical amounts are in range of 0.2-5g/L. This will also determine the conductivity of electrolyte - an important factor since the voltage drop on the electrolyte will alter the electrical field gradient through the coating thus affecting the dielectric breakdown voltage. A simple calculation was proposed in [53] allowing estimation of voltage drop caused by the electrolyte conductivity:

$$\Delta V = \frac{4hI}{\pi D^2 \sigma} \quad (1)$$

where h and D are the height and diameter of the pore at breakdown spot, I is a discharge current and σ is electrolyte conductivity. Although the equation does not fully translate to the real system, with all approximations (temperature, density, irregularity of pores etc.) allows one to conclude that the voltage drop caused by the change in electrolyte conductivity can be as drastic as tens of volts, even for relatively thin coatings (20 μm).

With the base of the electrolyte formed one can utilize the 4-component nature of the PEO, where substrate, oxide coating, electrolyte and gas are in contact with the plasma and thus participating in formation of the oxide and add additives in the electrolyte to alter the properties of the coating. Both soluble and insoluble additives will work, with great scientific interest devoted to suspension electrolytes [54].

Quite quickly it became evident that insoluble particles present in the electrolyte will still participate in PEO as they will come close to the discharges and thus incorporate in the coating. This opens a new range of possibilities to alter the properties of the coating and thus suspension electrolyte (sometimes called "slurry electrolytes" [55]) studies can be considered as the separate category. Successful application of nanoparticle suspension was reported to be useful for improvement of wear and friction characteristics as well as corrosion resistance [54] [56] [57]. While the former utilizes the adapted characteristics of the implemented particles (e.g. hardness of Al_2O_3 alpha particles is much higher than the alumina coating in gamma phase) the latter uses the ability of the particles to fill pores and cavities in the coating thus preventing the contact of metal with the environment. The mechanism of practice inclusion in PEO was briefly described in [58] where a distinction was made between particles that participate in the coating creation maintaining the particle form and crystal structure and those undergoing thermolysis in plasma discharges thus partially or fully mixing atomic structure of the particle with the coating. Both of the cases are feasible and experimentally observable, although the use of stabilizer/anticoaugulant (e.g. $Na_6P_6O_{18}$ [55]) does favor the degradation of particles in arc discharges.

Pore filling technique described in detail in chapter 4.1.2 can also be considered a "suspension" electrolyte as the processes occurring during particle inclusion in the coating are similar to the suspension electrolytes; however, requiring much smaller amount of powder, thus making it even more suitable for modification of optical properties where relatively expensive rare earth oxides often are used.

Since the small changes in electrolyte (be it quality of reagents, measurement errors or other factors) influencing the voltage-current characteristics of the system and coating quality in a major way, the comparison of the results acquired in different laboratories and systems is

extremely hard. This is one of the factors why mainly only general relations and concepts are presented as conclusions of studies rather than a step-by-step instruction for one or another type of coating. Nevertheless, some studies propose a "universal" type of electrolyte optimized for both aluminium and magnesium coatings [59].

Electrical parameters

As PEO can be performed in a broad range of electrical regimes, a row of power supply parameters can be controlled: maximum voltage and current, AC/DC mode of operation, current density, overall power applied to the sample, pulsed DC frequency, assymetric bipolar ratio and others.

Although consistency of parameters between studies is hardly observable, some general considerations are outlined. For a successful PEO process couple of requirements should be met – firstly, maximum voltage should be sufficient to cause a discharge through coating depending on the material itself (aluminium usually requires slightly higher voltages than magnesium [53] [60]) and the stage of the process (the longer the process – the thicker the oxide – higher voltage needed to cause a discharge). Another important factor is the DC/AC mode of operation. Often, a simple high voltage DC power supply is used; however, various studies reported the benefits of using pulsed DC sources to control the duration of the plasma discharge thus gaining more uniform structure of the coating [61][62]. Pulsed DC current, however, can cause additional polarization of the electrode – an undesirable effect leading to the drift of current density – a crucial parameter in PEO processing. To limit that, the unbalanced AC or DC sources can be used with different positive and negative voltages [63]. Decades of studies on PEO electrical parameters involve research of processes on macro scale. In praxis, for each application, electrolyte and experimental setup the set of electrical parameters will be adjusted uniquely based on the general observations in other studies.

2.1.4 The doping possibilities of PEO coatings

The large number of variable parameters implies the many possible ways to alter the composition of the coating. Firstly, it is evident that the substrate composition is the main determining factor for coating composition. Naturally, the effects of alloying elements if PEO is performed on the alloy will cause structural changes of the coating – some studies reporting the changes of corrosion performance and wear caused by the alloying elements [64] [65] and unless the study is performed on a pure metal surface (extremely rare due to the lack of practical

applications), the elements from the alloy will always be present in the coating and should be taken into consideration. For luminescence applications, the Eu alloyed aluminium was used to insert europium ions in the coating [66] and this study is presented in-depth in chapter 4.1.1.
The most popular way of doping the coatings is inserting the needed atoms from the electrolyte by using insoluble particle addition. A significant amount of studies were performed with the aim to improve wear performance, coating growth characteristics and anti-corrosion properties using "slurry" electrolytes – reviewed in a paper by A.Borisov et.al. [58]; however, row of studies by S.Stojadinovic and R. Vasilic utilize the approach for enhancement of luminescence properties of the coating. Papers on PEO coatings on Zirconium [67] [68] [69][70][71], Niobium [72] [73], Tantalum [74], Aluminium [75] [76] [77] [78] and Titanium [79] [80] [81] [82] [83], all doped with various dopants demonstrate the effectiveness of the method to alter photoluminescent properties of the coatings and enhance the application possibilities of the technology. The method was also successfully applied to create a complex strontium aluminate structure consisting of three different dopants added from the suspension electrolyte [84], [85] and will be discussed further in chapter 4.3.
A derivation of the suspension electrolyte method – a pore filling technique - was demonstrated in [86] and will be discussed in detail in chapter 4.1.2.

2.1.5 Applications of PEO coatings

Historically, PEO coatings are used for their outstanding mechanical and chemical properties – the benefits of a thick layer of oxide on a metal prone to corrosion and scratching are hard to replicate with other coating methods (paints, anodization). However, the variability of composition, possibility to obtain crystalline structures and relative simplicity of experimental setups motivated scientists to expand the list of possible applications and create functional, optical and other non-conventional coatings. Therefore, the applications of PEO coatings can be divided in two categories – structural and functional. The first one utilizes the mechanical and chemical properties to enhance the performance of the part that is coated and the second one utilizes the properties of the layer itself rather than improves the material.

Structural applications

PEO coatings are mainly used due to the two properties – firstly, great corrosion resistance and secondly, high hardness and adhesion ensuring great wear characteristics. Apart from the scientific studies, PEO is commercially applied to create coatings on car parts, marine components, medical equipment, consumer electronics and aviation industry (e.g. Keronite

International Ltd. [87] or IBC Coatings Technologies, Inc. [88]) Thermal/electrical insulation is another prominent feature of coatings [89] [45].

Due to the PEO being electrolytic approach, a uniform coverage of complex parts can easily be achieved – another important feature of the process utilized to cover highly-porous or composite structures [90] [91] [92] [93]. Rapidly developing metal additive manufacturing field is another possibility for application of PEO technology [94] [95]

Functional applications

Outstanding mechanical and chemical properties of coatings motivated the search for more advanced, enhanced applications of the technology. Notable examples of such applications are antibacterial [96] [97] [98], biocompatibility [99] [100], photovoltaic [101], photocatalysis [102] [103] [104][79][105] and many more due to the versatility of the process.

Luminescent PEO coatings are a relatively new field of study; however, in the last 5 years some luminescence-based applications were developed: luminescence thermometry [106] [107], gas sensitivity [38], dosimetry [108] and long lasting luminescence [84] [85].

2.2 Luminescence

Luminescence is a spontaneous emission of light by electron radiative transition from higher energy level to lower [109]. For electron to emit a photon by decrease of its energy, firstly the energy should be increased via the "excitation" process; therefore, a broad field of luminescence is usually divided into the subsections by specifying the excitation process – e.g. photoluminescence (PL) is the increase of electron energy by light photons, x-ray luminescence (XRL) is the excitation of electrons using X-rays, bioluminescence is the increase of energy due to the biological activity in the sample, chemiluminescence – excitation in chemical reactions and so on. Some luminescence methods require complex mechanisms of electron trapping in metastable positions, thus only a way of stimulation of charge carrier release is specified in the name: thermostimulated (TSL) luminescence uses heat to initiate release of already trapped electrons, optically stimulated luminescence (OSL) uses light in the same manner. There are tens of possible luminescence mechanisms with most of them tied to the practical applications. Light emitting displays, most of the modern lighting options, glow-in-the-dark toys and emergency signs all use some type of luminescence and even more possible applications are still under investigations in medicine, transportation, science, space, military and sport industries.

This work will mainly focus on the TSL, PL and XRL studies of materials. One of the main applications of TSL is the field of dosimetry – detection and quantification of ionizing radiation used mostly in medicine and nuclear energy.

2.2.1 Solid State dosimetry

Since the beginning of radiation research and first observations of ionizing radiation by Pierre Curie, Marie Curie, and Henri Becquerel, the detection of radiation became the important aspect of the field. While benefits of high-energy radiation became evident almost immediately, the dangers associated with them were not obvious until the first studies of high flux ionizing radiation effects on living organisms. Damage done by high intensity X-ray light can be seen almost immediately; however, the high dose over prolonged period of time was proven to cause cell mutations and increased risk of development of cancerous cells in the organisms. With the first observations of such effects it was evident that accumulative acquired dose is an important factor to control. A challenge was proposed – development of precise, simple and cheap measurement device of acquired dose over a certain period of time. A subsection of physics under the name of "personal dosimetry" was thus founded.

With ever increasing use of ionizing radiation in medicine, energy production and manufacturing, the demand for personal and industrial dosimetry motivated scientific groups to devote a lot of attention to this complex topic. Different approaches all tailored to a specific application were developed mostly in the last century connecting many science fields (biology, physics, chemistry, medicine, engineering etc.); however, there is still a demand for a specific type of dosimeters, improved characteristics of existing dosimeters or development of completely new ones meeting particular specifications.

2.2.2 Types of dosimeters

There are various possibilities to measure the presence of ionizing radiation and quantify the intensity of it. Since the ionizing radiation can significantly affect various properties and parameters of the materials, a range of physical effects can be used to detect it. Perhaps the most notable is the temperature change of material upon irradiation – calorimeter-type dosimeters detect the absorbed dose by measuring the temperature change of the measuring medium. Ionizing radiation can also induce chemical reactions and promote destruction of chemical bonds and formation of others – thus, chemical dosimetry can also be used. One of the most popular chemical dosimeters is Frickle dosimeter [110] – a color-changing liquid

suitable for large dose measurements. Notable chemical dosimeter is the radiographic film – usually silver bromide particles in a transparent medium extensively used in medicine due to the great spatial resolution. Another widely popular high energy radiation detection system is the ionization chamber detectors – a gas filled chambers with high voltage (400-900V) applied to distant electrodes in direct contact with the gas. High energy photon will cause ionization of the gas thus lowering resistivity of the chamber causing an electric discharge channel to occur. Electronics device then registers number of pulses in a timeframe – a unit proportional to the radiation flux. Ionization can also occur in solid materials – ionizing radiation photon can transfer its energy to detach an electron from an atom in a solid material (e.g. crystal) promoting electron to the higher energy state, which then finds another vacant position and "relaxes" to it emitting the difference in energy as a light photon. Solid state dosimetry studies the effects and electron transitions in order to detect and quantify the radiation and will be discussed in the next chapter.

Clearly, there are many techniques developed for detection of ionizing radiation and there is no universal way to measure radiation. Most of the materials and approaches are specifically tailored for a particular application, therefore different properties are utilized – high sensitivity (for applications in power plants), spatial resolution (for X-ray scans and detection screens), large measurable dose range (for personal dosimeters), high maximum dose (in industry), immediate data output (for environment control) or quick operation (for pulsed radiation measurement).

2.2.3 Solid state dosimeters

Solid state dosimeters are a type of dosimeters where a solid material is used for storage of some of the energy acquired from ionizing radiation with the ability to "trigger" the energy release by a specific process. The mechanism of energy storage an release is not trivial and varies by the material, but the majority of solid state dosimeters use crystalline lattice of a semiconductor with intrinsic or impurity defects, which create electron traps in the band gap of the material. Since these traps are located above valence band of the semiconductor the energy of electrons in these traps is increased (thus the electron is called "excited") and an additional energy is required to release the electron from the trap to the conduction band and promote recombination with energy output in a form of light (luminescence). The simplest and most used method for the application of this additional energy is temperature increase - the method is therefore called thermostimulated luminescence and will be described in the next chapter.

Other method for energy release is optical stimulation (in case of OSL) often used in the more modern measurement systems. A main feature of the TSL and OSL materials is retrospective analysis of the acquired dose, thus the approach gained a lot of use in personal dosimetry field or environmental radiation analysis as it provides a convenient way to tell the dose acquired during some defined period of time. Although the technology is well-studied and widely used, TSL-based personal dosimeters have limitations and drawbacks described below.

TSL signal can be observed in a wide range of materials; however, a set of requirements was defined for a material to be successfully used as a dosimeter for any application either in personal dosimetry, medicine, environmental monitoring or powerplants:

1) Dose response – TSL based dosimeters exhibit some relation between TSL intensity and absorbed dose. The best scenario for dose quantification is linearity range, where intensity I is proportional to the acquired dose. However, the linear response is not possible for the infinite range of doses – minimum detectable dose and saturation dose limit the usable range of the dosimeter. Minimal detectable dose is dependant on many factors: e.g. material itself, sensitivity of the detection system, size of the detector. Often, a technical specification requires the use of complex bleaching procedures between each measurement (usually heating) to ensure correct reading of low signals. Different dosimeters exhibit different usable dose ranges and therefore are more suitable for one or another application. It is important to note that the dosimeter can be used outside its linearity range, but that scenario will lead to the increased error and complexity of data analysis thus losing the reliability. Another factor affecting linearity region is the rate of irradiation of the material. Fast "impact" irradiation can skew the results thus adding to the reading error. Some materials like BeO or LiF [111] have the dose-rate-independent effects, albeit in a much smaller usable dose ranges. In addition, dose response repeatability over time should be taken into the account by providing an expiration date to the dosimeters.

2) Energy response – the amount of energy absorbed from the ionizing radiation source is not the full energy of irradiation, thus the intensity of TSL signal during readout will only be proportional to the absorbed radiation. Different materials absorb radiation differently, thus absorption coefficient should be taken into the account when choosing the correct dosimeter for application. The photon energy response value S(E) is used for that and is defined as the ratio of mass energy absorption coefficient (μ_{en}/ρ) of the dosimeter to the μ_{en}/ρ of the reference (air, tissue, water). The μ_{en}/ρ is formed by the radiation losses occurring due to the photoelectric

interaction, Compton scattering or pair production. All those processes are dependent on the energy of the radiation and material properties: its isotopic content and effective atomic number Z_{eff}. However, to compare different dosimeters, a relative energy response (RER) value is defined as the ratio of S(E) to the ^{60}Co γ-rays of energy 1.25MeV: $(RER)_E=S(E)/S(1.25MeV\ ^{60}Co)$. By plotting $(RER)_E$ on a graph for LiF, CaF_2 and material with effective nuclear charge Z_{eff} = 55 (fig. 2.5), one can see that different materials will react to the same absorbed dose differently depending on the photon energy. Thus, a conclusion can be made – the desired energy response of the material should be as constant as possible for the measurement ranges of irradiation. This is rarely the case, thus additional corrections should be performed. This relation is true only for photon irradiation (X-rays, γ-rays). For other types of irradiation the response of the material will behave differently and should be considered accordingly.

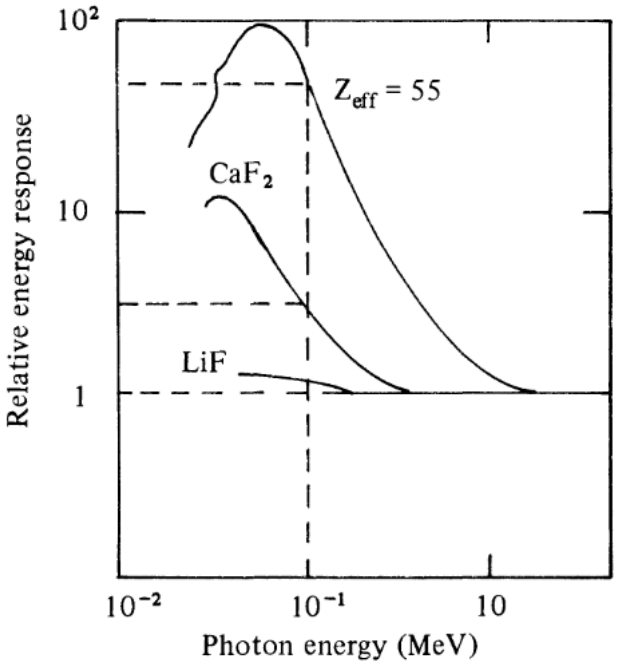

Fig. 2.5. Relative energy response as a function of photon energy for LiF (Z_{eff}=8.14), CaF_2 (Z_{eff}=16.3), and a theoretical material with Z_{eff}=55 [112]

3) Fading and stability – In the simplified case, the recombination rate of excited electrons will be proportional to the *exp(-E/kT)*, therefore any increase of the temperature will increase the probability of each excited electron to recombine. Therefore, a fading is inevitable – gradual loss of acquired energy after the irradiation. However, if a dosimeter is chosen correctly, fading can be minimized to insignificance: for that, one must choose a TSL peak occurring at much higher temperatures than the environment in which dosimeter will be used (large values of

activation energies E_k for a trap). If chosen incorrectly, the dosimeter will emit all the light even before the TSL measurement losing all usability. A stability of the materials at a set environment temperature should be correctly defined and the unnecessary increases of temperature should be avoided. In addition, TSL and OSL are often related, therefore, dosimeters should be kept in dark environments to exclude bleaching effects.

4) Physical and chemical changes – some dosimeters will lose their properties and display incorrect dose values if a physical damage was done producing additional defects in the structure. Another way to damage the material unintentionally altering the dosimetric properties is chemical effects – high humidity, acidic environment or concentrated chemicals can be a factor for incorrect reading. Both of these factors can be minimized with the enclosed box physically protecting the dosimeter from the environment, granted the box does not absorb the radiation the dosimeter will acquire.

The undeniable usability and performance of solid state TL based dosimeters stimulated the quick technology transfer to the various industries. Although there are no defined specifications for a particular dosimeter for each application, there are some preferred materials in every field. Since the great amount of systematic research was performed over the decades, couple of dosimeters stand out as "standard" choice. The TLD (Thermo-Luminescet Dosimeter) designation is often used to mark a commercially available standard dosimeter [113].

One of the "classical", most studied and widely used materials for dosimetry of ionizing radiation is α-Al_2O_3:C (aluminium oxide crystalline matrix in trigonal symmetry). Due to the excellent thermal stability, effective atomic number (Z_{eff} = 10.2) close to human body, and intense TSL signal [114] [113], carbon-doped α-Al_2O_3 is well established as a personal dosimeter and is usually represented with the designation "TLD-500". Although the undoped Al_2O_3 for dosimetric applications is extensively studied for decades, only with the works of Akserod and Kortov in 1990s [114] [115] [116] [117] [118] the doping with carbon drastically increased the usability of the alumina for detection of ionizing radiation due to the increase in TL intensity. The effect is descried with the increase of the amount of F and F^+ centers responsible for the visible luminescence output. The F centers - two electrons in the anion (oxygen) vacancy field are the main luminescence centres in Al_2O_3 host lattice, with F^+ center – one electron in the anion (oxygen) vacancy field - forming by compensating the charge of heterovalent impurity C^{2+} ions [119] [120]. The main emission of the α-Al_2O_3:C is at 460K and 420nm – well within the acceptable range for both the heater devices and photomultiplier tube sensitivity range.

Dopants like Si and Ti [121], Mg [122] and Ca [123], Cr and Ni [124] are often used in Al_2O_3.

Another large group of dosimeters is based on lithium fluoride doped with Mg, Ti, Cu, and P. The designation used for LiF:Mg, Ti is MTS with the symbol representing if natural, 6Li-enriched or 7Li-enriched lithium is used (MTS-N, MTS-6 and MTS-7 respectively). The use of isotopes in production of LiF dosimeters allows the material to be used for detection of neutron exposure in addition to gamma radiation. MTS-type detectors have the linear TSL dose dependence up to 1Gy irradiation with a negligible fading of couple percent per year [125]. LiF:Mg, Cu, P are called MCP-type dosimeters with different isotopic composition, same as MTS: MCP-N, MCP-6 and MCP-7, suitable for measuring doses from mGy to hundreds of kGy due to the presence of high temperature peak [126][127]. This allows the MCP-type dosimeters to be used in measurement of secondary fields of high-energy accelerators. Outside of LiF, different Li-based dosimeters are often used: $Li_2B_4O_7$ with dopants [128] and $LiAlO_2$ [129] exhibit TSL signal proportional to the radiation dose too.

Another matrix used for dosimetry is CaSO4 with Dy [130] [131] , Mn [132] or Tm [133] [130] as dopants with studies on CaSO4:Dy Teflon discs available [134]. These materials are often used for the personnel dosimetry due to the low minimal detectable exposure, manageable fading (1-2% per month) [130] as well as the good amount of measurable cycles.

MgO- based dosimeters [135], CaF_2- based dosimeters [136][137], BaSO [138] should be noted, all exhibiting their different strengths and weaknesses. For most applications, the type of dosimeter used is chosen by the convenience, availability, and price of respective material, which can be easily replaced by another material with similar properties, with small modifications in the readout system.

Recently, a new form of a dosimeters gained attention – devices with spatial resolution or 2D dosimeters. Mainly for use in IMRT (intensity modulated radiation therapy), couple of good approaches can be outlined: the classical radiographic [139], ionization chamber arrays [140] and diode arrays [141], optically-stimulated luminescence films [142] and thermoluminescence-based devices [143].

To conclude, there are many different materials used in solid state dosimetry – rarely universal, each is tailored for a specific application in mind. The different parameters that a material should meet to be considered as a dosimeter and the amount of optimization of each system already performed produced a field where materials are used mostly for their strength while ignoring the weaknesses (e.g. the tradeoff of sensitivity to linear dose range etc.) However, weaknesses inherit to all dosimetric materials are present: cost of production, stability (mechanical and chemical), repeatability of the readings, scalability, uniformity and others. Addressing any of the weaknesses to produce a novel material can promote a replacement of

inferior material in existing application or even create a tailored material for emerging application or technology.

2.2.4 Persistent luminescence

Another field of study of luminescence materials is the persistent luminescence (often called phosphorescence, although the name is dated as most of the phosphorescent materials do not contain phosphorus). The field investigates the long afterglow materials widely used in emergency signage and lighting. Although the physical processes occurring in the phosphorescent materials are similar to those in dosimetry (electrons are trapped in a metastable states with gradual release dependent on the temperature), a crucial difference is present: while fading in dosimetry is a parasitic effect on the property, it is necessary for the performance of phosphorescent materials. The TSL maximum is therefore located near the desired operating temperature (usually, room temperature) to cause a gradual recombination of electrons emitting light photons. Two of the most popular phosphorescent materials are zinc sulphide and strontium aluminate. Both, however, require dopants to enhance performance: Cu and Mn for zinc sulphide [144] [145] with additions of radioisotopes (Radium, Tritium and Promethium) to prolong the afterglow and Eu and Dy for strontium aluminate [146]. The outstanding performance of strontium aluminate with detectable afterglow of more than 10h requires [147] is replacing the use of radiation isotopes in ZnS in addition to providing better performance. However, most of the applications of phosphorescent materials require the material to be coated on a surface, and since the materials are in form of powder or ceramics, the coating is usually performed by mixing of the particles in laques and paints – an inefficient, two-step process decreasing overall intensity of the afterglow and promoting the waste of material by implementing it in the whole paint volume while only surface layer is participating in the desired effect.

3 Materials and methods

3.1 PEO setup

To successfully perform PEO research a three-component system is required: reaction chamber, power supply and PC. The configuration is shown on fig. 3.1.

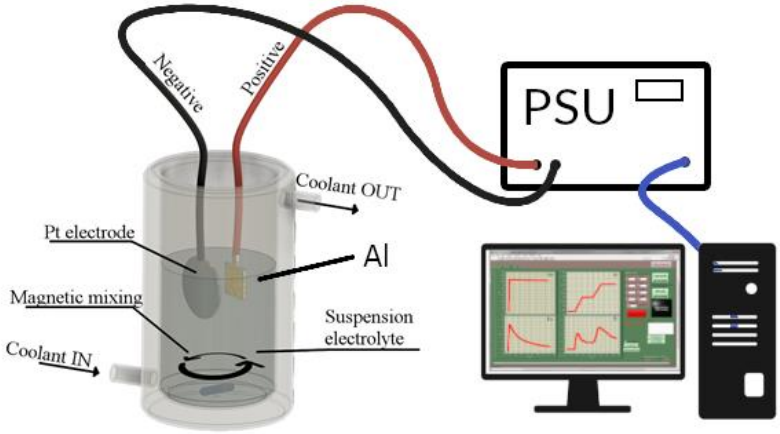

Fig. 3.1. The overview of the PEO setup – reaction chamber with two electrodes is connected to the PSU, which is managed using a PC.

3.1.1 Reactor chamber

A distinctive feature of PEO process is the use of high voltage and current. While high electrical power is necessary, it will be unavoidably converted to heat. Most of the heat will be dissipated in electrolyte, thus increasing its temperature. This can have drastic effects on the process pace and reduce coating quality, especially if the electrolyte reaches boiling temperatures since vapor not only has lower conductivity, but also lacks soluble salts and any insoluble particles. Vapor bubbles reduce surface area covered by the conductive electrolyte, and if power supply operates in constant current mode the current density will be much larger than defined and thus coating structure will be hardly controllable. Great care should be taken for reducing the electrolyte temperature, thus the vast majority of the reaction chambers (electrolyte baths) have some kind of active cooling. Industrial high-throughput setups require water-cooled heat collector coils in the electrolyte with constant water flow through the appropriately-sized radiator ensuring effective heat removal. Some scientific setups utilize the same approach (heat collector inside

electrolyte); however, additional elements in the reaction chamber do bring in additional contamination to the electrolyte as well as provide additional surfaces to be cleaned between synthesis sessions where drastically different electrolytes are used (e.g. residuals of rare earth oxide particles even in low concentrations can affect luminescence properties of the coatings).
Our setup uses double-walled glass beaker with 1L volume. Water inlet and outlet are used to provide constant flow of low-quality cold water (tap water) thus preventing contamination of the electrolyte. Inside glass surfaces are easily cleaned and are chemically inert as opposed to copper or aluminium heat collectors used in the industry. Use of glass chamber also provides the ability for using the magnetic stirrer - a better solution for improving convection of electrolyte than widely used bubble stirrer technique. Constant flow of electrolyte around the sample is even more important with the use of suspension electrolytes as particles tend to segregate in liquids, thus magnetic stirring is preferred.
Despite all the advantages of the double-walled glass reaction chamber, its use is limited due to the poor heat conduction between electrolyte and coolant as a plane of glass is present between them (heat conductivity of glass is 80-100 times lower than aluminium alloys [148]). In addition, the area of cooling surface is small (only the inside of the reactor) when compared to conventional heat collectors and the scalability is limited. With all the drawbacks this approach most probably will not be suitable for industrial application, especially taking into account the absence of most advantages (e.g. electrolyte is usually held constant thus cleaning and contamination are not as big of an issue).
Another requirement for the reaction chamber is high air flow above the electrolyte. As described before, electrolytic process will produce hydrogen gas on the cathode, which will eventually gather on top of the electrolyte. If the bubbles are formed, the hydrogen gas will ignite from the plasma discharges occurring close to the electrolyte surface thus causing an explosion. While harmful, the explosions can potentially cause the electrolyte reservoir cracking or other excessive mechanical stress on the glass or the sample holding device. To minimize the explosion probability a high air flow should be ensured to vent out the hydrogen and prevent bubbling. For this purpose, an attachment was developed and manufactured with electric ventilators blowing air to the electrolyte surface and appropriately sized venting holes for effective removal. The 3D render of the venting device and electrolyte reservoir is shown in fig. 3.2.

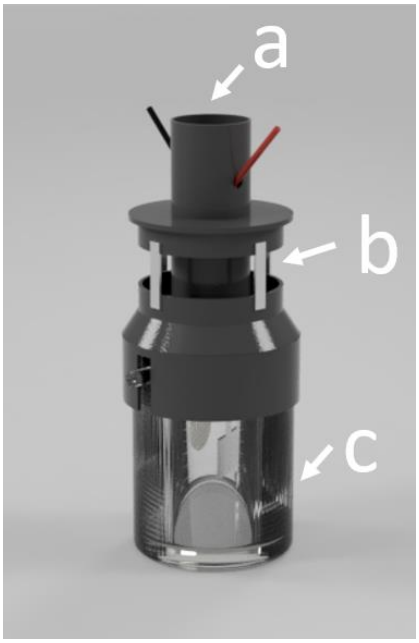

Fig. 3.2. 3d model of reactor chamber with a cooling head attached. a – air fan inside tube, b – outlets of gas, c – double-walled electrolyte reservoir

3.1.2 Power supply

A custom power supply unit (PSU) for PEO was developed and provided by "ElGoo Tech SIA". The total output power of PEO PSU is 10kW – max current of 10A and voltage of 1000V can be achieved. An important property of the PSU is the ability to precisely control electrical parameters in various regimes (unipolar, bipolar, pulsed) with currant and voltage limits in place. The precise modulation of high power square pulses allows pulse durations as small as 1μs. The PSU is fully automated through MODBUS communication protocol – if programmed correctly, no human intervention is needed throughout the whole process. The PC control also allows linear parameter change throughout the process enabling in-depth research of discharge characteristics. Full readout of applied voltage and current data is ensured. In addition, a regular manual control through front panel is also possible.

3.1.3 Software

For most industrial applications, a steady, purpose-built power supply is sufficient for production of PEO coatings. Similar to anodization, PEO production lines are tailored for a specific substrate material and electrolyte, therefore only minimal adjustments are necessary on the power supply. Reducing the number of variable parameters leaving only the surface area of different parts ensures constant quality of the coating. However, this is not the case for the

scientific research, where not only flexibility of the hardware is crucial, but also the correct control and readout of various parameters is necessary for successful analysis of the process and making the correct adjustments. Custom-built power supply described previously offers complete off-panel control through the RS232 port using standard MODBUS protocol, therefore a PC software was developed.

General tasks for the software package are:

1) Automated control of the parameter setpoints
2) Readout of the parameters
3) Data storage and visualization
4) User interface

A graphical programming environment National Instruments “Labview” was used to create the software. The environment is widely used for industrial applications, automation of large arrays of devices and laboratory setups. Offering powerful tools for data analysis, visualization, user interface, device input/output and memory management, Labview is suitable for automation of PEO power supply.

The software is divided in 3 major modules. First one is a process creator tool - an application that can be used to create rows of setpoints - desired values for the power supply to reach. By design, power supply is voltage or current limited based on what is achieved first, therefore the user is able to define only setpoint parameters and real output values may differ. Every variable parameter (including time constants) can be defined by selecting points in time for the value to reach (e.g. 400V at t=0s; 500V at t=600s and so on) and the software will calculate interim values for linear change between points automatically. Other than linear change algorithms can be implemented in the future if necessary. The process creator tool will then evaluate the user input to prevent various mistakes (non-increasing time, values outside limits, wrong value format etc.) and save the process in a separate, human-readable .txt file that can be later loaded to the main program for execution. This approach accelerates workflow for operators (there is no need to input hundreds of parameters to repeat the coating cycle) as well as removes all human factors from the setup.

Second, and most important module is a main program - consisting of data communication with the power supply itself, algorithms to change the variable parameters by the predefined routes (setpoint file from the process creator tool) and user interface for on-line monitoring of setpoints and real values. The window for process file loading contains a visualization graph for easy evaluation and prevention of wrong file loading. Main operation window contains 4 graphs - current and voltage for both polarities, as well as buttons for setting the parameters manually,

launching/stopping the power supply, running the process and a window for adding a comment during the process to save it in the log file. The software is also configured to save data in convenient format - all graphs, parameters, log file, errors (if any) will be stored in a pre-defined folder in human-readable .txt files and marked in a measurement table. This allows straightforward reference of measurements from any point in time and long-term troubleshooting capabilities. Safety features are also implemented in the software - notifications, warnings and alerts are still in place.

Third module is used for organized storage and management of recorded measurement data. This is done in the form of a table with timestamps, as well as path to the measurement files.

3.2 Characterisation

3.2.1 Structure and morphology

Throughout the studies, various setups were used for evaluation of crystalline structure, analysis of elements in the coatings as well as morphology and coating thickness.

X-ray diffraction (XRD) was measured using two setups: a table-top device Rigaku MiniFlex 600 and more advanced device PANalytical X'Pert Pro diffractometer with Cu Kα radiation (1.5418 Å).

SEM top-view and cross-section images were taken using either table-top SEM Phenom Pro or a Tescan Lyra SEM equipped with energy dispersive X-ray spectrometer (EDX) operated at 15 kV for element mapping.

Transmission electron microscopy (TEM) measurements in Al_2O_3:C and strontium aluminate coatings were done on Tecnai G2 F20, FEI operated at 200 kV. The samples for TEM studies were scratched from coating using diamond pen and placed on a lacy carbon coated grid AGS166-4 (Agar Scientific).

Although most PEO studies use the wide range of mechanical and chemical testing equipment to evaluate the performance of the coating from a structural stand point, the studies in this work disregarded those measurements as the focus was set on enhancing the luminescence properties. However, the assumption of good mechanical durability can be made from the large thickness of the coatings and the harder crystalline phases of alumina present in some coatings.

Reader is advised to refer to the publications associated with "Results" chapters to get the full list of characterisation devices used in a particular study.

3.2.2 Luminescence

For luminescence measurements, two setups were used: Andor Shamrock SR-303i spectrometer coupled with Andor iDus401 charge coupled device (CCD) was used for the acquisition of photoluminescence spectra, TSL studies and XRL. Additionally, Horiba iHR320 imaging spectrometer coupled with SampleMax sample chamber and Jobin Yvon/Horiba TRIAX320 excitation monochromator was used for photoluminescence and luminescence decay kinetics. This spectrometer is coupled with photomultiplier tube (PMT) and CCD. A list of parameters is provided below:

Andor Shamrock SR-303i: spectrometer: Czerny-Turner arrangement with imaging toroidal optics; focal length of 303mm, aperture f/4; wavelength resolution 0.1nm (<0.2nm with 25μm pixel CCD detector), wavelength reproducibility ± 0.05nm, wavelength accuracy ± 0.2nm. Gratings are mounted on interchangeable triple grating turret equipped with following gratings: 150 lines/mm, 600 lines/mm and 1200 lines/mm

Andor iDus401 (DU401A-BV) CCD: active pixels 1024x128, pixel size 26x26μm, air cooling up to -55°C, max. 81 spectra per second.

Horiba iHR320: imaging spectrometer: Czerny-Turner arrangement, 320mm focal length, aperture f/4.1. Spectral range 150 to 1500nm with 1200 l/mm grating, triple grating turret. Spectral resolution of 0.06nm, wavelength accuracy ±0.20nm, repeatability ± 0.075nm, spectral dispersion 2.35 nm/mm, scan speed 159 nm/sec, step size 0.002nm. Three different gratings are available: 1200 grooves/mm, 950 grooves/mm and 150 grooves/mm.

Jobin Yvon/Horiba TRIAX320: single grating excitation monochromator. Three different gratings are availabe: 1800 grooves/mm, 1200 grooves/mm, 600 grooves/mm.

For luminescence measurements, different excitation sources were used: YAG:Nd laser (266nm, 532nm), conventional Deuterium and Xenon lamps as well as X-ray source which is directly connected to sample chamber in the Andor setup.

Spectra measured with CCD in PL, XRL and TSL were not corrected to accommodate differences in detection at different wavelengths as only the comparison study was performed. For a precise specification of hardware used for luminescence measurement please refer to the corresponding papers of research presented in this work.

Reader is advised to refer to the publications associated with “Results” chapters to get the full list of luminescence devices used in a particular study.

3.2.3 Thermostimulated luminescence

The first recorded observations of TSL phenomena were in 17th century; however, only in 20th century the measurement technique was systematically studied immediately forming two main use cases – ionization radiation dosimetry and archeological dating of minerals. Both directions require comprehensive understanding of underlying mechanisms for TSL and efforts of many scientific groups led to the development of related measurement technique – OSL. While TSL based archeological dating is a complimentary technique in a vast field of archeology, ever growing demand for good quality radiation control devices boosted the transition of TL dosimeters from the laboratories to the practical application.

From experimental point of view, TSL is a luminescence of a pre-irradiated sample caused by the increase of temperature. A graphical representation of TSL setup is shown in fig. 3.3 A with the according graphs in fig. 3.3 B.

Here, a picture – left side is a basic main element scheme of TSL setup, right – T(t), I(t), N(t) graphs

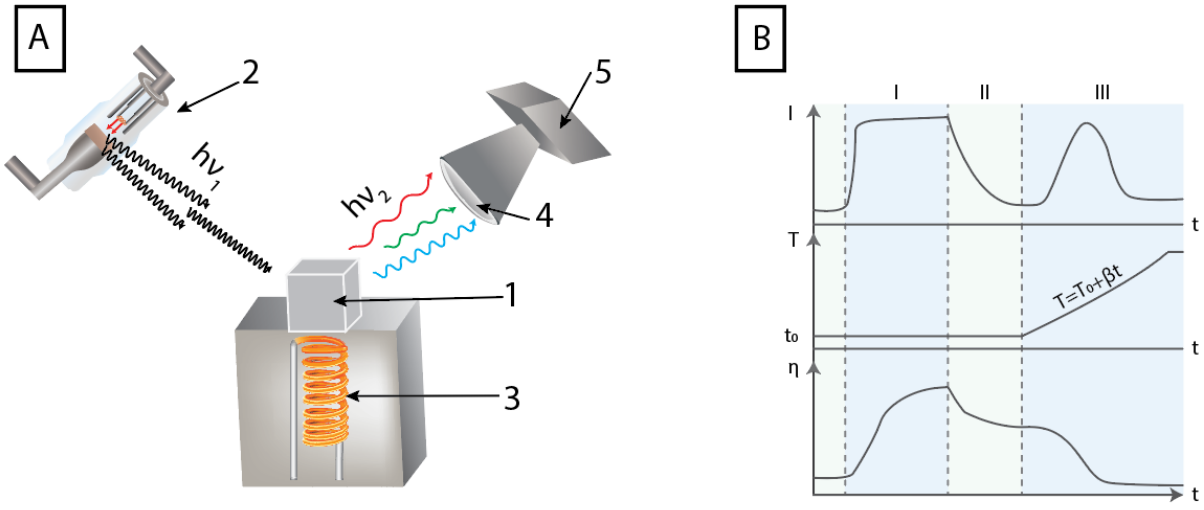

Fig 3.3 A - schematic of a simplest TSL setup, 1 – sample, 2 – ionizing radiation source, 3 – heater element, 4 – lens system/monochromator, 5 – detector; B – light intensity, temperature and number of excited electrons during the TSL measurement – I – excitation stage, II – afterglow stage, III – TSL readout stage

The solution of Schrodinger equation for electrons in a periodic potential (e.g. in a non-conductive crystal) shows the separation of "allowed" energy states dividing the energy band graph to valence, conduction and forbidden band. At absolute zero temperature in a non-metallic crystal all the electrons are located in a valence zone, with the possibility to be

"excited" to the conduction band to form the conductivity of the crystal. The minimal energy required for the electron to reach lowest level in a conduction band from the highest level of the valence band is called band gap. Although electrons are bound to the atoms in the lattice, once electron in moved to the conduction band it can move freely in the crystal. When excited, electron leaves a "hole" in a valence band (positively charged atom) and since there is a non-zero possibility for electron from a nearby atom to "jump" to the positively charged atom, the "hole" in valence band is mobile and can contribute to the conductivity of the crystal. However, perfect crystals are nonexistent in a real world and some number of defects (intrinsic or impurity) will always be present. Study of various defects in a crystal structure is one of the main points of interest of a wide field of solid state physics and is crucial in almost any research of optical properties of materials. Several well-defined defect types can be outlined:

Point defects – vacancy (missing lattice atom), interstitial defects (host lattice atom in a wrong lattice spot), impurity defects (foreign atoms in-between the host lattice atoms). Frenkel defects (one atom - usually a cation in ionic crystal - shifted from the position creating a vacancy), Schottky defects (two nearby oppositely charged ions leaving their location creating vacancies) and others.

Line and plane defects – dislocations (shift of a crystalline plane due to insertion of a half-plane), grain boundaries (meeting point of two crystalline grains), stacking faults (shift of a crystal structure by a fraction of lattice constant), twin boundaries (mirror symmetry plane) and others.

Other important defect is the **surface** of a crystal – a disordered lattice structure often in contact with the atmosphere. This defect is especially important in studies of nanoparticles, as surface to body ratio is orders of magnitude higher than that of macroscopic materials.

To explain the TSL process from a theoretical standpoint a simplified "one trap one center" (1T1C) model is used, sometimes also called OTOR for "One Trap One Recombination center" or GOT – "General One Trap" approach. The basis for the model is a highly ordered crystalline lattice of atoms with one type of defects creating a "trapping state" for the electron with the corresponding "recombination center". The schematic representation of the band structure in shown in fig. 3.4. A with the corresponding electron paths marked.

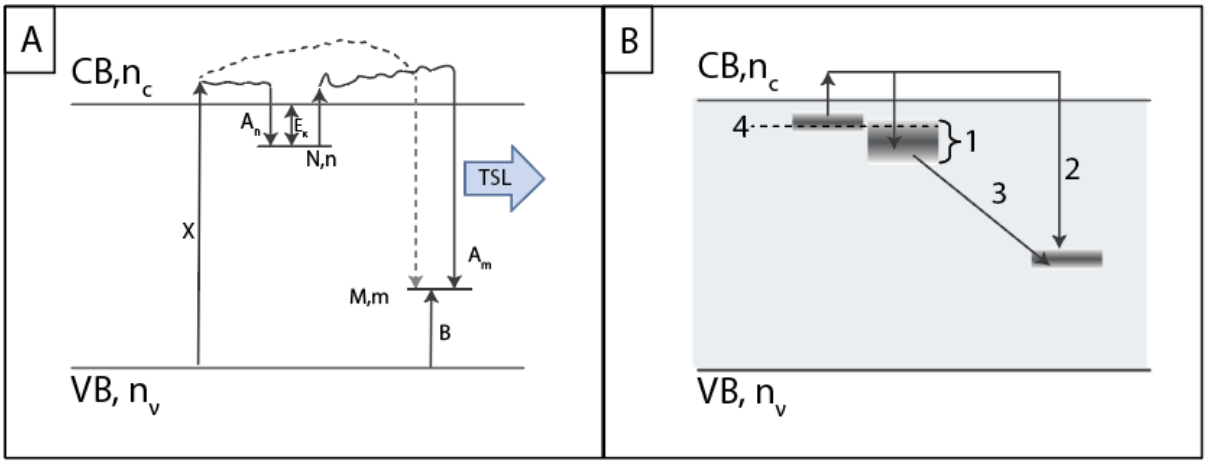

Fig 3.4. A – schematic representation of band structure for a simple OTOR model; B – more complex system with 1 – distribution of energies for a single trap, 2 – irradiative recombination from both traps, 3 – tunneling processes, 4 – overlapping of trap energies.

A set of differential equations was developed to describe the change in concentration of electrons or holes in each of the possible states: n – amount of trapped electrons in traps per volume unit, m – amount of trapped holes per volume unit, n_c (amount of free electrons in a conduction band) and n_υ (amount of free holes in a valence band). During the irradiation, the equations are as follows:

$$\frac{dn}{dt} = A_n(N-n)n_c - s * n * \exp\left(-\frac{E}{kT}\right) \quad (2)$$

$$\frac{dm}{dt} = B(M-m)n_v - A_m m n_c \quad (3)$$

$$\frac{dn_c}{dt} = X - A_n(N-n)n_c - A_m m n_c \quad (4)$$

$$\frac{dn_v}{dt} = \frac{dn}{dt} + \frac{dn_c}{dt} - \frac{dm}{dt} \quad (5)$$

The first equation (2) describes the increase of trapped electrons in time, with two concurring parts: first term of the right hand side $A_n(N-n)n_c$ describes the trapping probability A_n (cm^3cm^{-1}) multiplied by the amount of free traps $N-n$ (where N is the total amount of traps) and total electron count in conduction band n_c. The second term is the temperature dependent rate of excitation of electrons in the traps, thus the term *s*n*exp(-E/kT)* is used, where s (s^{-1}) is a frequency factor, E (eV) is the activation energy of the trap (marked as E_k in fig. 3.4 A), k (eV

K^{-1}) is the Boltzmann constant and T is the temperature. This term will be crucial during the release of electrons during the heating cycle and will be described later.

Second equation (3) shows the development of the amount of holes in a material with, again, two concurring processes – $B(M-m)n_v$ describing the rate of hole trapping from the valence band where B (cm^3 s^{-1}) is a trapping probability of holes and M(cm^{-3}) is a concentration of recombination centres and $A_m m n_c$ describing the rate of electron recombination with holes, where A_m (cm^3 s^{-1}) is a recombination probability of electrons in a conduction band.

Third equation (4) shows the progression of the amount of electrons in the conduction band and consists of three main components: X (cm^3 s^{-1}) – rate at which the electrons are excited to the condiuction band (the intensity of ionizing radiation applied to the material); $A_n(N-n)n_c$ – rate at which electrons "fall" into the traps (same as the one in the first equation) and $A_m m n_c$ – rate at which electrons recombine with holes.

And final equation (5) describing the rate of change of electrons in a valence band ties all three states together, specifying that the valence band is the only source of electrons in the system and assuming that no electrons are lost in the process.

The set of four differential equations provide general description of processes occurring under ionizing irradiation in the simple material with one type of electron traps and one type of recombination center. However, TSL technique does not examine the system under constant flow of photons that excite electrons from valence band (VC) to the conduction band (CB), but rather describes the processes occurring upon heating of the sample without other external energy sources. As mentioned previously, sample at the start of the TSL measurement is already excited – some amount of traps is filled with electrons (n>>0), the irradiation is not present (X=0), all electrons in conduction band recombined or relaxed into traps (n_c=0), all holes in the valence band are filled (n_v=0) and thermal release of electrons from traps is negligible ($s*n*exp(-E/kT)$=0). The last factor is what can be manipulated externally – the electron release rate from the traps by increasing temperature. Usually, a linear temperature profile is used $T=T_0+\beta t$ ensuring a gradual increase of $s*n*exp(-E/kT)$; however, some researchers report the use of non-linear heating profiles.

The set of differential equations contains undefined probability values, therefore further simplifications of the process are needed. An important assumption was proposed by Halperin and Braner [149] stating that the amount of electrons in the conduction band during the heating is much less than the amount present in traps (which is true for experimentally possible heating rates) and the amount of free electrons in the conduction band does not change as quickly as does the amount of electrons in the traps. Another assumption that can be made is that retrapping

(trapping of thermally released electrons) probability during TSL is essentially zero (A_n=0). The basis for this assumption is twofold: firstly, the amount of electrons in the conduction band during TSL is much lower than during irradiation as it is limited by the amount of trapped electrons present in the system and not the flux of electrons from VB thus lowering the number of interaction between free electron in CB with unoccupied trap. Secondly, even in the retrapping scenario the electron will immediately be released back to the conduction band as *E/kT* energy is sufficient. Moreover, as OTOR model explains the processes with one type of trapping centers and one type of recombination centers, an assumption can be made that the amount of electrons in traps is equal to the amount of holes (n=m)

The TSL measurement is an optical measurement approach, therefore the intensity of acquired signal during TSL is the value interest. The intensity of the TSL signal during heating at a specific temperature *I(T)* will be proportional to the speed (first derivative) of recombination of electrons or inversely proportional to the amount of excited electrons in traps -*dn/dt*. Taking into the account all assumptions, a simplified equation for the intensity of TSL signal can be written as follows:

$$I = -\frac{dn}{dt} = s * n * \exp\left(-\frac{E}{kT}\right) \quad (6)$$

This equation (6) describes a first order process (single type of traps); however, majority of real world systems contain a range of traps at different activation energies. The OTOR model then can be expanded to simulate the intensity curve of a more complex, second or general order process. The explanation of the formulae and all aspects required for deriving the intensity of general order process is beyond the scope of this work. The end result is similar to the first order process, but with addition of b – the order of kinetics and s' – a value with the units of ($cm^{3(b-1)}\ s^{-1}$):

$$I = -\frac{dn}{dt} = s' n^b \exp\left(-\frac{E}{kT}\right) \quad (7)$$

From all models it is evident that the two most important parameters of traps in materials are the frequency factor *s* and activation energy *E*. The determination of these parameters is of great interest as it will give the direct insight on the lattice distortions caused by defects in crystals. In addition, trapped electron interaction with other defects in a crystal will widen the range of possible activation energies for each trap thus widening the TSL maximum causing overlapping and increasing complexity of analysis. Complex systems exhibit overlapping peaks of different intensities and full widths at half maximum (FWHM). The knowledge of activation energies of overlapping traps will help distinguish peaks and correctly build theories of electron paths in a

structure. A valuable feedback for the synthesis of the samples can then be provided to alter the properties in a desired way. Two main directions of activation energy research are present – TSL peak shape analysis and experimental techniques such as initial rise methods. Former method relies on the iterative fitting of obtained TSL glow curves to find best combination of theoretical peaks, sum of which will match the signal the best. The latter group relies on the correct realization of some heating algorithm thus partially releasing electrons from the trap and analyzing the rate of release through luminescence measurements. Simple mathematical operations can then be performed to derive activation energy value and frequency factor.

In this work, a previously described luminescence setup was used for TSL measurements with the heater attachment. TSL heating is achieved by using custom made heating device (with different heating rates available) which is connected to computer. A full-spectrum registration is implemented using CCD camera – this allows analysis of the luminescence spectral distribution dependence of the temperature in a single measurement.

4 Results and discussion

The results of this work are divided into three main sections. The first section comprises of the results on the exploration of different doping possibilities to obtain luminescent coatings. Two separate studies are presented – one focusing on doping from the metal itself and the other describes a novel pore-filling approach. The second section will contain studies of two types of radiation-sensitive alumina coatings: carbon-doped alumina close in composition to commercially available dosimeter TLD-500 and chromium doped alumina. The third section will include a research of the more complex material – strontium aluminate coating with long lasting luminescence properties produced in a one-step process. All sections will relate to the respective thesis and are accompanied by the publications.

4.1 Doping of PEO coatings

The modification of the PEO coatings by changing their chemical composition is of interest in various applications as it might affect all properties commonly associated with the PEO – high coating hardness, crystalline structure, wear resistance, chemical stability and others. With every changing parameter of the process there is a possibility to modify the coating and influence its structure and/or composition. Moreover, known mechanisms of PEO coating growth agree that formation occurs in the presence of four parts – substrate, electrolyte, previously formed oxide and plasma. First two of them are obvious candidates for the implementation of the foreign atoms – dopants – in the coating.

4.1.1 Alloying the aluminium with dopant atoms

Without a doubt, the metals present in the substrate – be it pure metal or alloy – will participate in the formation of the coating creating the metal-oxide. Therefore a very first method that was realized to produce a coating with the specific purpose of enhancing its luminescence properties was done by using alloyed metal on the surface. The study was then considered as a scientific exercise to gain additional knowledge on coating formation mechanisms and without the particular application in mind, therefore a well-known ion in alumina matrix should be chosen as a dopant. The rare-earth element europium fits well – Eu^{3+} exhibits very distinctive luminescence in red region of spectrum – sharp lines representing transitions from $^5D_0$ to ^7F levels with the most intense line observable at 613 nm (transition $^5D_0 \rightarrow {}^7F_2$) The lines are quite distinctive and the position varies only slightly with the different crystalline matrices. In

addition, it is known that the Eu atom can incorporate in alumina matrix in Eu^{2+} state exhibiting blue luminescence that can be separated from intrinsic luminescence of the alumina.

A crucial element in this study – the Eu-Alloy was obtained from American Elements (CAS#7429-90-5) containing 1wt% Eu. For a comparison, the pure Al (99.999%, NewMet) alloy was used. After polishing with 1μm diamond paste, samples with surface area of $15cm^2$ were processed under a relatively low voltage pulses +350V and -100V, both for 1ms with a process time of 10-20 minutes ("PEO" and "PEO-Eu"). In addition, a Eu-containing sample with $300V^+$ for 5ms and $100V^-$ for 1ms pulses at 180 and 90 mA/cm^2 respectively ("PEO-Eu-2") was prepared to compare the luminescence output with varying PEO parameters.

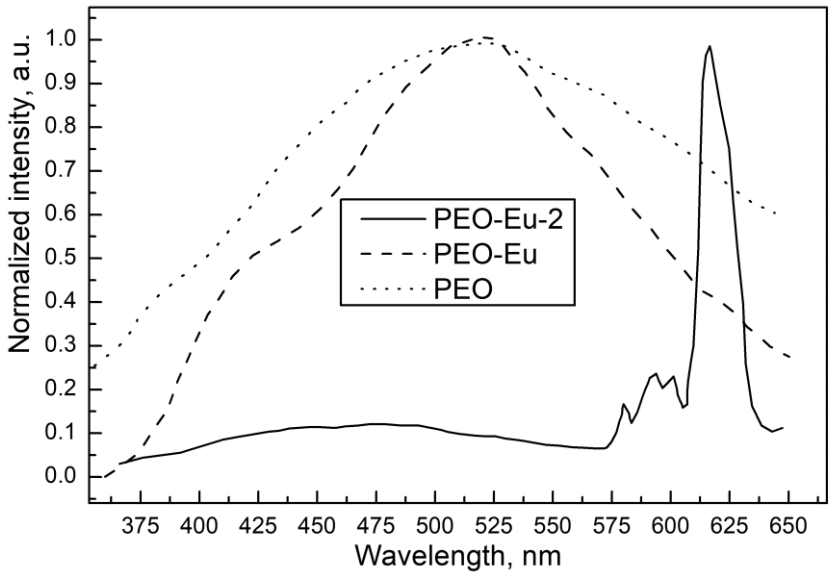

Fig. 4.1. Normalized photoluminescence spectra of PEO, PEO-Eu and PEO-Eu-2 samples.

The resulting photoluminescence spectra under 266nm laser irradiation are shown in fig. 4.1. The undoped coating (PEO) exhibits only the alumina intrinsic green luminescence band peaking at 500nm. On the other hand, doped coatings ("PEO-Eu" and "PEO-Eu-2") with two different PEO processes both have significant changes in the spectral distribution and intensity of the luminescence – sample "PEO-Eu" exhibits increased luminescence in the blue region of spectrum – a possible Eu^{2+} ion in alumina matrix. It is well-known that Eu incorporates in a divalent configuration in various aluminates [150] [151] [152]. On the other hand, coating with the greater current density ("PEO-Eu-2") exhibits luminescence in the red region of spectrum – sharp lines, although overlapping and not clearly resolved, indicate the presence of Eu^{3+} in the coating. The difference of luminescence between samples "PEO-Eu" and "PEO-Eu-2" indicate the possibility of Eu recharging in the coating, thus the presence of Eu^{2+} in the coating

should be explored in detail. First factor confirming the presence of Eu^{2+} in the "PEO-Eu" coating is the greatly increased photoluminescence intensity – the maximum intensity is approx. 50 times higher than that of sample "PEO". Second factor is the analysis of fast decay kinetics obtained from the sample (fig. 4.2) – "PEO" and "PEO-Eu" samples show drastically different decay curves. The undoped sample ("PEO") kinetic can be approximated by two exponents with decay times of 23ns and 1.3μs, while the decay kinetic of Eu-doped sample ("PEO-Eu") shows a significantly longer, complex decay curve – a typical characteristic of partially forbidden Eu electron transition.

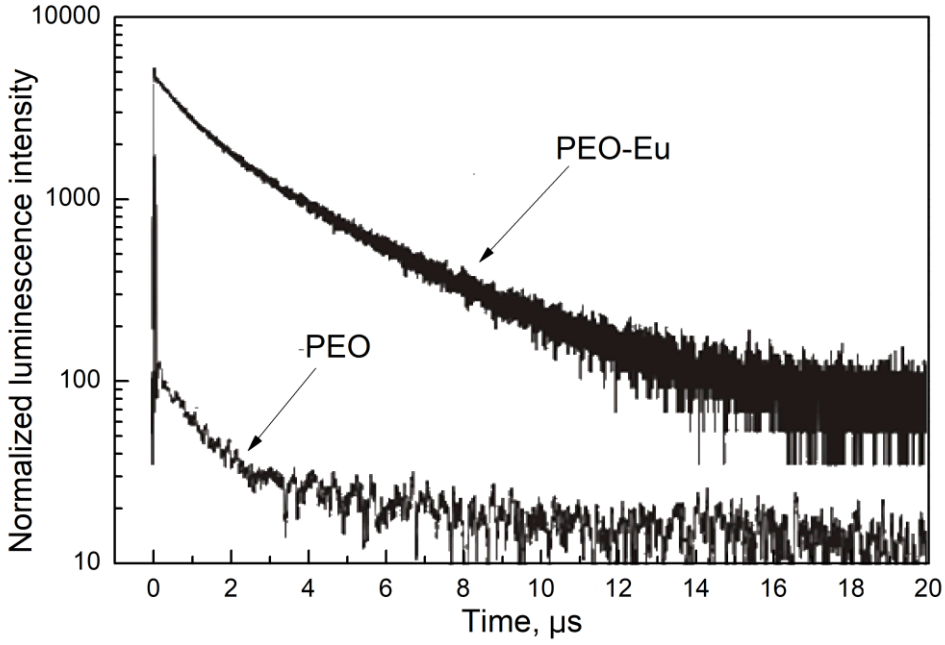

Fig 4.2 Fast decay kinetics of photoluminescence for samples PEO and PEO-Eu

This first of its kind study was performed as a proof of concept – indeed, luminescence output of PEO coatings can be altered by doping of the coating through one of the routes – use of specific alloy to bring needed atoms in the coating structure. In addition, study shows the ability to alter the luminescence of the coating by changing PEO parameters – voltage, current, pulse width and process time can all change structure of the coating thus changing the luminescence output. Complimentary, the luminescence of the doped PEO coatings can be used to better understand coating formation mechanisms and adjust theoretical approaches with the obtained information.

Although the study was performed without practical application as a main goal, it should be noted that the use of Eu containing aluminium alloy will not be commercially viable in most of the cases due to the high cost of alloy preparation. Moreover, if other dopants or concentrations

are needed in the coating for a specific application, preparation of new alloy will be necessary making research and production expensive and labor intensive. It is evident that other doping possibilities should be explored unless the luminescence of the coating is based on a dopant already present in readily-available aluminium alloys (like Cr, Mg, Mn and others often present in industrial-grade aluminium alloys).

4.1.2 Pore filling method

A range of studies indicates the benefits of the use of "slurry electrolytes" [58] – electrolytes with high concentration of insoluble micro- or nano-particles. Some studies indicate the increased growth rate of the coatings with nanoparticles acting as the reinforcement of the coating, especially when particles with high hardness are used. Some of the properties of the particles will be transferred to the coating. [55] This confirms the inclusion of solid particles in the formation process of the coating; therefore, the same principle can be used to alter the luminescence properties of the coating. However, one of the most used dopants in luminescent materials are rare earth elements (RE) – lanthanides + yttrium and scandium. Although REs are plentiful in Earth's crust, their containing compounds are often expensive due to the dispersion of RE-containing minerals requiring large amounts of ore to be processed [153]. Thus, a great care should be taken when developing a process with the commercial application in mind – excessive use of RE-containing chemicals and waste will render the technology not viable. Slurry electrolytes require large amounts of powder for a volume of the electrolyte, thus the approach is not feasible in the industrial setting. The present study is based on the two main concepts – firstly, only the particles in a near vicinity of the plasma discharge participate in the formation of the coating and can be implemented in the structure; secondly, pores of the PEO coating can be filled with some sort of material. Therefore, the aim of this study is to create highly-porous coating on the surface of the aluminium, fill pores with appropriately-sized powder of RE oxide and perform the PEO on the porous filled coating fusing the oxide in the structure. The schematic representation of the process is shown on figure 4.3. This approach could minimize the required amount of powder by placing it in the discharge channels directly rather than relying on the electrolyte to bring the powder to the coating.

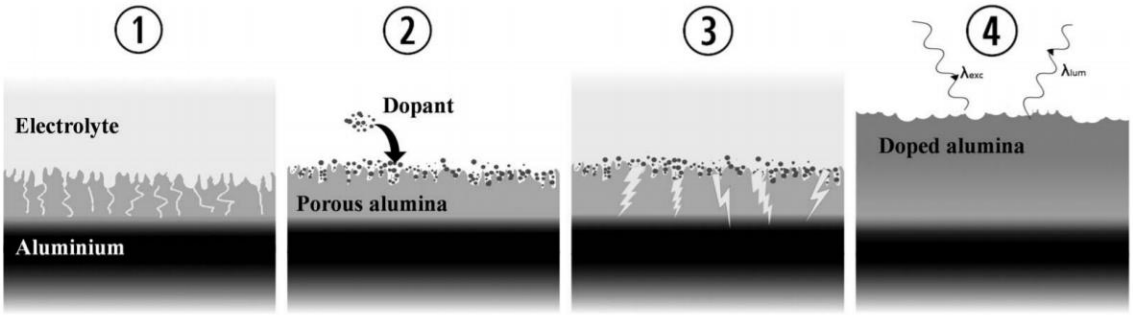

Fig.4.3 Schematic illustration of sample preparation stages: 1 – production of porous coating, 2 – filling the pores with powder, 3 – PEO processing, 4 – resulting doped oxide layer exhibiting luminescence.

First stage in achieving the goal is to find the best parameters to produce homogeneous porous structure. It is well-known that pores are naturally occurring during PEO process due to the formation of discharge channels; however, the increase of porosity of the coating still proposes a challenge that can be solved by altering power supply parameters and initial surface morphology. An iterative study on the surface of Al1050 alloy was performed to acquire the coating with large amount of differently sized pores in order of a couple of micrometers. The best example is shown in fig. 4.4 A. Important factor to note is the importance of the surface quality prior to the first PEO step - aluminum samples were polished using SiC sandpapers followed with Cr_2O_3 and diamond paste and rinsed off with acetone. This step ensured removal of the initially formed oxide on the aluminium and low surface roughness. Additionally, a special three-stage algorithm was developed for the porous coating production, with all stages performed in bipolar 10kHz regime: first stage - positive voltage held at 350V (negative pulse voltage held at 400V (or less), current unlimited) for 5 minutes; second stage - linearly increased positive voltage from 350V to 400V in 5 minutes (keeping all the other parameters same); and third stage - positive voltage held at 400V for 5 minutes (keeping all the other parameters same). Although complex, the algorithm can be easily executed and repeated using software-controlled power supply described in methods section. The coating was produced in 2 g/L KOH, 7.5 g/L Na_3PO_4 and 6 ml/L glycerin electrolyte. After the total of 15 minutes of PEO the coating was removed from the electrolyte, rinsed with deionized water and dried in air. Highly porous coating produced in this way will show weak performance in corrosion resistance and mechanical integrity and is only considered as a first step in a multi-step synthesis.

Second stage is to fill the pores with $Eu(OH)_3$ powder. The powder was prepared in a sol-gel synthesis from 10 gL^{-1} $Eu(NO_3)_3$ powder and 120gL^{-1} urea stirred in a 100ml of deionized water

for 60min at 90°C. Resulting product was filtered and dried at room temperature. To insert the $Eu(OH)_3$ powder in the pores, it was first ground in a mortar for 10 minutes with addition of ethanol to prevent the agglomeration of the particles. The resulting highly concentrated dispersion of particles in ethanol was dripped on the porous alumina coating from the first step. After drying, the excess of $Eu(OH)_3$ was removed from the surface of coating. The SEM image (fig. 4.4. B) gives an overview of the distribution of the Eu powder on the coating. One can see that the size of the powder grains is in range of 300 nm to 2 μm – mostly significantly smaller than the pores of the PEO coatings. This allows the grains to stay in the pores even after rinsing with water, during immersion in the constantly flowing electrolyte in the third stage and during the plasma discharges in the oxidation process.

Third, and final stage is a final PEO process – porous coating filled with the powder containing the desired dopant (Eu in this case) is submerged in the simple electrolyte of 1L deionized water with $2gL^{-1}$ of KOH and unipolar DC 530V voltage-limited regime is applied for the extended periods of time. Current density is set at 0.15 A/cm^2. Uniform plasma discharges are achieved on the surface of the sample, fusing the oxide with the powder in the pores and implementing the dopant atoms in the oxide structure. The visual analysis of the SEM images of the final coating with and without filling of the pores with Eu^{3+} (fig. 4.4 C and 4.4 D) shows that there is virtually no difference in morphology of the samples and Eu atom inclusion in the crystalline matrix does not affect the growth dynamics of the coating. This can also be confirmed with the assumption that any foreign atoms in the lattice in such low concentrations do not have scalable effects, especially with large amounts of intrinsic defects.

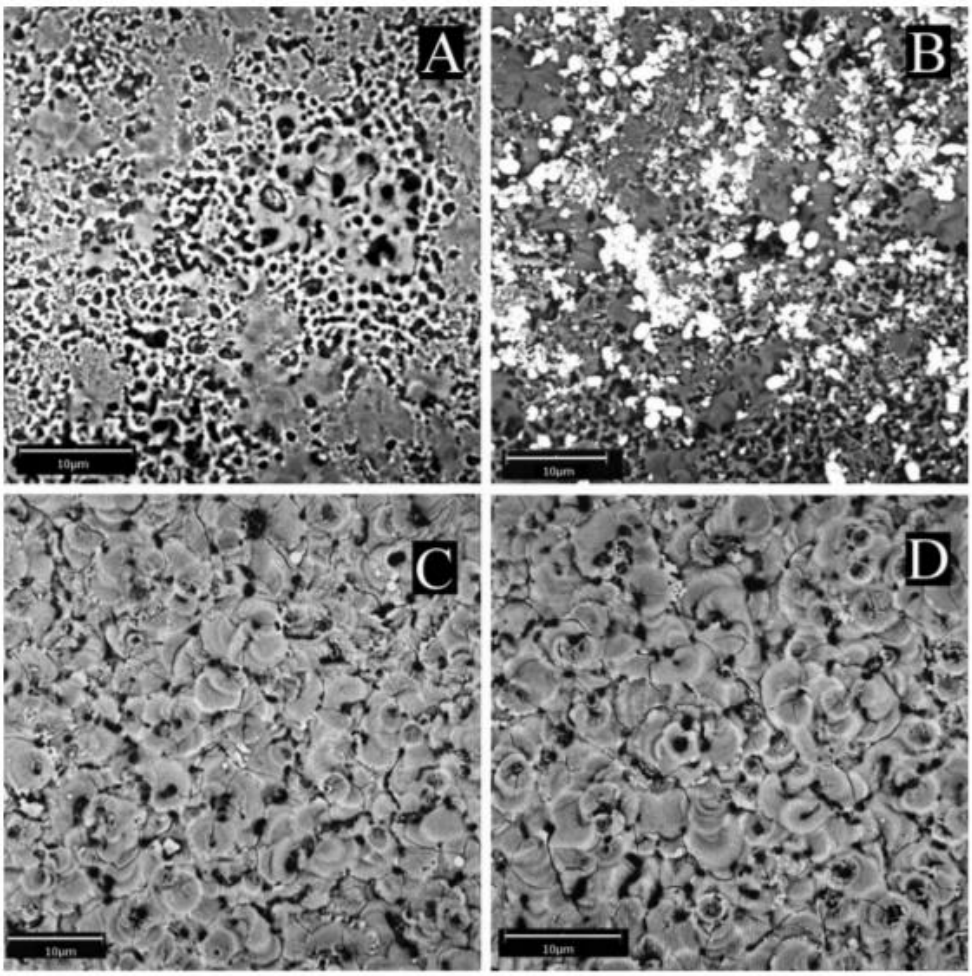

Fig. 4.4. Backscattered-Electron (BSE) top view images of each stage of the process – A – first stage porous coating, B – filled porous coating after second stage, C – PEO-processed coating after third stage and D – same process without second stage (without Eu-containing powder)

To verify and control the presence of Eu ions in the pores in stage 2, a photoluminescence measurement was used in addition to SEM. The luminescence was excited with a 266nm UV laser with the average output from all sample surface accumulated in spectra. Figure 4.5 summarizes the spectra. A distinct Eu^{3+} luminescence (red) was observed from the $Eu(OH)_3$ powder - the transitions from level $^5D_0$ to ^7F in Eu^{3+} ion. The most intense line, which is observable at 613 nm marks the transition $^5D_0 \rightarrow {}^7F_2$. A combination of broad intrinsic alumina band peaking at 450nm and Eu^{3+} bands is observable from porous alumina filled with $Eu(OH)_3$ powder, as expected.

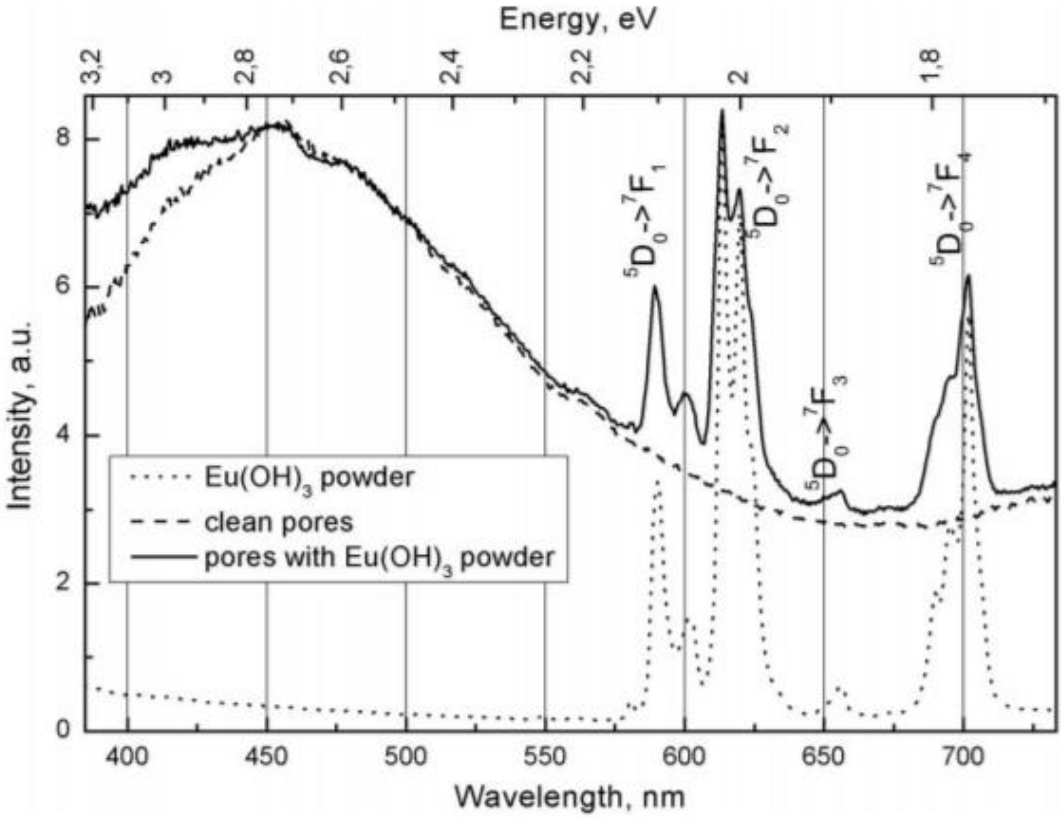

Fig. 4.5. Normalized photoluminescence spectra of $Eu(OH)_3$ powder, clean porous coating (first stage) and filled pores with $Eu(OH)_3$ powder (second stage)

The application of a high voltage (third stage) leads to the plasma electrical discharges leading to the almost immediate Eu^{3+} luminescence disappearance from the spectra. However, a new broad band of luminescence appears in the blue region. The same observation was made in [66] where it has been reported as Eu^{3+} recharging to Eu^{2+}. The recharge of the Eu could be linked to oxygen vacancies: Eu incorporates in the divalent state to compensate the charge difference. The luminescence of Eu^{2+} in blue region of spectrum was also observed in other alumina materials like translucent ceramics [154] and alkaline-earth aluminates [155] [156]. Fig. 4.6 presents a summary of the spectra obtained from the samples after the 3rd stage.

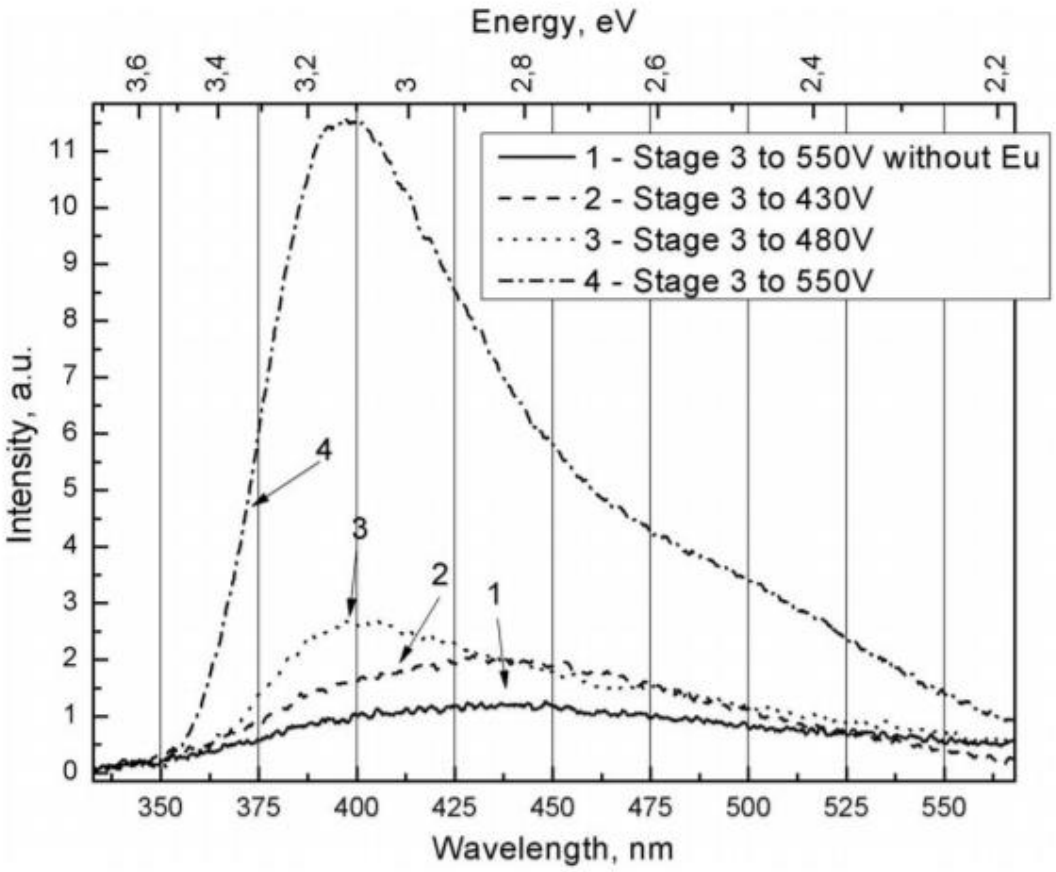

Fig. 4.6 – Luminescence of coatings after third stage with varying voltage in third stage.

Thirteen samples were prepared with varying maximum voltage in the third stage to study the effect of increased electric field on the implementation and recharging of europium. A tenfold increase in the photoluminescence intensity at 400 nm compared to the undoped alumina (pores were not filled in stage 2) was achieved for the 550V sample. The correlation between the maximum PEO voltage applied to the sample in the third stage and the increase in 400nm luminescence intensity is shown in fig. 4.7. The 400nm band occurs with the first anode sparks (450V) and saturates at 500V. An unexpected plateau is observed at 480-490V – with no other changes in the process it is assumed that the reason for this is measurement error.

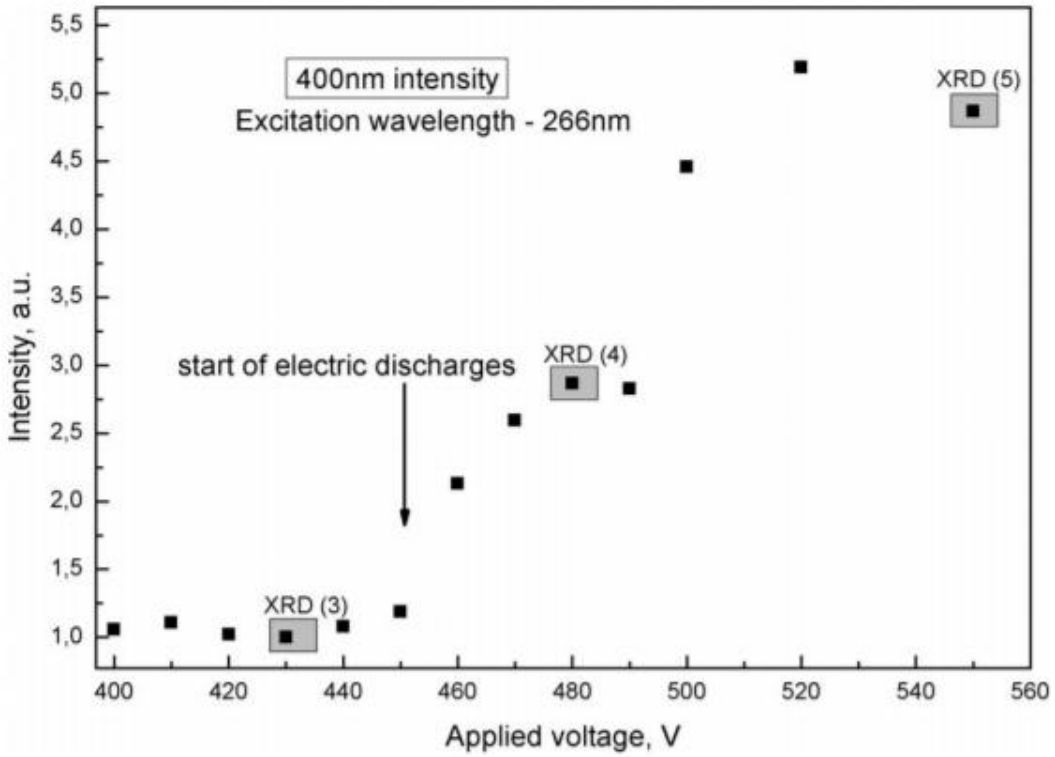

Fig. 4.7 Relation between 400nm photoluminescence intensity and applied voltage in the third stage.

To analyze coating structure throughout the Eu^{2+} line growth, XRD spectra were captured at 430, 480 and 550V. The results are shown on Figure 4.8. Main characteristics of XRD are the presence of Al metallic lines (38.5 and 44.5 deg.) as well as magnesium silicate lines (marked "b" in fig.4.8) indicating a range of intermetallic phase particles in raw material [157]. The absence of lines indicating the alumina crystalline structure indicates that the porous alumina after first stage has amorphous structure – this correlates with a range of studies indicating the need for long processing times with high voltage for production of crystalline phases. This is also evident by the appearance of η-Al_2O_3 lines [158] with processing voltage over 480V.

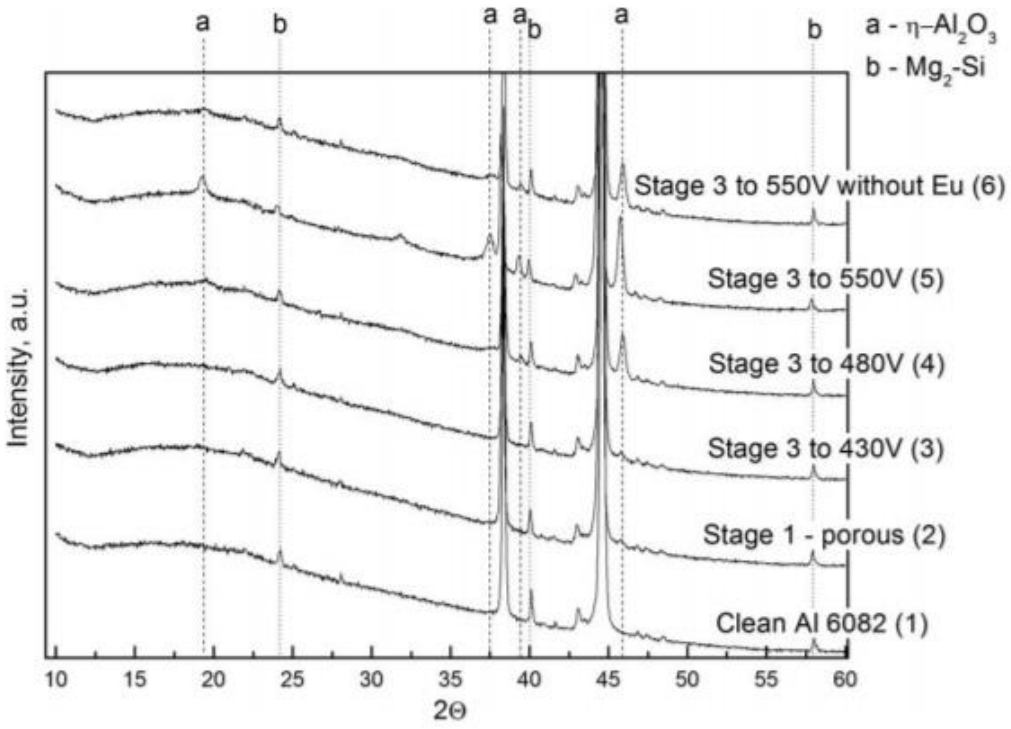

Fig. 4.8 XRD spectra of samples after third stage with varying voltage.

In conclusion, the developed pore filling method is a valid approach for doping of PEO coatings. The results clearly demonstrate the successful implementation of Eu ions in the coating structure. However, several drawbacks of the technology still persist: the high dependence on the initial surface quality – vigorous polishing is required prior to the PEO for the production of high quality pores. In addition, complex power supply is needed allowing the precise change of bipolar pulsed voltage. Powder grain size also should be controlled to meet the pore size of the coating after first stage. Most importantly, the process is performed in three separate stages, which limits the applicability of the technology in the industrial setting. All these factors and complications, however, might still be ignored due to the main advantage of the approach – minimum amount of wasted powder. Pore filling technique offers extremely efficient use of dopant-containing powder in comparison with widely used suspension or slurry electrolytes, where the concentration should be factored for the whole volume of the electrolyte. With industrial processes often using tens of liters of electrolyte per coating with frequent changes due to the degradation, the approach could offer a feasible way for better resource management.

This study enables economically-feasible way of production of modified PEO coatings even if the insoluble dopant-containing reagents have high cost. Thus, a whole range of PEO studies

that utilize costly materials (e.g. RE-containing powders or precious metals) can be scaled and transferred to production.

This chapter demonstrated experimental process for altering the luminescence properties of PEO coatings using two completely different methods. In combination with the previously known data from the literature, the following thesis is therefore drawn:

Thesis 1: The doping of alumina PEO coatings to alter their luminescence properties can be achieved in three ways: alloying the metal substrate; using three-stage pore filling process and by adding dopants to electrolyte

4.2 Dosimetric coatings

Radiation protection and monitoring will always be an important field of research, especially due to the rapidly growing use of radiation in medicine, nuclear powerplants and countless industrial applications of ionizing radiation. Big part in personal and industrial radiation protection is the use of solid-state dosimeters – devices for detection and quantification of the acquired ionizing radiation dose. Lately, interest in 2d dosimeters emerged for applications in medicine [159][160][161][162][163] motivating further research of possible materials for emerging technologies. In addition, a scaling of the already developed and widely used ceramic or crystalline dosimeters possess a challenge due to the large cost of production and lack of repeatability between the samples preventing the use of dosimeter arrays. With other drawbacks like low spatial resolution and small detection area [161], the need for unconventional production methods is needed. Since many of the already developed dosimeters are based on the metal oxides, PEO stands as a promising technology since it produces a thick coat of oxide on metal surfaces that is easily scalable and manufacturable to specs required for the particular application. This chapter will explore the two possible PEO alumina-based dosimeters: carbon-doped Al_2O_3 and chromium-doped Al_2O_3. Both dosimeters will be TSL-based. The schematic representation of the proposed technology is shown in fig. 4.9.

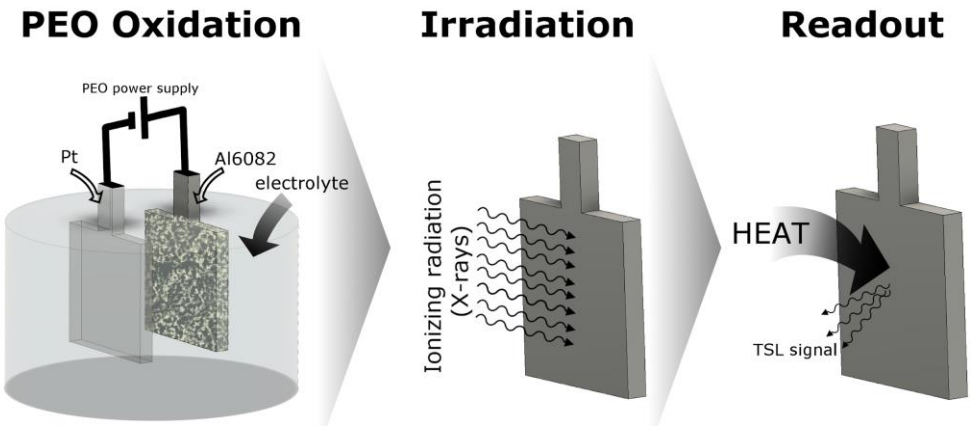

Fig. 4.9. Schematic representation of the production and use of TL-based PEO dosimeter.

Couple of factors will be kept in mind: both studies will be performed on a conventionally available aluminium alloys (Al6082 and Al1052) and will be considered as a single-step process with one electrolyte composition to fit industrial setting and make the process commercially-viable.

4.2.1 Al_2O_3:C coating

Historically, one of the main materials for PEO processing is aluminium and its alloys. Alumina coatings produced with PEO are widely used for their mechanical characteristics and chemical stability, therefore there is no lack of studies for production of tens of microns thick alumina coatings even with the alpha-phase crystalline structure for maximum hardness. Naturally, for production of PEO coating based dosimeter, an obvious idea is to mimic the already used dosimeter of similar structure. The conventional and readily available dosimeter based on Al_2O_3 is TLD-500 – carbon doped alumina. Since the first studies of the material for dosimetry [115] it was evident that Al_2O_3:C will perform well as TL dosimeter due to the intense and narrow TSL peak showing linear intensity response to the wide range of gamma-ray doses (10^{-6}Gy – 1Gy). The material is grown as a single crystal rod and cut with diamond tool for the desired shape [114]. The replication of the material using PEO possesses a row of challenges, with the major one being the source of carbon. Conventional PEO is performed in electrolyte containing KOH, on aluminium alloy surface with no intentional carbon doping, therefore carbon atoms will have to be implemented manually. A reliable source of carbon is needed – highly soluble substance, like ethanol; however, other carbon-based chemicals can be used. To keep the research as close as possible to real application, a single step synthesis is required with the same electrolyte kept throughout the process.

Al6082 aluminium alloy is used in this study. Main allying elements are Cr, Cu, Fe, Mg, Mn, Si, Ti, Zn and other metals with concentrations varying from 0.1% to 1.3%. No initial preparation of the surface was performed other than rinsing in deionized water. Simple, 3-component electrolyte was used – deionized water, 2 gL^{-1} KOH and 60ml/L ethanol. Square voltage-limited non-symmetrical 5 ms pulses were used with the voltages of +700 V and −233 V. 1 ms pauses were set in-between pulses. Current density was 0.6kA m^{-2} with minimal decline over 15 minutes of processing time. The AC regime with the 1/3 ratio of positive and negative pulses was chosen to reduce porosity [164].

The row of samples with varying concentration of ethanol and electrical parameters was made; the sample with the mentioned parameters exhibited the most intense TSL signal and therefore was analyzed further.

Firstly, the surface of the coating and thickness was evaluated using SEM (fig. 4.10). The cross-section image shows the average thickness of 20μm, top view reveals some porosity – a characteristic property of PEO coatings which sometimes can be used as an advantage [165]. Overall, the use of ethanol in the electrolyte does not seem to affect coating morphology.

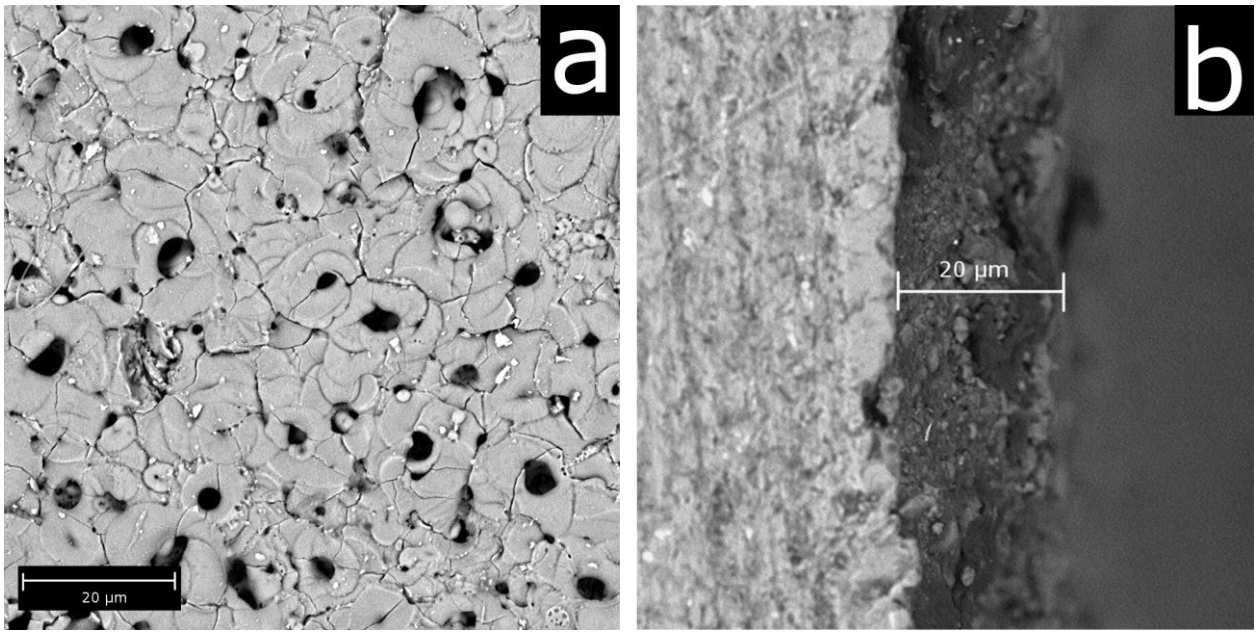

Fig 4.10. SEM images of the coating, a – top view and b – cross-section.

The TEM EDX study was performed to verify the amount of carbon in the coating. Figure 4.11 shows the analysis of two samples – carbon-doped coating (with ethanol in electrolyte as described previously) and undoped coating – same parameters except no ethanol in the electrolyte. The Kα line of the carbon at 0.277 KeV shows that the ethanol in the electrolyte does indeed result in a significant amount of carbon atoms in the coating, with the inset

demonstrating the repeat measurement of five samples. The variation in C/Al line ration is quite high – probably due to the combination of factors like inhomogeneity of carbon distribution in the coating and specifics of sample preparation for TEM measurements. Nevertheless, the increase of carbon in the coating is apparent. A signal from Cu and Mg is also observed – originating from the Cu TEM grid or from the dopants in aluminium alloy. A weak C signal is also observed in the undoped sample originating from the TEM grid.

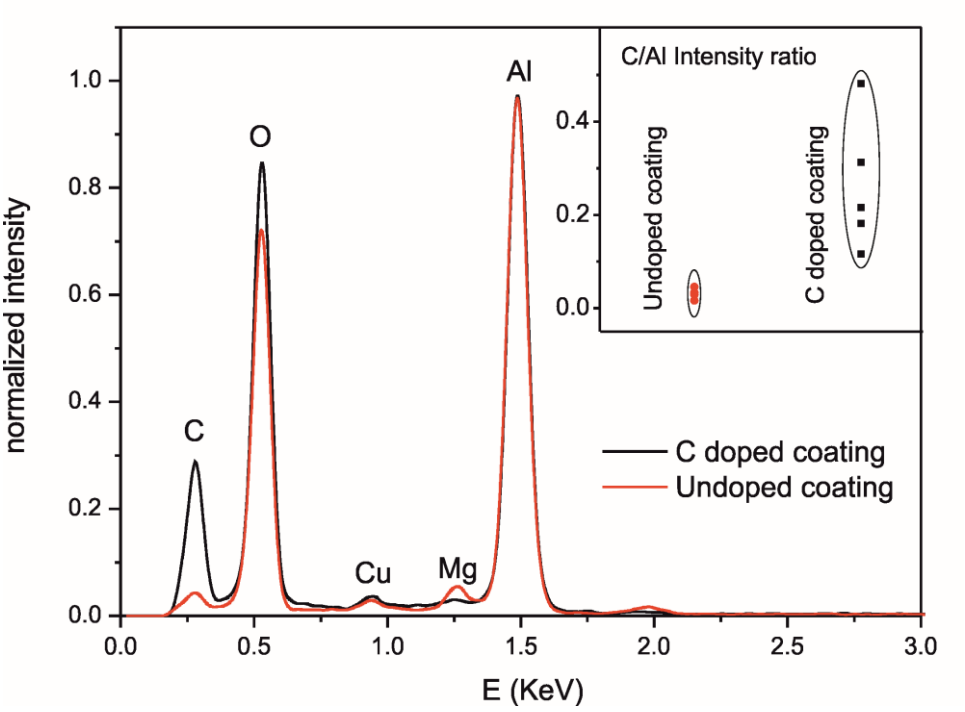

Fig. 4.11. TEM EDX measurements of two coatings – with and without ethanol in the electrolyte. Inset shows repeated measurements from 5 samples.

Next, TSL measurements were performed and compared to the signal from commercially available TLD-500 sample. The samples were irradiated with X-ray lamp with W anode operating at 30kV and 10mA. Then, sample was heated with the rate of 12K/s with simultaneous detection with PMT. The results are shown on fig. 4.12 – carbon-doped PEO coating demonstrates a wide TSL peak from 300K to 630K while TLD-500 sample maximum occupies much smaller temperature range. The signal from TLD-500 is in a good agreement with other studies of the material [166] [167] [168]. The broad TSL maximum of PEO coating indicates the wide distribution of activation energies of traps – a characteristic of disordered crystalline structure and large amount of defects in the structure.

Although the width of the maxima is much larger for PEO coating, the maximum occurs at the same temperature – this leads to believe that the same recombination centers are participating in the luminescence in both samples. To verify that, the spectral distribution of TSL as well as X-ray excited luminescence was measured for both samples and results are shown in fig. 4.13.

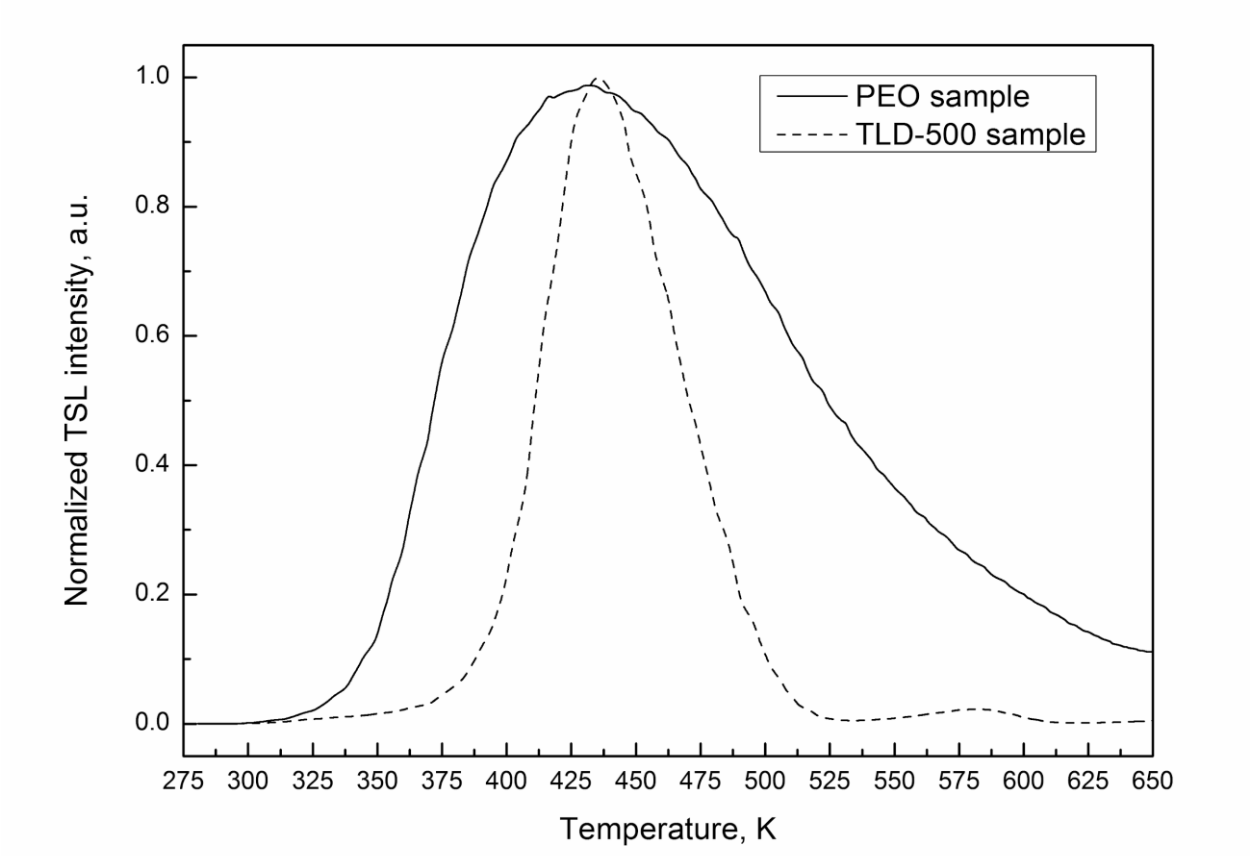

Fig. 4.12. TSL glowcurves of the obtained carbon-doped coating and TLD-500 sample.

The analysis of spectral distribution of both samples shows that main luminescence of TLD-500 sample is located at 420nm and is described as the F^+ center that is charge compensated by C^{2+} ions in trigonal crystalline lattice of alumina in α-phase [115]. Additional complex luminescence band of TLD-500 in red region of spectrum that is also present for PEO coating is described as various metal oxides present in the samples. It is well-known that Mg [169], Mn [170] and Cr [171] oxides exhibit luminescence in the red region of spectrum; however, due to the mix of the metals as traces in both samples the distinction between the each band is impossible (apart from intense Cr^{3+} R-line doublet at 693-694nm). However, main band for the TSL in PEO samples is located at 530nm. With the amount of tracing oxides that were brought from the aluminium alloy, the identification of this line is challenging. Similar luminescence band was found in alumina doped with Mg and C [172], where F_2^{2+} (2Mg) center is a result of charge compensation for the substitutional Mg^{2+} ion in Al^{3+} site.

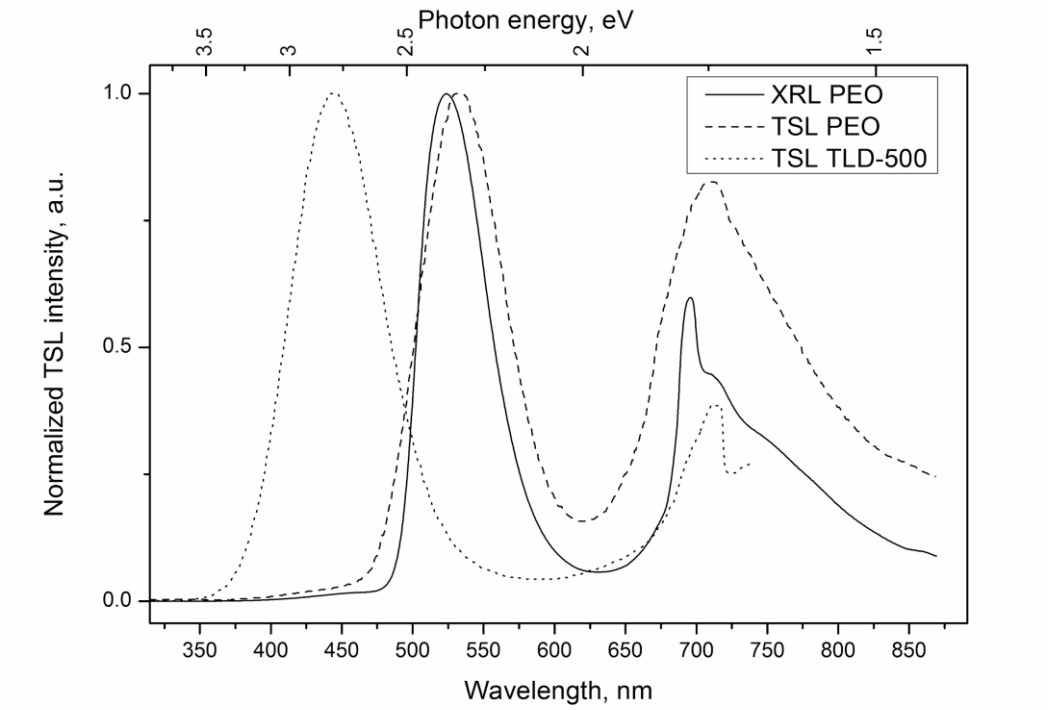

Fig. 4.13. Spectral distribution of TSL and XRL signal for carbon-doped PEO coating as well as TLD-500.

Both the TSL glowcurve and signal distribution studies indicate the irregular structure of the alumina – to verify that the XRD spectra were registered for undoped (without ethanol in the electrolyte) and doped (with ethanol in the electrolyte) coatings. The results are presented in fig. 4.14. Apart from the main aluminium peaks at 38.44, 44.69 and 65.07 deg and various intermetallic phases in 39–44° region (as well as peak at 48.7°) from the substrate, eta- or gamma- phase alumina maxima are present in the "undoped" coating. The process, however, is proven to be suitable for the production of α-Al_2O_3 [173] [174] but the processing time needs to be much longer – in order of hours. The optimization of the coating in this study led to the shorter processing times – 15 minutes only. A reason for that is probable evaporation of the ethanol from the electrolyte preventing further growth of carbon-doped alumina. Such low processing time only allows the creation of "softer" phases of alumina – as seen on the undoped XRD. However, the inclusion of ethanol in the electrolyte does alter the process in a significant manner preventing any crystalline structure to appear. Thus, amorphous alumina is created – combined with the addition of defects due dopant atoms this can explain to the broad TSL maximum.

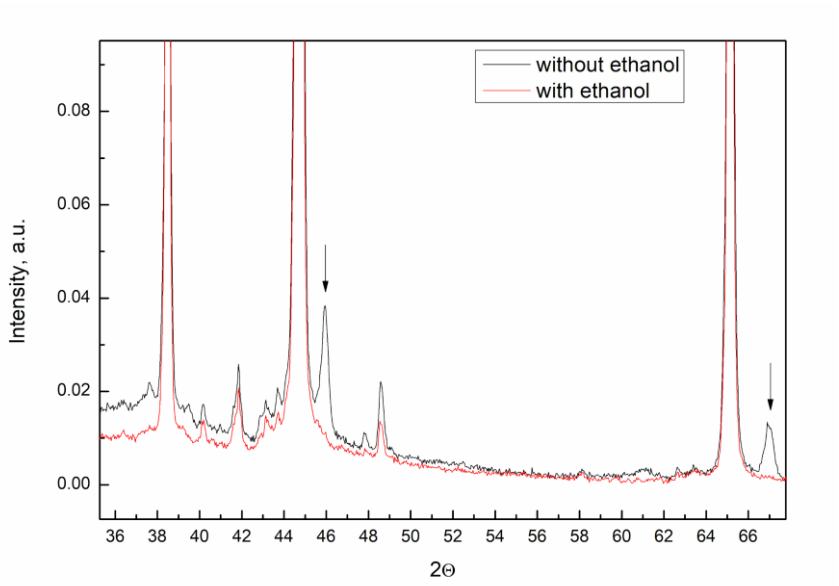

Fig. 4.14. The XRD graph of coating prepared with ethanol in the electrolyte (doped coating) and without ethanol (undoped coating). Arrows indicate the peaks for η- or γ- phase alumina.

Since one of the possible applications of dosimetric PEO coatings is the production of 2D dosimeters, the Al_2O_3:C coating should be tested for the ability to measure a spatial distribution of radiation. Four identical samples with the dimensions of 25x25x3mm were coated and combined in a 2x2 grid to form a single surface with the area of 50x50mm. The "screen" was then inserted in the path of unfocused X-ray beam, irradiated for 30 min from 10cm distance. After the irradiation, the whole grid was quickly placed on the pre-heated to 300°C conventional chemical beaker heater. A commercially available camera with complementary metal–oxide–semiconductor (CMOS) sensor and long exposure of 35s was focused on the "screen" placed on the heater. Throughout the whole heating process, the camera acquired light to form an image seen in fig. 4.15. The color image reveals couple of interesting details –

1) the distribution of X-ray irradiation can be seen well indicating poor alignment of the X-ray lamp in the housing – the circle is not uniformly illuminated.
2) the color of the image varies greatly – from dark green to bright green to red. This can lead to the conclusion that the distribution of defects and dopants is irregular on the surface – brighter and darker green spots can be observed. In addition, the larger current density and poor heat conductivity on the edges of each of four tiles forming the "screen" lead to the greater impact of "red" part of the emission – it seems that alloying atoms from the aluminium alloy better incorporate in the coating with higher current densities.

3) Repeatability of the samples in PEO process is sufficient for this application with only slight variation in overall intensity from each tile. This can be improved with thorough control of electrolyte composition and pre- and postprocessing of the tiles.

The best case scenario in this application would be to create a single tile in a single PEO process rather than combining tiles to achieve needed dimensions of the screen. Unfortunately, this was impossible in the available setup due to the limitations of maximum current provided by the power supply.

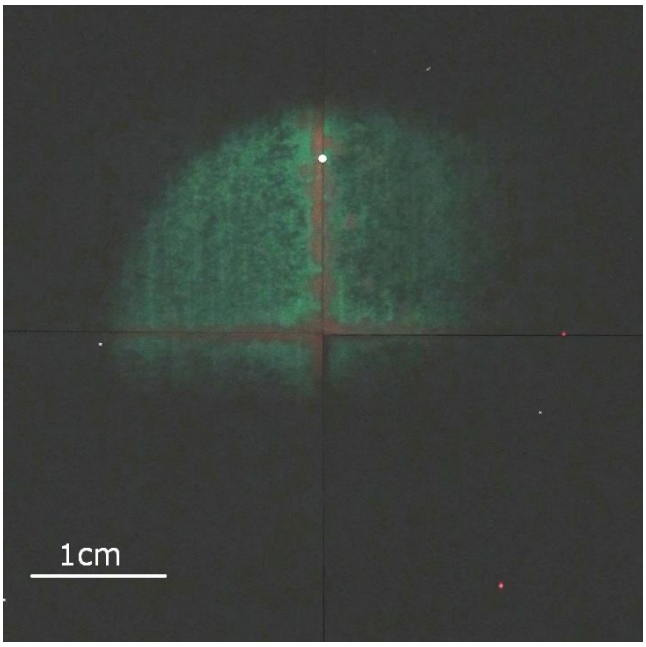

Fig. 4.15. Integrated image of PEO dosimetric "screen" placed on the hot plate heater after irradiation with X-rays.

In conclusion, this study shows a valid approach to create a PEO coating with TL sensitivity for ionizing radiation. The resulting coating exhibits a range of drawbacks preventing its use as a dosimeter at room temperatures – the large width of the TSL peak allows the trapped electrons to recombine at room temperature leading to quick fading of acquired signal. Other drawbacks include the non-uniform distribution of TSL intensity on the surface of the coating, evaporation of ethanol from electrolyte and requirement for short PEO processing times preventing the synthesis of harder, desired alumina phases. Some of the drawbacks can be addressed by the use of other carbon sources in the PEO – replacing the ethanol could not only add a more controllable way of doping of the oxide, but also extend the PEO processing time to acquire at least some crystalline structure.

4.2.2 Al_2O_3:Cr coating

The carbon doped alumina is, although most popular, not the only alumina-based material exhibiting intense TSL signal. One of such materials is chromium-doped alumina – however, previously noted by Akselrod et. al. that the use of Chromium dopant, although increasing the sensitivity, shifted the TL glowcurve maximum to 580K and 699nm – "inconvenient for reading" with the devices available in 1990. [114] Nowadays, the red region of spectrum is easily detectable by the conventional, cheap and readily available CCDs [175] thus making Al_2O_3:Cr as a viable option for dosimetry.

During our previous PEO dosimetric studies we noticed the increase of "red" luminescence from oxides with increased acidity of the electrolyte. This led us to believe that acidic electrolytes can produce coatings with increased dopant concentration in the oxide coating without any other dopant needed in the electrolyte itself or without the use of pore-filling method. As it was proven previously, if the substrate itself is alloyed with some element, the same element will easily incorporate in the structure of the coating (chapter 4.1.1.) The combination of these two observations motivated the search of a particular electrolyte that will bring alloying elements from commercial aluminium alloy (e.g. Al1052 with alloying elements of Cr, Cu, Fe, Mg, Mn, Si, Ti, Zn and other metals with concentrations of up to 0.4%) in the coating thus altering the luminescence properties.

In this study, a 2mm thick Al1052 aluminium sheet was cut into samples 25×25×2 mm^3 in size, each having the total surface area of approx. 14cm^2 (used in calculations of current density, a bit less than geometric value due to the non-constant waterline). No special treatment, apart from rinsing with water, was implemented before the PEO process.

The electrolyte for "doped" sample consisted of 3 components: deionized water, 1 g L^{-1} KOH (Stanlab) and 10 g L^{-1} citric acid (Sigma Aldrich, 99.5-100.5% based on anhydrous substance). For comparison, the second sample (marked "undoped" in this chapter) was prepared without the addition of citric acid in the electrolyte. The pH of the electrolyte before the PEO process was 3.7 and 12.2 for doped and undoped samples, respectively. The temperature of the electrolyte was maintained at 30±5°C.

DC constant voltage electrical parameters were chosen and kept constant throughout the whole process. The total process time was set to 30min. Voltage was set to 700V while current density remained mostly constant (178 mA cm^{-2}) in the first half of the process and declined in the second half to 121 mA cm^{-2}. The current density for the undoped sample (without citric acid in the electrolyte) was approx. 25 mA cm^{-2} larger throughout the whole synthesis. Pt plate was

used as a counter electrode. Although the setup uses water-cooled reactor with a substantial flow of water, evaporation of the electrolyte was still present. To compensate, a constant influx of deionized water was supplied to the reactor keeping the water level constant.

SEM measurements were performed to study the surface of the coating and compare the two samples. It is evident that the samples prepared with citric acid (a and b in fig. 4.16) have larger porosity than undoped samples, which can be attributed to the slightly larger current density during the PEO of the undoped sample. Both coatings have many features characteristic to PEO, like porosity, which sometimes can be used to an advantage [165], and cracks. Zoomed in images (b and d in fig. 4.16) show a similar ceramic-like structure with visible grain boundaries and irregular cracks formed by large temperature gradients.

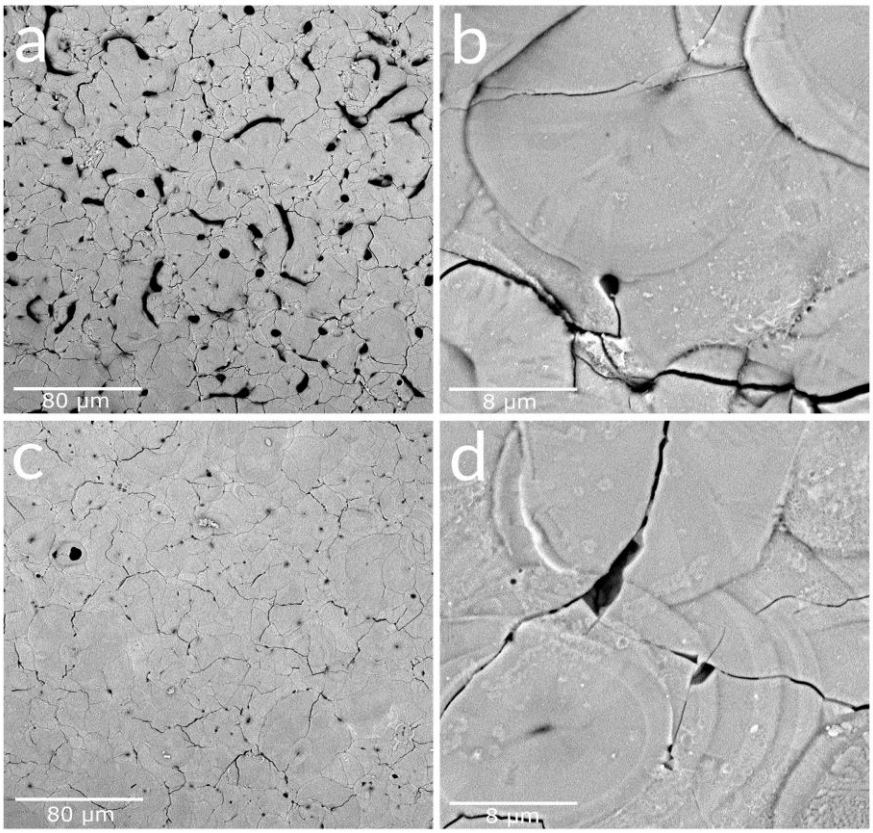

Fig. 4.16. Scanning electron microscope image of doped coating (a and b with different scales) and undoped coating (c and d with different scales)

The XRD measurements are crucial in almost any study of PEO coatings as the presence and type of crystalline structure in the coating will manifest most mechanical properties and capabilities. Figure 4.17 shows the XRD graph of doped coating with most major peaks identified and connected to different alumina phases. Two main crystalline phases were

identified – α-Al_2O_3 rhombohedral and γ-Al_2O_3 cubic [176]. One can see that the 30 min processing time is enough to produce α-Al_2O_3, which correlates well with literature [173], [174] and previous investigations. By applying phase determination and peak index fitting using Rietveld analysis in "Profex" software [177], the concentration of phases were 40.9% and 41.7% for α- and γ- phases respectively with the remainder as amorphous alumina. Although there is a close to 1:1 mixture of the hardest α- phase and a "softer" γ- phase, the coating is still expected to perform well in wear and hardness tests.

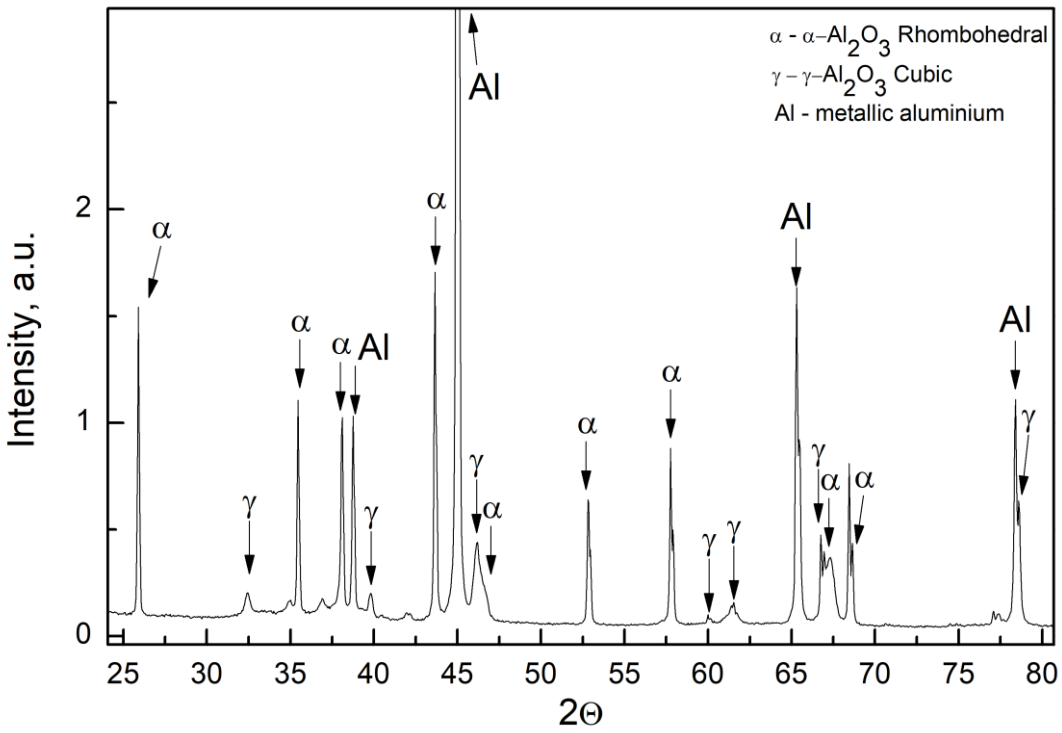

Fig. 4.17 XRD measurement of doped coating with all major peaks marked with the corresponding phase

The substrate for the coating (Al1050) is not pure, and during PEO process the coating is formed at the interface of the substrate, previously formed coating and electrolyte. Therefore, some presence of impurities from the aluminium alloy are expected in the coating too. The question remains of the effect that citric acid inclusion in the electrolyte has on the concentration of impurity metal ions in the resulting coating. To study that, XRF measurements were performed and presented in fig. 4.18. One can clearly see that although some concentrations of Cr, Mn and Fe are present in the coating even without the citric acid in the electrolyte, the addition of it increased Cr content drastically. This correlates well with the PL and TSL measurements presented later. The intensity of XRF presented in fig. 4.18 was normed to the sharp Al Kα line

at 1.486keV (not presented in the graph for scaling purposes); however, it is important to note that the detected concentrations of dopants are close to or less than 1wt%, therefore the intensities are almost at the detection limit of this setup. Despite that, one can clearly see an increased Cr content in doped sample.

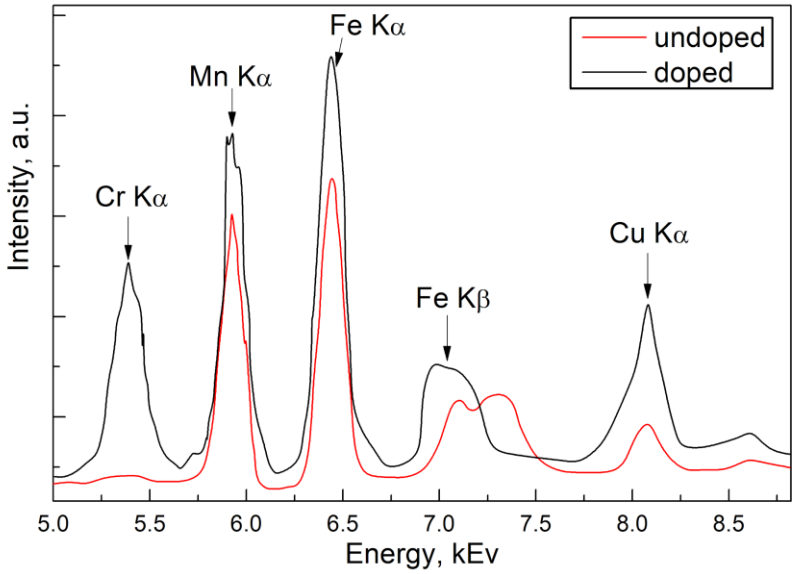

Fig. 4.18 Minor bands of XRF measurements of the undoped and doped PEO coatings.

Sample luminescence consists of three major parts – blue, green and red, representing visible light spectrum parts, as seen on fig. 4.19.

Blue luminescence (maximum at 425-450nm) appears only under UV irradiation in both samples and it relates to alumina F and F^+ (oxygen vacancies with one or two electrons) centers and are often observed in anodic aluminium oxide films. Both F^+ and F centers are present, and the maxima are overlapping thus producing a broad emission band. [178]. Slight variation in integrated intensity in this region between samples is due to the overlap of maxima (F and F^+) with different intensities as intensities of both bands are highly sensitive to the structure, internal stresses and preparation conditions of the coating. [179]–[181]

Green luminescence band with maximum at 525nm is present under both UV and X-ray irradiation and in both samples. Well-known band in amorphous and crystalline alumina is due to intrinsic defects of alumina matrix, specifically F_2 centers. The band is observed in alumina prepared by a wide range of methods. [182]–[185]

Red luminescence is a complex band consisting of two sharp peaks (679nm and 693nm) and a broad-band covering the whole red part of the spectrum. The sharp peak at 679nm is interpreted as a result of the $^2E_g \rightarrow {}^4A_{2g}$ transition in Mn^{4+} ions incorporated in alpha-alumina [186], [187].

The presence of this peak confirms the inclusion of Mn ions in crystalline lattice of the coating. The maximum is well observed under UV irradiation; however, virtually not present under X-rays irradiation. The 693nm sharp line dominates the XRL spectrum completely quenching the Mn^{4+} luminescence and is associated with widely studied and abbreviated in literature as R1 and R2 line doublet of Cr^{3+} ions in Al sites of the α-Al_2O_3 matrix. The inability to distinct R1 and R2 (692.5nm and 694nm [188]) lines is explained by the irregularities in the crystalline lattice of the coating the presence of other impurities. [188], [189] Cr^{3+} luminescence is also the only one present in TSL glow-curves (fig. 4.20).

PL measurements show additional, wide and complex red luminescence band. Based on previous observations (from XRF), it is evident that broad red luminescence originates from different metal ions (besides Mn and Cr) present in alumina structure which are obtained from the alloy itself during the growth of the coating. [183]

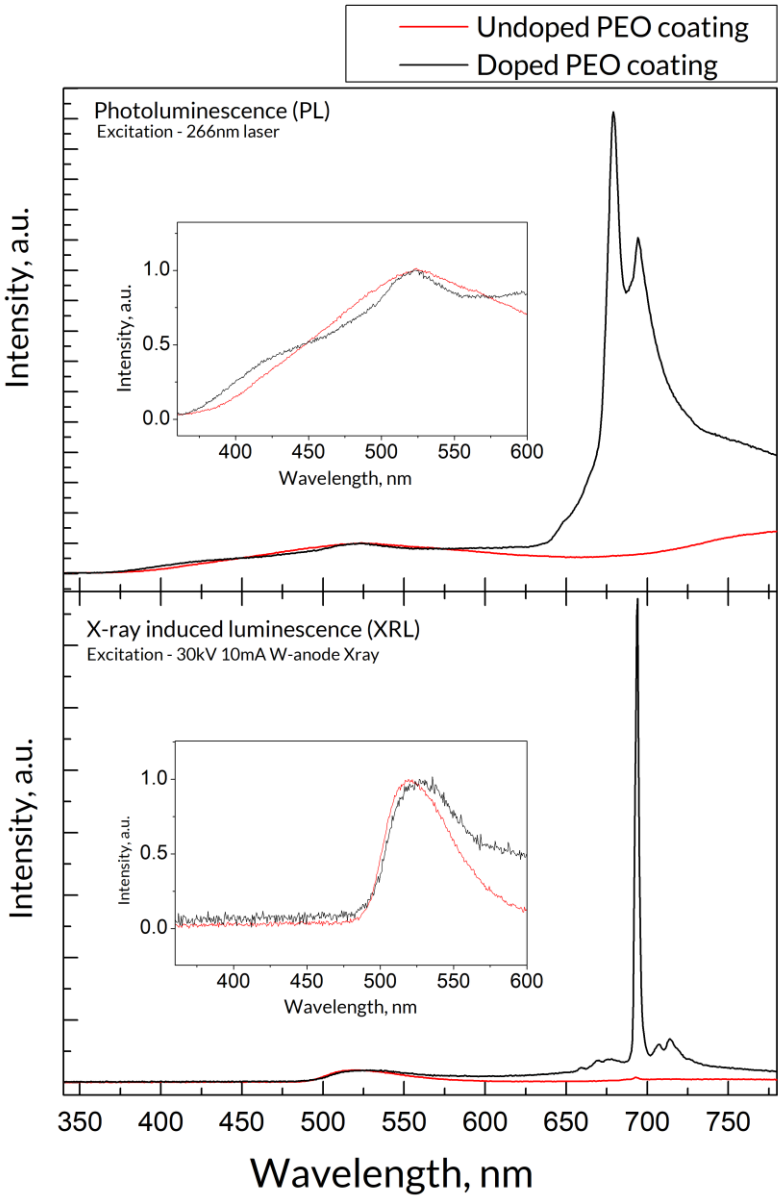

Fig. 4.19 Top half - PL spectra of undoped and Cr-doped samples, inset – intrinsic defect range 340-600nm; bottom half - XRL spectra of undoped and Cr-doped samples, inset - intrinsic defect range 340-600nm.

TSL glow curves were measured with CCD, therefore quick analysis of the full spectral distribution can be performed. The glow curve and 3d matrix is presented in fig. 4.20. Only Cr^{3+} luminescence is observed in TSL, meaning that any energy traps present in the lattice recombine exclusively on Cr atoms, which correlates well with previous observations even in other matrices. By analyzing only the 693nm line, one can observe that the Cr doped sample exhibits intense TSL signal in temperature ranges above room temperature consisting of two or more overlapping maxima. Low temperature maximum (centered at about 375K) is producing

afterglow at room temperature and its intensity relates to the delay between the "impact" ionizing radiation dose and the measurement itself. The most intense glow curve maximum (at 442K with FWHM of 60K) represents the trap center with an activation energy of approximately 1eV (estimated Randall-Wilkins equation [190]–[192]); well within the broad band-gap of the alumina. The intensity of this maximum might correlate with the acquired radiation dose, so long as the center is stable enough at room temperature. Additionally, high temperature complex maximum is observed (from 575K and up); however, the intensity is relatively low and the limitations of the measurement setup deny complete study of this part of the glow curve). It is important to note that no TSL signal above room temperature was observed for the undoped sample; therefore, all glow curve maxima are due to the increased concentration of defects (impurity ions) in the alumina matrix.

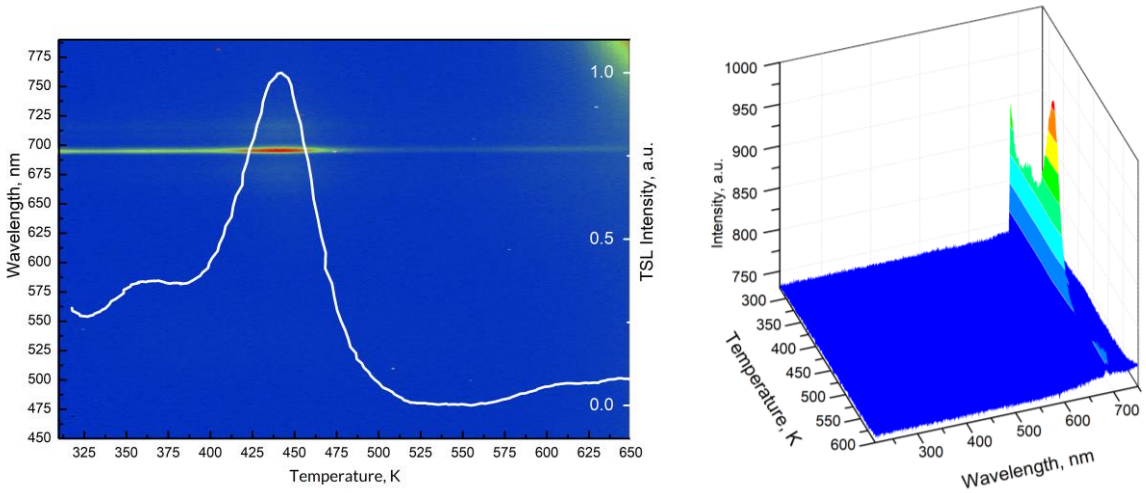

Fig. 4.20 TSL glow curve at 693nm (white line, right Y scale) overlayed on top of full measurement matrix (left Y scale). X-scale is joint between overlay and matrix. Color represents the intensity of the 2d graph (temperature to wavelength). Right – 3D surface graph of the TSL measurement.

A new approach to produce Cr^{3+} doped hard ceramic alumina coating on aluminium alloy (Al1050) surface is proposed. The coating is prepared during the PEO process with the use of a modified KOH-based electrolyte by the addition of citric acid. Obtained material exhibits outstanding luminescence properties promising for use in detection and quantification of ionizing radiation. Strong Cr^{3+} emission is observed in PL, XRL and TSL, providing basis for a range of sensor applications.

Since the proposed technique does not require an artificial dopant to be added to the electrolyte and rather uses the atoms already present in most aluminium alloys, this method is easily and inexpensively scalable and is more environmentally friendly than conventional Cr-based electrolytes.

To evaluate the coating for use as a dosimeter, additional measurements should be performed. Moreover, although the alpha phase is well present in the coating, mechanical properties should be studied if the approach is considered to be used for coating preparation with both mechanical stability and functional properties.

Both of the studies (Al_2O_3:C and Al_2O_3:Cr) present a feasible approach for production of dosimetric coatings on various parts. As an example, a mobile phone case can be covered in such coating providing excellent protection of the device from the environment while simultaneously providing the ability to read the acquired ionizing radiation dose if necessary, thus removing the burden of carrying personal dosimeters.

The research presented in last two chapters is a basis for the thesis 2:

Thesis 2: The PEO process is applicable for the doping of alumina coating with carbon or chromium atoms thus making the material promising for applications in detection of ionizing radiation.

4.3 Phosphorescent coatings

The persistent luminescence mechanism is close to dosimetry – the acquisition of energy with subsequent release of it in a form of light by gradual recombination of excited electrons. However, while materials used in dosimetry should not release any of the stored energy while at operating temperature (room temperature), the persistent luminophores should. TSL maximum of such materials, therefore, should be close to room temperature. As described previously, one of the materials often used for “glow in the dark” devices is rare-earth doped SrAl – a $SrAl_2O_4$:Eu^{2+}, Dy^{3+} structure that, when prepared correctly, can exhibit long afterglow (> 10 h [193]–[196]) and high quantum efficiency [197]–[199], good thermal and chemical stability [200], [201], environmental friendliness and no signs of toxicity [201]–[203]. However, the production of SrAl is complicated, and if the intended use of material is to create any type of surface for illumination or signage [199], [204] [201], [205], the material then should be prepared in powder form and mixed with lacquers or paints. This action creates a row of complications both in material performance (powder will not perform as well in any medium

for coating) and manufacturing (additional production step is required). PEO might be the answer for that – it is used for production of alumina on flat metal surfaces and the oxide can be doped using various methods. The idea therefore is to develop a process for the creation of rare-earth doped SrAl using single step PEO process.

The method of doping from suspension electrolyte was chosen, and the appropriate electrolyte should be prepared: strontium carbonate ($SrCO_3$, 6 gL^{-1}), europium oxide (Eu_2O_3, 0.5 gL^{-1}), dysprosium oxide (Dy_2O_3, 1 gL^{-1}) were used as the starting materials, all obtained from the large supplier Alfa Aesar. The ratio of powders was chosen based on the assumption of the same incorporation probabilities of all components and with intended end composition in SrAl matrix as in $SrAl_2O_4:Eu^{2+}$, Dy^{3+}. No purification was performed on the powders. All three components have low solubility in deionized water, therefore an addition of 1 gL^{-1} of KOH was used to create needed ions in the electrolyte. As a substrate, Al6082 was used : 25×25×3 mm samples were cut with the "leg" for holding and electrical contact.

A voltage-limited (with voltage 700 V and a current density around 0.18 A cm^{-2}) unipolar regime was applied. For the first 150 seconds of the process no plasma discharges were observed – the anodization process took place. Anodization stage was observed with no plasma discharges for the first 150 s of the process, and for the rest of the 60 min process the uniform plasma discharge distribution occurred on the surface of the sample, with minimal current drop of 0.02 A cm^{-2} due to the growth of the oxide. The resulting coating was rinsed in HCl solution to remove traces of $SrCO_3$ from the surface. The image of the uncoated, coated and emitting sample is shown in fig. 4.21.

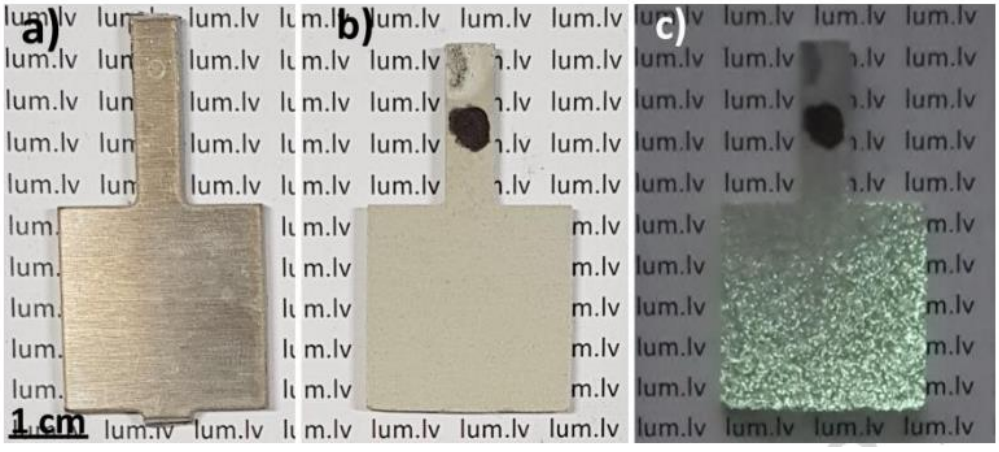

Fig. 4.21 – The photo of uncoated sample (a), PEO-processed sample in normal lighting (b) and PEO-processed sample after irradiation with UV light in low-light environment (c).

Right away one can observe that indeed, after 60 min long PEO processing time the coating visually looks similar to the conventional coatings. After short irradiation with 405nm UV light, the luminescence from the sample in a dark environment is observed for a couple of minutes indicating the formation of persistent luminophore. By analyzing SEM images (Fig. 4.22) one can see that with low magnification the coating looks like a classical PEO coating with slight amount of pores and irregular surface; however, closer inspection reveals microcrystal formations on the surface of the coating. The microcrystals have the length of 1-5μm with the thickness of 100-150nm. It might be that microcrystals contain the crystalline structure needed for persistent luminescence. Additionally, cross-section of the sample was prepared to analyze the thickness of the coating (fig. 4.23 left) as well as perform EDX analysis to see the distribution of the elements. The thickness is approximately 40 μm – the expected value for the electrolyte and processing time. Cross-section also reveals absence of direct channels to the substrate and large number of closed pores that might affect mechanical properties of the coating.

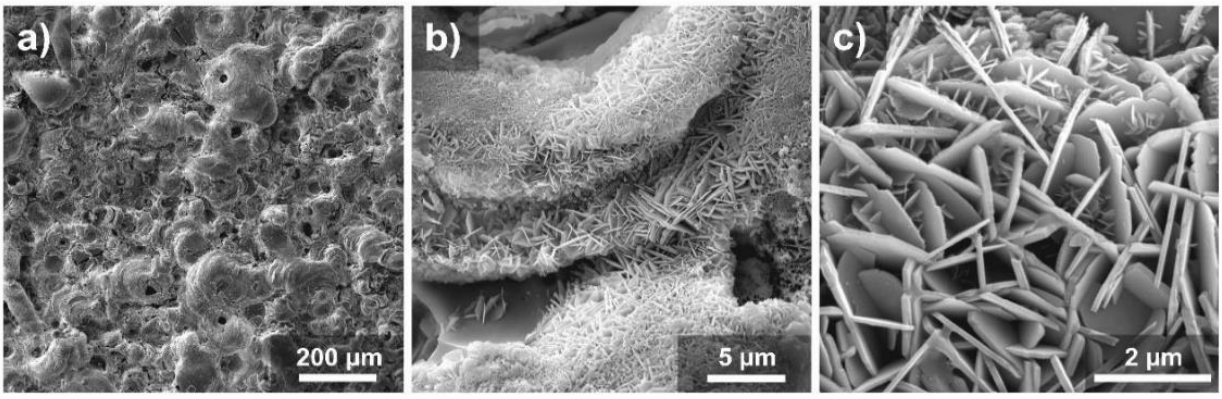

Fig. 4.22 – SEM images of the obtained coating. a – low magnification, b and c – high magnification

EDX map (fig. 4.23 right) of the cross section confirms the presence of Eu, Sr and Dy atoms in the coating; however, the concentration of Eu and Dy is close to the detection limit of the setup thus large amount of noise is present seemingly in the substrate.

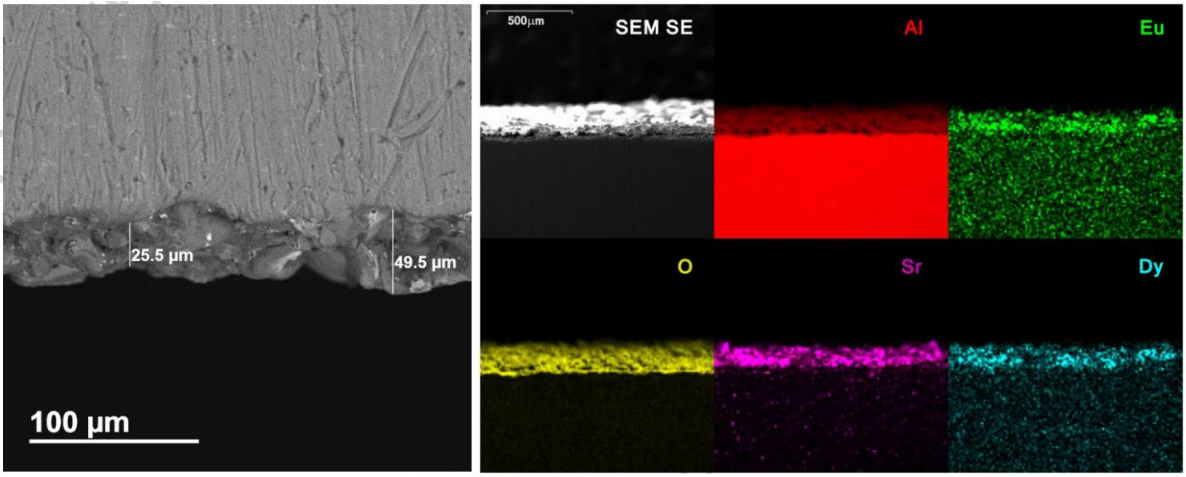

Fig. 4.23. Left - Cross section SEM image of the coating with two extreme values of thickness marked; Right - EDX map of the elements present in the coating.

Finally, XRD pattern as well as EDX pattern from the top of the coating was measured – presented in fig 4.24. The XRD pattern reveals several peaks corresponding to γ-alumina crystalline structure as well as monoclinic $SrAl_2O_4$ phase. Another strontium aluminate phase was also detected – $SrAl_{12}O_{19}$. No crystalline phases of rare-earth ("dopant") oxides were detected, therefore one can assume that the atoms are incorporated in the SrAl or alumina matrix. EDX revealed the approximate ration of elements as 67% Al, 22% Sr, 4% Eu and 7% Dy at. % - a combination fitting with the intended composition of $SrAl_2O_4:Eu^{2+}, Dy^{2+}$.

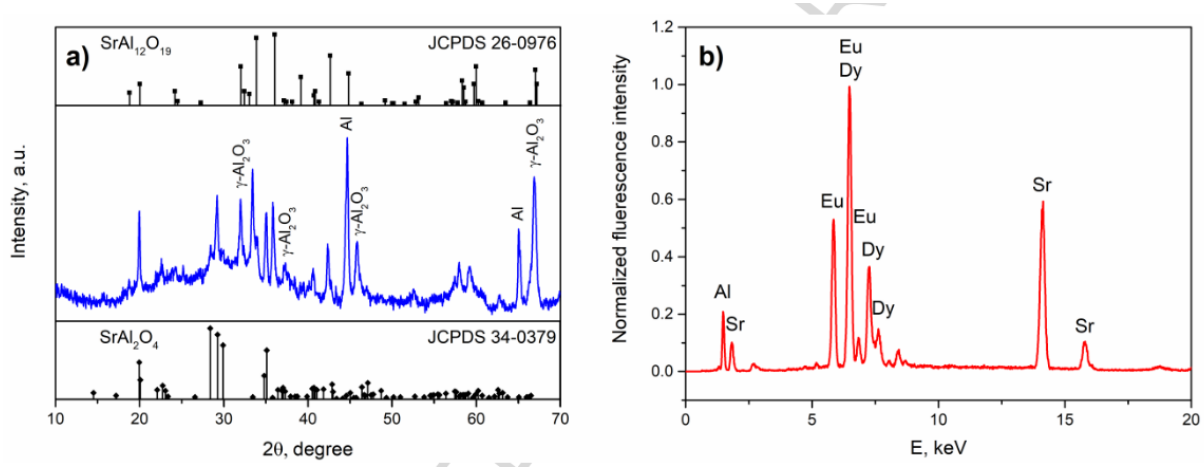

Fig. 4.24 a - XRD spectrum of obtained coating and b – EDX spectrum of the coating.

To further analyze the luminescence properties of the coating, the excitation-emission spectrum was recorded and is shown on fig. 4.25. For a comparison, a commercially available SrAl was used as a reference (obtained from Sigma Aldrich). Firstly, the afterglow of the obtained coating

and commercial SrAl do match indicating the same recombination centers responsible for afterglow in both samples. This luminescence is a 5d-4f emission of Eu^{2+} [206] – therefore, a correct incorporation of Eu in the structure of PEO coating occurred due to the reduction of Eu^{3+} from the powder. The similar process did occur in the PEO pore-filling study described in section 4.1.2. The second maximum in the photoluminescence emission spectrum of the coating under UV irradiation at 455nm is associated with the Eu^{2+} incorporation in another Sr position in SrAl matrix [207] with some contribution from the intrinsic amorphous alumina luminescence [208], [209]. Although some reports are suggesting that this maximum is quenched above 150K [198], [210], the peak can also be explained with other SrAl phases present in the coating [211] (as observed in XRD spectra in fig. 4.24). Other aluminate matrices can also exhibit Eu^{2+} luminescence in blue region of spectrum (e.g. barium-magnesium aluminates BaMgAl or barium-europium aluminates BaEuAl) [145], [212].

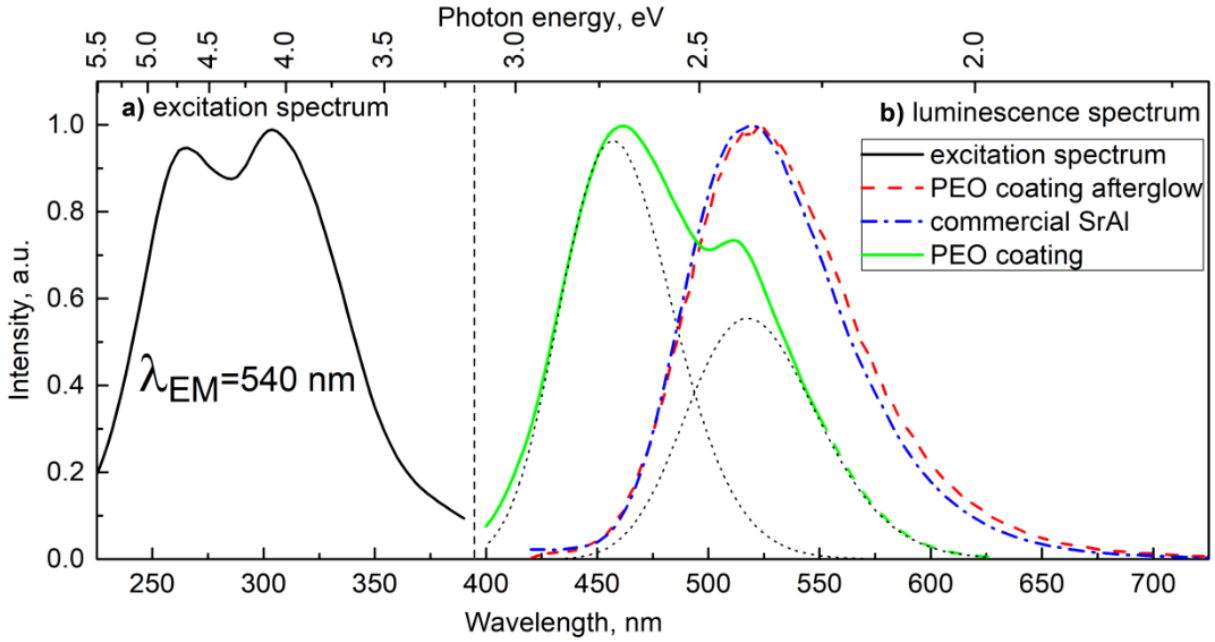

Fig. 4.25. Excitation and emission spectrum obtained from the coating and reference sample. a – excitation spectrum measured at 540nm emission and b – emission spectrum for PEO sample (green line) and afterglow spectrum of PEO coating and commercially available SrAl.

Long afterglow of the luminescence is caused by thermally assisted charge release from electron traps causing electron recombination at luminescence center with difference of energy released in a form of light. To study the electron traps and recombination process the TSL method is used, similar to the analysis performed for dosimetry. The TSL glowcurve obtained from the sample is presented in fig. 4.26 with the data on the spectral distribution of the emission

presented in the background. A single, broad (FWHM=144K), possibly multi-component glow peak is observed with a maximum at 425K. The overlapping of the glow peak with the room temperature enables gradual release of charged electrons.

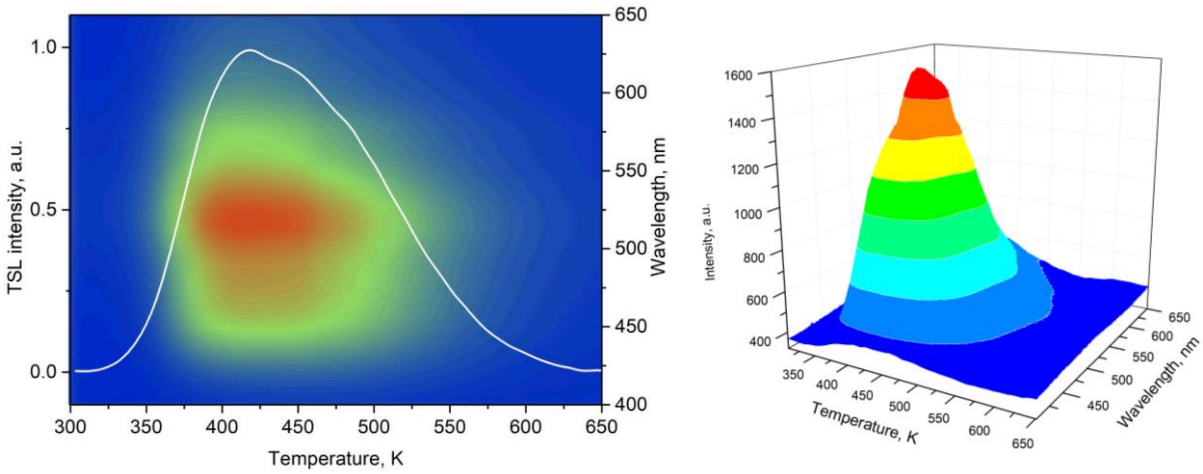

Fig. 4.26 TSL glowcurve of the coating (measured at 520nm) with 3D matrix on the background: temperature/wavelength measurement with colors indicating intensity of the signal. Right – 3D surface graph of the TSL measurement.

To evaluate long afterglow performance of the material, the decay kinetics were measured at room temperature (fig. 4.27). The sample was irradiated for 10s and luminescence intensity of 520nm band was measured as a function of time for 3 hours. The stretched exponent function was used for approximation of the curve (red dashed line in fig. 4.27). The physical interpretation of approximation function can be found in [213]. The inability to approximate the decay kinetics with a single or double exponent indicates the presence of a wide distribution of energy levels (also confirmed by the relatively large FWHM of TSL maximum). It is assumed that multiple trapping and detrapping events occur simultaneously during the afterglow process causing a superposition of a number of exponential decay [214], [215].

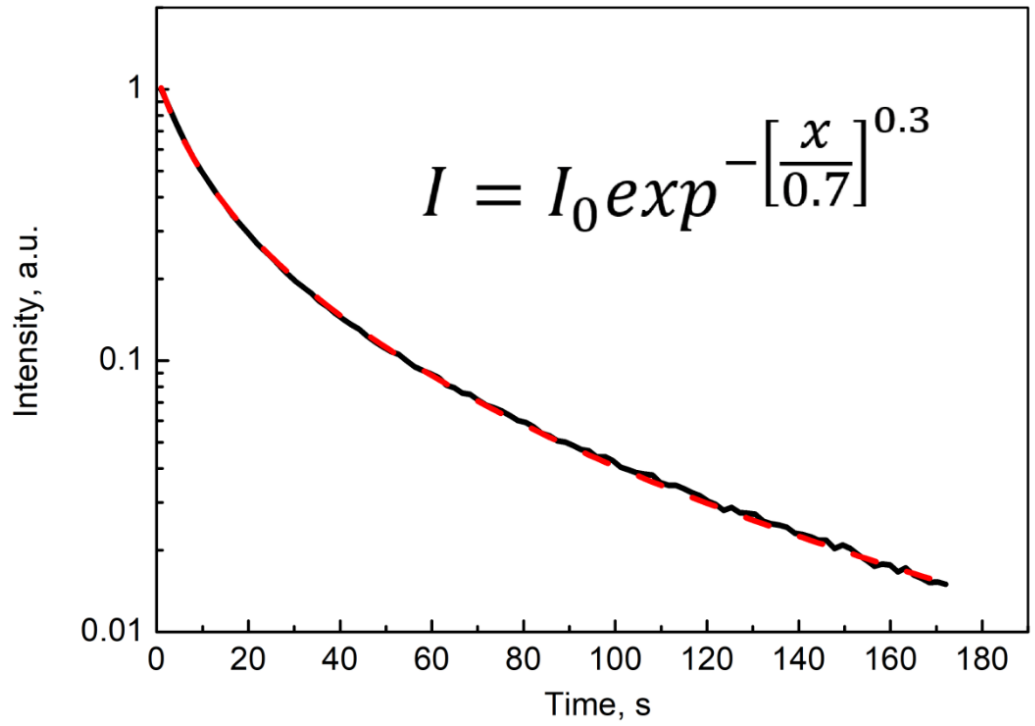

Fig. 4.27. The luminescence decay kinetic measurement from obtained coating with a stretched exponent decay approximation (red dashed).

The method and reactions occurring during PEO process is described in detail in [84]. Thus, a novel approach for production of SrAl coatings is presented. Although certain optimization routes should be explored to make the performance of the phosphorescent coating comparable to the commercially available powder samples, the approach exhibits a row of crucial advantages. When compared to most popular SrAl production method – solid-state reaction – PEO process offers much smaller processing time, no need for pre- and post-processing to obtain material in a coating form, the ecological friendliness of the process, less energy requirements and efficient use of materials. The approach is also easily scalable and transferrable to the industrial setting to produce a range of products like vehicle body panels, road and emergency signs and others.

The research of a production of strontium aluminate coating in a single-step PEO leads to the third thesis of this work:

Thesis 3: PEO process is a viable alternative to the solid state reaction in production of complex oxide phosphorescent coatings.

5 Conclusions

PEO is a complex process with the large number of varying parameters, therefore for a successful application of the technology the great care should be taken in choosing of the material, electrical parameters and electrolyte. However, the large number of variable parameters can also be used as an advantage – for a controlled implementation of atoms in small concentration (dopants) in the structure of the oxide coatings. The role of dopants in luminescence materials is crucial, and many of the materials used for various luminescence applications are based on metal oxides; therefore, a PEO process can be used to produce coatings with a specific luminescence output. The aim of this dissertation was to explore the possibilities for PEO coating technology to be used for production of coatings with enhanced luminescent properties. As the work covers three distinctive topics, the conclusions are divided into three sections.

Firstly, different possibilities to dope the crystalline structure of PEO coating to alter its luminescence properties were explored. By implementing europium in the alloy, its luminescence can be observed from the coating after PEO processing. Moreover, the Eu ion in the lattice undergoes the transition from Eu^{3+} charge state to Eu^{2+}. However, the creation of specific alloys is often expensive, and the mechanical properties can be altered to disadvantage, therefore other methods for implementation of ions should be considered. One of these methods is the use of suspension electrolyte – the insoluble powder is mixed in a PEO electrolyte. With the nature of the process, inevitably the particles will come in contact with plasma discharges thus participating in the formation of the coating structure. This approach, although effective, has one crucial drawback often preventing the commercial application possibilities – the use of large amount of powder is necessary, and with large electrolyte volume the financial cost becomes high very quickly, especially so in production of luminescence coatings where expensive rare earth elements are used. One of the solutions to this problem is the developed pore-filling approach – this work demonstrated that by filling the pores on the PEO coating with a Eu-containing powder one can achieve the same effect as in the use of suspension electrolytes – the powder particles participate in the formation of the coating with the same effect of Eu charge state change that was observed in a study with Eu-containing alloy. The pore-filling approach can significantly reduce the amount of powder needed to achieve some sort of doped PEO coating, although a minor drawback can be defined – with prolonged PEO processes that are required to obtain hardest alpha-phases of alumina the amount of Eu in the

coating will reduce minimizing the effect of the doping. To mitigate that a repeated pore-filling should be performed adding additional steps in the process – an undesired factor for commercial applications.

Secondly, to further explore the possibilities of PEO to create coatings with luminescence-based applications, the enhanced thermostimulated luminescence signal was obtained from two different coatings – Al_2O_3:C and Al_2O_3:Cr coatings on aluminum surface. The carbon-doped coating was used by implementing the organic soluble additive in the electrolyte, while the chromium was implemented from the alloy itself, similar to the Eu implementation from the Eu-containing alloy previously. Both coatings exhibit enhanced thermostimulated luminescence intensity, however, with different spectral and thermal distribution. The broad distribution of traps in a carbon-containing alumina produced a wide thermostimulated luminescence maximum peaking at 520nm, while chromium doping enhanced Cr^{3+} R-line doublet luminescence at 613nm. Both studies describe a viable approach to produce dosimetric coatings, and with combination of other PEO advantages (low cost, scalability and energy efficiency) they present an interesting proof of concept for further research: the performance of both approaches should be improved and re-evaluated. Additional TSL, dose response curve and OSL measurements should be performed to fully understand the mechanisms, drawbacks, and applicability of the technology.

Thirdly, the attempt at replicating of another type of luminescence-based material using PEO was made in the field of persistent luminescence. Previous knowledge was used to create a complex suspension electrolyte and an electrical parameter set that enabled the synthesis of a PEO coating with strontium aluminate structure exhibiting observable persistent luminescence. This is a unique approach to create a complex crystalline structure of strontium aluminate doped with europium and dysprosium. Notable advantages of the PEO process to create phosphorescent coatings when compared to the conventional approaches include the single-step nature of the process, energy efficiency and great adhesion of the coating to the part. Despite the success of the research, the coating luminescence output should be optimized (afterglow is observed for 10 minutes after the end of UV irradiation while the similar material created by other synthesis methods demonstrates tens of hours of afterglow) before any commercial application. Nevertheless, the research demonstrated the possibility of PEO process to create not only doped metal-oxide coatings, but also complex, multi-component doped oxide structures enabling further search of other PEO applications.

6 Thesis

Thesis 1: The doping of alumina PEO coatings to alter their luminescence properties can be achieved in three ways: alloying the metal substrate; using three-stage pore filling process and by adding dopants to electrolyte.

Thesis 2: The PEO process is applicable for the doping of alumina coating with carbon or chromium atoms thus making the material promising for applications in detection of ionizing radiation.

Thesis 3: PEO process is a viable alternative to the solid state reaction in production of complex oxide phosphorescent coatings.

Please refer to the chapter 7.1 on the next page for the list of publications of experimental proofs for the thesis.

7 List of conferences and publications

7.1 Authors publications reflecting the thesis

Thesis 1:

- K. Smits, D. Millers, **A. Zolotarjovs**, R. Drunka, M. Vanks, Luminescence of Eu ion in alumina prepared by plasma electrolytic oxidation, Appl. Surf. Sci. 337 (2015) 166–171. doi:10.1016/j.apsusc.2015.02.085.
- **A. Zolotarjovs,** K. Smits, A. Krumina, D. Millers, L. Grigorjeva, Luminescent PEO Coatings on Aluminum, ECS J. Solid State Sci. Technol. 5 (2016) R150–R153. doi:10.1149/2.0401609jss.

Thesis 2 :

- **A. Zolotarjovs**, K. Smits, K. Laganovska, I. Bite, L. Grigorjeva, K. Auzins, D. Millers, L. Skuja, Thermostimulated luminescence of plasma electrolytic oxidation coatings on 6082 aluminium surface, Radiat. Meas. 124 (2019) 29–34. doi:10.1016/j.radmeas.2019.02.020.
- **A. Zolotarjovs**, K. Smits, I. Bite, K. Laganovska, K. Auzins, E. Einbergs, V. Vitola, D. Millers Chromium luminescence in plasma electrolytic oxidation coatings on aluminium surface. In publishing.

Thesis 3:

- I. Bite, G. Krieke, **A. Zolotarjovs**, K. Laganovska, V. Liepina, K. Smits, K. Auzins, L. Grigorjeva, D. Millers, L. Skuja, Novel method of phosphorescent strontium aluminate coating preparation on aluminum, Mater. Des. 160 (2018) 794–802. doi:10.1016/j.matdes.2018.10.021.
- K. Auzins, **A. Zolotarjovs**, I. Bite, K. Laganovska, V. Vitola, K. Smits, D. Millers, Production of Phosphorescent Coatings on 6082 Aluminum Using $Sr_{0.95}Eu_{0.02}Dy_{0.03}Al_2O_4$-δ Powder and Plasma Electrolytic Oxidation, Coatings. 9 (2019) 865. doi:10.3390/coatings9120865.

7.2 Other authors publications

(total: 36 publications, h-index: 9)

- Vitola, I. Bite, D. Millers, **A. Zolotarjovs**, K. Laganovska, K. Smits, A. Spustaka, The boron effect on low temperature luminescence of $SrAl_2O_4$:Eu,Dy Ceram. Int. (2020). doi:10.1016/j.ceramint.2020.01.208.
- E. Butanovs, S. Piskunov, **A. Zolotarjovs**, B. Polyakov, Growth and characterization of PbI_2-decorated ZnO nanowires for photodetection applications, J. Alloys Compd. 825 (2020) 154095. doi:10.1016/j.jallcom.2020.154095.
- Antuzevics, A. Fedotovs, D. Berzins, U. Rogulis, K. Auzins, **A. Zolotarjovs**, S.L. Baldochi, Recombination luminescence of X-ray induced paramagnetic defects in BaY_2F_8, J. Lumin. 223 (2020) 117216. doi:10.1016/j.jlumin.2020.117216.
- L. Grigorjeva, **A. Zolotarjovs**, I. Bite, J. Grube, D. Millers, Electronic processes in doped ZnO nanopowders, IOP Conf. Ser. Mater. Sci. Eng. 503 (2019). doi:10.1088/1757-899X/503/1/012017.
- P. Bohacek, A. Krasnikov, M. Nikl, S. Zazubovich, **A. Zolotarjovs**, On low-temperature luminescence quenching in $Gd_3(Ga,Al)_5O_{12}$:Ce crystals, Opt. Mater. (Amst). 95 (2019) 109252. doi:10.1016/j.optmat.2019.109252.
- J. Cipa, A. Zarins, A. Supe, G. Kizane, **A. Zolotarjovs**, L. Baumane, L. Trinkler, O. Leys, R. Knitter, X-ray induced defects in advanced lithium orthosilicate pebbles with additions of lithium metatitanate, Fusion Eng. Des. 143 (2019) 10–15. doi:10.1016/j.fusengdes.2019.03.096.
- M. Korzhik, V. Alenkov, O. Buzanov, A. Fedorov, G. Dosovitskiy, L. Grigorjeva, V. Mechinsky, P. Sokolov, Y. Tratsiak, **A. Zolotarjovs**, V. Dormenev, A. Dosovitskiy, D. Agrawal, T. Anniyev, M. Vasilyev, V. Khabashesku, Nanoengineered $Gd_3Al_2Ga_3O_{12}$ Scintillation Materials with Disordered Garnet Structure for Novel Detectors of Ionizing Radiation, Cryst. Res. Technol. 54 (2019) 1–10. doi:10.1002/crat.201800172.
- V. Liepina, D. Millers, K. Smits, **A. Zolotarjovs**, I. Bite, X-ray excited luminescence of $SrAl_2O_4$:Eu,Dy at low temperatures, J. Phys. Chem. Solids. 115 (2018) 381–385. doi:10.1016/j.jpcs.2017.12.040.
- E. Auffray, R. Augulis, A. Fedorov, G. Dosovitskiy, L. Grigorjeva, V. Gulbinas, M. Koschan, M. Lucchini, C. Melcher, S. Nargelas, G. Tamulaitis, A. Vaitkevičius, **A. Zolotarjovs**, M. Korzhik, Excitation Transfer Engineering in Ce-Doped Oxide

Crystalline Scintillators by Codoping with Alkali-Earth Ions, Phys. Status Solidi Appl. Mater. Sci. 215 (2018) 1–10. doi:10.1002/pssa.201700798.

- E. Butanovs, J. Butikova, **A. Zolotarjovs**, B. Polyakov, Towards metal chalcogenide nanowire-based colour-sensitive photodetectors, Opt. Mater. (Amst). 75 (2018) 501–507. doi:10.1016/j.optmat.2017.11.010.
- L. Grigorjeva, **A. Zolotarjovs**, S.Y. Sokovnin, D. Millers, K. Smits, V.G. Il`ves, Radioluminescence, thermoluminescence and dosimetric properties of ZnO ceramics, Ceram. Int. 43 (2017) 6187–6191. doi:10.1016/j.ceramint.2017.02.016.
- L. Rozenberga-Voska, J. Grabis, **A. Zolotarjovs**, Synthesis of Eu^{2+} and Dy^{3+} doped strontium aluminates and their properties, Key Eng. Mater. 721 KEM (2017) 311–315. doi:10.4028/www.scientific.net/KEM.721.311.
- K. Smits, D. Olsteins, **A. Zolotarjovs**, K. Laganovska, D. Millers, R. Ignatans, J. Grabis, Doped zirconia phase and luminescence dependence on the nature of charge compensation, Sci. Rep. 7 (2017) 1–7. doi:10.1038/srep44453.
- V. Babin, P. Bohacek, L. Grigorjeva, M. Kučera, M. Nikl, S. Zazubovich, **A. Zolotarjovs**, Effect of Mg^{2+} ions co-doping on luminescence and defects formation processes in $Gd_3(Ga,Al)_5O_{12}$:Ce single crystals, Opt. Mater. (Amst). 66 (2017) 48–58. doi:10.1016/j.optmat.2017.01.039.
- Zarins, O. Leys, G. Kizane, A. Supe, L. Baumane, M. Gonzalez, V. Correcher, C. Boronat, **A. Zolotarjovs**, R. Knitter, Behaviour of advanced tritium breeder pebbles under simultaneous action of accelerated electrons and high temperature, Fusion Eng. Des. 121 (2017) 167–173. doi:10.1016/j.fusengdes.2017.06.033.
- J. Cipa, G. Kizane, A. Supe, **A. Zolotarjovs**, A. Zarins, L. Baumane, Luminescence of X-ray induced radiation defects in modified lithium orthosilicate pebbles with additions of titanium dioxide, Energetika. 63 (2017) 113–120. doi:10.6001/energetika.v63i3.3562.
- V. Vitola, D. Millers, K. Smits, I. Bite, **A. Zolotarjovs**, The search for defects in undoped $SrAl_2O_4$ material, Opt. Mater. (Amst). 87 (2019) 48–52. doi:10.1016/j.optmat.2018.06.004.
- L. Grigorjeva, J. Grube, I. Bite, **A. Zolotarjovs**, K. Smits, D. Millers, P. Rodnyi, K. Chernenko, Sub-nanosecond excitonic luminescence in ZnO:In nanocrystals, Radiat. Meas. 123 (2019) 69–73. doi:10.1016/j.radmeas.2019.02.016.

- T. Gavrilović, K. Laganovska, **A. Zolotarjovs**, K. Smits, D.J. Jovanović, M.D. Dramićanin, High resolution luminescence spectroscopy and thermoluminescence of different size $LaPO_4:Eu^{3+}$ nanoparticles, Opt. Mater. (Amst). 82 (2018) 39–46. doi:10.1016/j.optmat.2018.05.042.
- L. Grigorjeva, **A. Zolotarjovs**, D. Millers, K. Smits, P. Krug, J. Stollenwerk, A. Osman, T. Tenostendarp, Magnetron sputtering fabrication of α-Al_2O_3:Cr powders and their thermoluminescence properties, Radiat. Meas. 119 (2018) 140–143. doi:10.1016/j.radmeas.2018.10.009.
- K. Laganovska, I. Bite, **A. Zolotarjovs**, K. Smits, Niobium enhanced europium ion luminescence in hafnia nanocrystals, J. Lumin. 203 (2018) 358–363. doi:10.1016/j.jlumin.2018.06.069.
- L. Grigorjeva, K. Kamada, M. Nikl, A. Yoshikawa, S. Zazubovich, **A. Zolotarjovs**, Effect of Ga content on luminescence and defects formation processes in $Gd_3(Ga,Al)_5O_{12}$:Ce single crystals, Opt. Mater. (Amst). 75 (2018) 331–336. doi:10.1016/j.optmat.2017.10.054.
- E. Elsts, G. Krieke, U. Rogulis, K. Smits, **A. Zolotarjovs**, J. Jansons, A. Sarakovskis, K. Kundzins, Rare earth doped glass–ceramics containing $NaLaF_4$ nanocrystals, Opt. Mater. (Amst). 59 (2016) 130–135. doi:10.1016/j.optmat.2016.01.005.
- P.A. Rodnyi, K.A. Chernenko, **A. Zolotarjovs**, L. Grigorjeva, E.I. Gorokhova, I.D. Venevtsev, Effect of point defects on luminescence characteristics of ZnO ceramics, Phys. Solid State. 58 (2016) 2055–2061. doi:10.1134/S1063783416100309.
- E. Elsts, U. Rogulis, K. Bulindzs, K. Smits, **A. Zolotarjovs**, L. Trinkler, K. Kundzins, Studies of radiation defects in cerium, europium and terbium activated oxyfluoride glasses and glass ceramics, Opt. Mater. (Amst). 41 (2015) 90–93. doi:10.1016/j.optmat.2014.10.042.
- L. Grigorjeva, D. Millers, K. Smits, **A. Zolotarjovs**, Gas sensitive luminescence of ZnO coatings obtained by plazma electrolytic oxidation, Sensors Actuators, A Phys. 234 (2015) 290–293. doi:10.1016/j.sna.2015.09.018.
- V. Bondar, L. Grigorjeva, T. Kärner, O. Sidletskiy, K. Smits, S. Zazubovich, **A. Zolotarjovs**, Thermally stimulated luminescence of undoped and Ce^{3+}-doped Gd_2SiO_5 and $(Lu,Gd)_2SiO_5$ single crystals, J. Lumin. 159 (2014) 229–237. doi:10.1016/j.jlumin.2014.11.034.

- **Zolatarjovs**, A.N. Trukhin, K. Smits, D. Millers, TSL and fractional glow study of Ge-doped α-quartz, IOP Conf. Ser. Mater. Sci. Eng. 49 (2013) 0–4. doi:10.1088/1757-899X/49/1/012056.
- K. Laganovska, **A. Zolotarjovs**, M. Vázquez, K. Mc Donnell, J. Liepins, H. Ben-Yoav, V. Karitans, K. Smits, Portable low-cost open-source wireless spectrophotometer for fast and reliable measurements, HardwareX. 7 (2020) e00108. doi:10.1016/j.ohx.2020.e00108.

7.3 International conferences

The author of this work participated in over 10 international conferences and training courses/summer schools. The non-exhaustive list is as follows:

- «New materials for radiation detectors» in Peter the Great Saint-Petersburg Polytechnic University (SPbPU) (29.06.2015 – 3.07.2015)
- COST Training School on "Upconverting nanoparticles in bioaffinity assays - from bioconjugation to luminescence readout" in Turku, Finland, 3. - 5. April 2017
- RACIRI Summer School 2017 “Grand Challenges and Opportunities with the Best X-ray and Neutron Sources” in Ronneby, Sweden. 19-26 August 2017
- A number of “Functional Materials and Nanotechnologies FMNT” conferences in years 2013-2020
- „1st Conference and Spring School on Properties, Design and Applications of Upconverting Nanomaterials UPCON-2016”
- “Luminescent Detectors and Transformers of Ionizing Radiation LumDeTr” 9-14 September 2018, Prague, Czech Republic
- Various workshops and meetings in frame of COST action CM1403
- Various workshops and meetings in frame of COST action PortASAP CA16215

8 Acknowledgements

The author is wholeheartedly expressing his sincere gratitude to the scientific supervisor Dr. Phys. Krisjanis Smits and the team of Optical Materials Laboratory for the unwavering support throughout the research and day-to-day work. A separate acknowledgement is expressed to the more experienced colleagues: PhD. Phys. Donats Millers, Dr. Phys. Larisa Grigorjeva, Dr. Phys. Linards Skuja, Dr. Phys. Anatolijs Truhins for valued knowledge transfer through decades of work in the field of science.

The help of colleagues from other laboratories as well as staff of Institute of Solid State Physics is treasured and appreciated.

The author also wants to thank the Faculty of Physics, Mathematics and Optometry of the Univeristy of Latvia for the constant support in studies and research through various programmes, consultations, software licensing and seminars.

Financial support provided by Scientific Research Project for Students and Young Researchers Nr. SJZ2015/21 and SJZ/2016/12 realized at the Institute of Solid State Physics, University of Latvia is greatly acknowledged.

Part of this research work was done in frame of ERAF project No. KC/2.1.2.1.1/10/01/005 (LIAA contract No. L-KC-11-0006).

This research was partly supported by the ERDF Project No. 1.1.1.1/16/A/182.

This research was partly supported by the Scientific Research project LZP-2018/1-0361.

Institute of Solid State Physics, University of Latvia as the Center of Excellence has received funding from the European Union's Horizon 2020 Framework Programme H2020-WIDESPREAD-01-2016-2017-TeamingPhase2 under grant agreement No. 739508, project CAMART^2

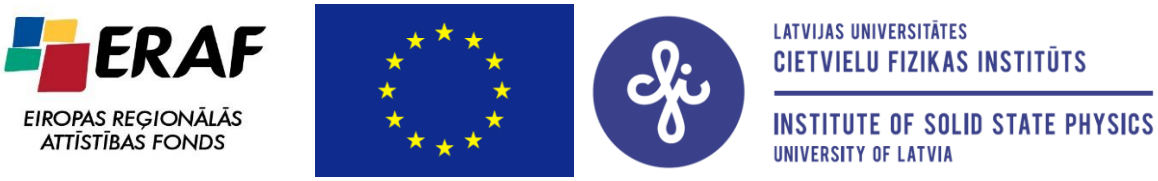

9 References

[1] D. A. . MacInnes, *The Principles of Electrochemistry*. Reinhold Publishing Corporation, 1939.

[2] R. S. Lillie, “The recovery of transmissivity in passive iron wires as a model of recovery processes in irritable living systems,” *J. Gen. Physiol.*, vol. 3, no. 2, pp. 129–143, Nov. 1920.

[3] P. G. S. and R.Pinner, *The Surface Treatment and Finishing of Aluminum and Its Alloys*. ASM International & Finishing Publications, 2001.

[4] W. Lee and S. Park, “Porous Anodic Aluminum Oxide : Anodization and Templated Synthesis of Functional Nanostructures,” 2014.

[5] F. M. Al-Kharafi and W. A. Badawy, “Corrosion and passivation of Al and Al-Si alloys in nitric acid solutions II—Effect of chloride ions,” *Electrochim. Acta*, vol. 40, no. 12, pp. 1811–1817, Sep. 1995.

[6] J. W. Diggle, T. C. Downie, and C. W. Goulding, “Anodic oxide films on aluminum,” *Chem. Rev.*, vol. 69, no. 3, pp. 365–405, Jun. 1969.

[7] F. Keller, M. S. Hunter, and D. L. Robinson, “Structural Features of Oxide Coatings on Aluminum,” *J. Electrochem. Soc.*, vol. 100, no. 9, p. 411, 1953.

[8] G. . Thompson, “Porous anodic alumina: fabrication, characterization and applications,” *Thin Solid Films*, vol. 297, no. 1–2, pp. 192–201, Apr. 1997.

[9] O’Sullivan JP and Wood GC, “Morphology and mechanism of formation of porous anodic films on aluminum,” *Proc Roy Soc Ser A Math Phys Sci*, vol. 317, no. 1731, 1970.

[10] S. Wernick, *The surface treatment and finishing of aluminium and its alloys*. Teddington: Robert Draper, 1956.

[11] G. E. J. Poinern, N. Ali, and D. Fawcett, “Progress in Nano-Engineered Anodic Aluminum Oxide Membrane Development,” *Materials (Basel).*, vol. 4, no. 3, pp. 487–526, Feb. 2011.

[12] C. Jeong, J. Lee, K. Sheppard, and C.-H. Choi, “Air-Impregnated Nanoporous Anodic Aluminum Oxide Layers for Enhancing the Corrosion Resistance of Aluminum,” *Langmuir*, vol. 31, no. 40, pp. 11040–11050, Oct. 2015.

[13] Y. Seo, J.-Y. Jung, J. Chung, and S. Lee, “Enhancement of Corrosion Resistance of Aluminum 7075 Surface through Oil Impregnation for Subsea Application,” *Appl. Sci.*, vol. 9, no. 18, p. 3762, Sep. 2019.

[14] G. Alcalá, P. Skeldon, G. E. Thompson, A. B. Mann, H. Habazaki, and K. Shimizu, "Mechanical properties of amorphous anodic alumina and tantala films using nanoindentation," *Nanotechnology*, vol. 13, no. 4, p. 302, Aug. 2002.

[15] S. H. Ko, D. W. Lee, S. E. Jee, H. C. Park, K. H. Lee, and W. Hwang, "Mechanical Properties and Residual Stress Measurements in Anodic Aluminium Oxide Structures Using Nanoindentation," *Glas. Phys. Chem.*, vol. 31, no. 3, pp. 356–363, May 2005.

[16] G. D. Sulka, *Nanostructured Anodic Metal Oxides: Synthesis and Applications*. Elsevier, 2020.

[17] C. J. Donahue and J. A. Exline, "Anodizing and Coloring Aluminum Alloys," *J. Chem. Educ.*, vol. 91, no. 5, pp. 711–715, May 2014.

[18] L. Iglesias, V. Vega, J. GarcÃ-a, B. Hernando, and V. M. Prida, "Development of electrostatic supercapacitors by atomic layer deposition on nanoporous anodic aluminum oxides for energy harvesting applications," *Front. Phys.*, vol. 3, Mar. 2015.

[19] S. Zheng *et al.*, "Fabrication of a micro-nanostructured superhydrophobic aluminum surface with excellent corrosion resistance and anti-icing performance," *RSC Adv.*, vol. 6, no. 83, pp. 79389–79400, 2016.

[20] C. V. Manzano, J. P. Best, J. J. Schwiedrzik, A. Cantarero, J. Michler, and L. Philippe, "The influence of thickness, interpore distance and compositional structure on the optical properties of self-ordered anodic aluminum oxide films," *J. Mater. Chem. C*, vol. 4, no. 32, pp. 7658–7666, 2016.

[21] A. Santos *et al.*, "Structural tuning of photoluminescence in nanoporous anodic alumina by hard anodization in oxalic and malonic acids," *Nanoscale Res. Lett.*, vol. 7, no. 1, p. 228, 2012.

[22] K. Huang, L. Pu, Y. Shi, P. Han, R. Zhang, and Y. D. Zheng, "Photoluminescence oscillations in porous alumina films," *Appl. Phys. Lett.*, vol. 89, no. 20, p. 201118, Nov. 2006.

[23] A. Santos *et al.*, "Nanoporous Anodic Alumina Barcodes: Toward Smart Optical Biosensors," *Adv. Mater.*, vol. 24, no. 8, pp. 1050–1054, Feb. 2012.

[24] P.-H. Lo, G.-L. Luo, C.-C. Lee, and W. Fang, "Nanoporous anodic aluminum oxide as a promising material for the electrostatically-controlled thin film interference filter," *J. Micromechanics Microengineering*, vol. 25, no. 2, p. 025001, Feb. 2015.

[25] L. Shen, M. Ali, Z. Gu, B. Min, D. Kim, and C. Park, "Preparation of anodic aluminum oxide (AAO) nano-template on silicon and its application to one-dimensional copper nano-pillar array formation," *Korean J. Chem. Eng.*, vol. 30, no. 1, pp. 221–227, Jan.

2013.

[26] A. AGUILERA *et al.*, “Porous alumina templates and nanostructured CdS for thin film solar cell applications,” *Sol. Energy Mater. Sol. Cells*, vol. 90, no. 6, pp. 713–726, Apr. 2006.

[27] H. Yazid, N. Z. Nekhia, R. Adnan, and A. M. Md Jani, “Synthesis and Characterization of Gold Nanoparticles Grafted on Nanoporous Anodic Aluminum Oxide (AAO) Membrane,” *Appl. Mech. Mater.*, vol. 752–753, pp. 77–80, Apr. 2015.

[28] Y.-L. Sung, F. Zhao, J. Li, and W.-C. Shih, “Gold nanoparticle decorated AAO filter membrane for SERS sensing of urine acetaminophen,” in *2016 IEEE SENSORS*, 2016, pp. 1–3.

[29] L. Wei *et al.*, “Low-Cost and High-Productivity Three-Dimensional Nanocapacitors Based on Stand-Up ZnO Nanowires for Energy Storage,” *Nanoscale Res. Lett.*, vol. 11, no. 1, p. 213, Dec. 2016.

[30] P. H. Lu, K. Wang, Z. Lu, A. J. Lennon, and S. R. Wenham, “Anodic Aluminum Oxide Passivation For Silicon Solar Cells,” *IEEE J. Photovoltaics*, vol. 3, no. 1, pp. 143–151, Jan. 2013.

[31] B. Abad, J. Maiz, and M. Martin-Gonzalez, “Rules to Determine Thermal Conductivity and Density of Anodic Aluminum Oxide (AAO) Membranes,” *J. Phys. Chem. C*, vol. 120, no. 10, pp. 5361–5370, Mar. 2016.

[32] Y.-N. Xu and W. Y. Ching, “Self-consistent band structures, charge distributions, and optical-absorption spectra in MgO, α- Al_2O_3” *Phys. Rev. B*, vol. 43, no. 5, pp. 4461–4472, Feb. 1991.

[33] R. H. French, “ChemInform Abstract: Electronic Band Structure of Al_2O_3, with Comparison to AlON and AlN,” *ChemInform*, vol. 21, no. 23, Jun. 1990.

[34] N. Kamarulzaman, M. F. Kasim, and R. Rusdi, “Band Gap Narrowing and Widening of ZnO Nanostructures and Doped Materials,” *Nanoscale Res. Lett.*, vol. 10, no. 1, p. 346, Dec. 2015.

[35] Ü. Özgür *et al.*, “A comprehensive review of ZnO materials and devices,” *J. Appl. Phys.*, vol. 98, no. 4, p. 041301, Aug. 2005.

[36] Y. Chen *et al.*, “Plasma assisted molecular beam epitaxy of ZnO on c -plane sapphire: Growth and characterization,” *J. Appl. Phys.*, vol. 84, no. 7, pp. 3912–3918, Oct. 1998.

[37] M. M. Lohrengel, “A Review Journal,” *Mater. Sci.*, vol. 12, pp. 243–294, 1993.

[38] L. Grigorjeva, D. Millers, K. Smits, and A. Zolotarjovs, “Gas sensitive luminescence of ZnO coatings obtained by plazma electrolytic oxidation,” *Sensors Actuators, A Phys.*,

vol. 234, pp. 290–293, 2015.

[39] L. White, Y. Koo, S. Neralla, J. Sankar, and Y. Yun, “Enhanced mechanical properties and increased corrosion resistance of a biodegradable magnesium alloy by plasma electrolytic oxidation (PEO),” *Mater. Sci. Eng. B*, vol. 208, pp. 39–46, 2016.

[40] M. Aliofkhazraei and A. S. Rouhaghdam, “Wear and coating removal mechanism of alumina/titania nanocomposite layer fabricated by plasma electrolysis,” *Surf. Coatings Technol.*, vol. 205, no. SUPPL. 2, pp. S57–S62, 2011.

[41] C. Martini, L. Ceschini, F. Tarterini, J. M. Paillard, and J. A. Curran, “PEO layers obtained from mixed aluminate-phosphate baths on Ti-6Al-4V: Dry sliding behaviour and influence of a PTFE topcoat,” *Wear*, vol. 269, no. 11–12, pp. 747–756, 2010.

[42] A. L. Yerokhin, X. Nie, A. Leyland, A. Matthews, and S. J. Dowey, “Plasma electrolysis for surface engineering,” *Surf. Coatings Technol.*, vol. 122, no. 2–3, pp. 73–93, 1999.

[43] X. Huang and Lord Famiyeh, “Plasma Electrolytic Oxidation Coatings on Aluminum Alloys: Microstructures, Properties, and Applications,” *Mod. Concepts Mater. Sci.*, vol. 2, no. 1, 2019.

[44] V. Dehnavi, X. Y. Liu, B. L. Luan, D. W. Shoesmith, and S. Rohani, “Phase transformation in plasma electrolytic oxidation coatings on 6061 aluminum alloy,” *Surf. Coatings Technol.*, vol. 251, pp. 106–114, Jul. 2014.

[45] J. A. Curran, H. Kalkancı, Y. Magurova, and T. W. Clyne, “Mullite-rich plasma electrolytic oxide coatings for thermal barrier applications,” *Surf. Coatings Technol.*, vol. 201, no. 21, pp. 8683–8687, Aug. 2007.

[46] J. Martín, M. Martín-González, A. del Campo, J. J. Reinosa, and J. F. Fernández, “Ordered arrays of polymeric nanopores by using inverse nanostructured PTFE surfaces,” *Nanotechnology*, vol. 23, no. 38, p. 385305, Sep. 2012.

[47] A. Lugovskoy and M. Zinigr, “Plasma Electrolytic Oxidation of Valve Metals,” in *Materials Science - Advanced Topics*, InTech, 2013.

[48] E. Kus, Z. Lee, S. Nutt, and F. Mansfeld, “A Comparison of the Corrosion Behavior of Nanocrystalline and Conventional Al 5083 Samples,” *CORROSION*, vol. 62, no. 2, pp. 152–161, Feb. 2006.

[49] M.-K. Chung, Y.-S. Choi, J.-G. Kim, Y.-M. Kim, and J.-C. Lee, “Effect of the number of ECAP pass time on the electrochemical properties of 1050 Al alloys,” *Mater. Sci. Eng. A*, vol. 366, no. 2, pp. 282–291, Feb. 2004.

[50] S. Aliasghari, P. Skeldon, and G. E. Thompson, “Plasma electrolytic oxidation of titanium in a phosphate/silicate electrolyte and tribological performance of the coatings,”

Appl. Surf. Sci., vol. 316, pp. 463–476, Oct. 2014.

[51] P. et al. HARTJEN, "Plasma Electrolytic Oxidation of Titanium Implant Surfaces: Microgroove-Structures Improve Cellular Adhesion and Viability," *In Vivo (Brooklyn).*, vol. 32, no. 2, Feb. 2018.

[52] B. L. Jiang and Y. M. Wang, "Plasma electrolytic oxidation treatment of aluminium and titanium alloys," in *Surface Engineering of Light Alloys*, Elsevier, 2010, pp. 110–154.

[53] T. W. Clyne and S. C. Troughton, "A review of recent work on discharge characteristics during plasma electrolytic oxidation of various metals," *Int. Mater. Rev.*, vol. 64, no. 3, pp. 127–162, Apr. 2019.

[54] X. Lu *et al.*, "Plasma electrolytic oxidation coatings with particle additions – A review," *Surf. Coatings Technol.*, vol. 307, pp. 1165–1182, 2016.

[55] V. N. Malyshev and K. M. Zorin, "Features of microarc oxidation coatings formation technology in slurry electrolytes," *Appl. Surf. Sci.*, vol. 254, no. 5, pp. 1511–1516, Dec. 2007.

[56] Y.-Q. Hou, D.-M. Zhuang, G. Zhang, M.-S. Wu, and J.-J. Liu, "Tribological performances of diamond film and graphite/diamond composite film," *Wear*, vol. 253, no. 7–8, pp. 711–719, Oct. 2002.

[57] M. Mu, J. Liang, X. Zhou, and Q. Xiao, "One-step preparation of TiO2/MoS2 composite coating on Ti6Al4V alloy by plasma electrolytic oxidation and its tribological properties," *Surf. Coatings Technol.*, vol. 214, pp. 124–130, Jan. 2013.

[58] A. M. Borisov, B. L. Krit, V. B. Lyudin, N. V. Morozova, I. V. Suminov, and A. V. Apelfeld, "Microarc oxidation in slurry electrolytes: A review," *Surf. Eng. Appl. Electrochem.*, vol. 52, no. 1, pp. 50–78, 2016.

[59] A. Kossenko and M. Zinigrad, "A universal electrolyte for the plasma electrolytic oxidation of aluminum and magnesium alloys," *Mater. Des.*, vol. 88, pp. 302–309, 2015.

[60] G. Barati Darband, M. Aliofkhazraei, P. Hamghalam, and N. Valizade, "Plasma electrolytic oxidation of magnesium and its alloys: Mechanism, properties and applications," *J. Magnes. Alloy.*, vol. 5, no. 1, pp. 74–132, Mar. 2017.

[61] R. O. Hussein, P. Zhang, X. Nie, Y. Xia, and D. O. Northwood, "The effect of current mode and discharge type on the corrosion resistance of plasma electrolytic oxidation (PEO) coated magnesium alloy AJ62," *Surf. Coatings Technol.*, vol. 206, no. 7, pp. 1990–1997, Dec. 2011.

[62] R. O. Hussein, X. Nie, and D. O. Northwood, "Effect of current mode on the plasma discharge, microstructure and corrosion resistance of oxide coatings produced on 1100

aluminum alloy by plasma electrolytic oxidation," 2019, pp. 3–16.

[63] A. B. Rogov, A. Yerokhin, and A. Matthews, "The Role of Cathodic Current in Plasma Electrolytic Oxidation of Aluminum: Phenomenological Concepts of the 'Soft Sparking' Mode," *Langmuir*, vol. 33, no. 41, pp. 11059–11069, Oct. 2017.

[64] Y.-J. Oh, J.-I. Mun, and J.-H. Kim, "Effects of alloying elements on microstructure and protective properties of Al_2O_3 coatings formed on aluminum alloy substrates by plasma electrolysis," *Surf. Coatings Technol.*, vol. 204, no. 1–2, pp. 141–148, Sep. 2009.

[65] M. Sieber, F. Simchen, R. Morgenstern, I. Scharf, and T. Lampke, "Plasma Electrolytic Oxidation of High-Strength Aluminium Alloys—Substrate Effect on Wear and Corrosion Performance," *Metals (Basel).*, vol. 8, no. 5, p. 356, May 2018.

[66] K. Smits, D. Millers, A. Zolotarjovs, R. Drunka, and M. Vanks, "Luminescence of Eu ion in alumina prepared by plasma electrolytic oxidation," *Appl. Surf. Sci.*, vol. 337, pp. 166–171, 2015.

[67] S. Stojadinović and R. Vasilić, "Formation and photoluminescence of Eu3+ doped zirconia coatings formed by plasma electrolytic oxidation," *J. Lumin.*, vol. 176, pp. 25–31, 2016.

[68] S. Stojadinović, R. Vasilić, N. Radić, and B. Grbić, "Zirconia films formed by plasma electrolytic oxidation: Photoluminescent and photocatalytic properties," *Opt. Mater. (Amst).*, vol. 40, pp. 20–25, 2015.

[69] S. Stojadinović, N. Tadić, and R. Vasilić, "Photoluminescence properties of Er^{3+}/Yb^{3+} doped ZrO_2 coatings formed by plasma electrolytic oxidation," *J. Lumin.*, vol. 208, no. December 2018, pp. 296–301, 2019.

[70] S. Stojadinović, N. Tadić, and R. Vasilić, "Down- and up-conversion photoluminescence of ZrO_2:Ho^{3+} and ZrO_2:Ho^{3+}/Yb^{3+} coatings formed by plasma electrolytic oxidation," *J. Alloys Compd.*, vol. 785, pp. 1222–1232, 2019.

[71] S. Stojadinović, N. Tadić, and R. Vasilić, "Down-conversion photoluminescence of ZrO_2:Er^{3+} coatings formed by plasma electrolytic oxidation," *Mater. Lett.*, vol. 219, pp. 251–255, 2018.

[72] S. Stojadinović and R. Vasilić, "Orange–red photoluminescence of Nb_2O_5:Eu^{3+}, Sm^{3+} coatings formed by plasma electrolytic oxidation of niobium," *J. Alloys Compd.*, vol. 685, pp. 881–889, 2016.

[73] S. Stojadinović, N. Tadić, N. Radić, P. Stefanov, B. Grbić, and R. Vasilić, "Anodic luminescence, structural, photoluminescent, and photocatalytic properties of anodic oxide films grown on niobium in phosphoric acid," *Appl. Surf. Sci.*, vol. 355, pp. 912–

920, 2015.

[74] S. Stojadinović, N. Tadić, and R. Vasilić, “Luminescence of oxide films during the electrolytic oxidation of tantalum,” *Electrochim. Acta*, vol. 152, pp. 323–329, 2015.

[75] S. Stojadinović and R. Vasilić, “Eu^{2+} photoluminescence in Al_2O_3 coatings obtained by plasma electrolytic oxidation,” *J. Lumin.*, vol. 199, no. March, pp. 240–244, 2018.

[76] S. Stojadinović, R. Vasilić, N. Radić, N. Tadić, P. Stefanov, and B. Grbić, “The formation of tungsten doped Al_2O_3/ZnO coatings on aluminum by plasma electrolytic oxidation and their application in photocatalysis,” *Appl. Surf. Sci.*, vol. 377, pp. 37–43, 2016.

[77] S. Stojadinović, N. Tadić, and R. Vasilić, “Photoluminescence of Sm^{2+}/Sm^{3+} doped Al_2O_3 coatings formed by plasma electrolytic oxidation of aluminum,” *J. Lumin.*, vol. 192, no. April, pp. 110–116, 2017.

[78] S. Stojadinović, N. Tadić, N. Radić, B. Stojadinović, B. Grbić, and R. Vasilić, “Synthesis and characterization of Al_2O_3/ZnO coatings formed by plasma electrolytic oxidation,” *Surf. Coatings Technol.*, vol. 276, pp. 573–579, 2015.

[79] S. Stojadinović, N. Tadić, N. Radić, B. Grbić, and R. Vasilić, “CdS particles modified TiO_2 coatings formed by plasma electrolytic oxidation with enhanced photocatalytic activity,” *Surf. Coatings Technol.*, vol. 344, pp. 528–533, 2018.

[80] S. Stojadinović, N. Tadić, N. Radić, B. Grbić, and R. Vasilić, “TiO_2/SnO_2 photocatalyst formed by plasma electrolytic oxidation,” *Mater. Lett.*, vol. 196, pp. 292–295, 2017.

[81] S. Stojadinović *et al.*, “Structural, photoluminescent and photocatalytic properties of TiO_2:Eu^{3+} coatings formed by plasma electrolytic oxidation,” *Appl. Surf. Sci.*, vol. 370, pp. 218–228, 2016.

[82] S. Stojadinović, N. Radić, N. Tadić, R. Vasilić, P. Stefanov, and B. Grbić, “Influence of iron doping on photocatalytic activity of TiO_2 coatings formed on titanium by plasma electrolytic oxidation,” *J. Mater. Sci. Mater. Electron.*, vol. 29, no. 11, pp. 9427–9434, 2018.

[83] S. Petrović, S. Stojadinović, L. Rožić, N. Radić, B. Grbić, and R. Vasilić, “Process modelling and analysis of plasma electrolytic oxidation of titanium for TiO_2/WO_3 thin film photocatalysts by response surface methodology,” *Surf. Coatings Technol.*, vol. 269, no. 1, pp. 250–257, 2015.

[84] I. Bite *et al.*, “Novel method of phosphorescent strontium aluminate coating preparation on aluminum,” *Mater. Des.*, vol. 160, pp. 794–802, 2018.

[85] K. Auzins *et al.*, “Production of Phosphorescent Coatings on 6082 Aluminum Using

$Sr_{0.95}Eu_{0.02}Dy_{0.03}Al_2O_4$-δ Powder and Plasma Electrolytic Oxidation," *Coatings*, vol. 9, no. 12, p. 865, Dec. 2019.

[86] A. Zolotarjovs, K. Smits, A. Krumina, D. Millers, and L. Grigorjeva, "Luminescent PEO Coatings on Aluminum," *ECS J. Solid State Sci. Technol.*, vol. 5, no. 9, pp. R150–R153, 2016.

[87] "Keronite International Ltd.," 2020. [Online]. Available: https://www.keronite.com/surface-technology/. [Accessed: 25-May-2020].

[88] "IBC Coatings Technologies, Inc.," 2020. [Online]. Available: https://www.ibccoatings.com/. [Accessed: 25-May-2020].

[89] J. A. Curran and T. W. Clyne, "Thermo-physical properties of plasma electrolytic oxide coatings on aluminium," *Surf. Coatings Technol.*, vol. 199, no. 2–3, pp. 168–176, Sep. 2005.

[90] C. S. Dunleavy, J. A. Curran, and T. W. Clyne, "Plasma electrolytic oxidation of aluminium networks to form a metal-cored ceramic composite hybrid material," *Compos. Sci. Technol.*, vol. 71, no. 6, pp. 908–915, Apr. 2011.

[91] L. Agureev *et al.*, "Study of Plasma Electrolytic Oxidation Coatings on Aluminum Composites," *Metals (Basel).*, vol. 8, no. 6, p. 459, Jun. 2018.

[92] S. V Savushkina, L. E. Agureev, A. A. Ashmarin, E. A. Vysotina, A. V Apelfeld, and K. A. Anikin, "The study of PEO coated zirconium doped aluminum composites," *J. Phys. Conf. Ser.*, vol. 1121, p. 012027, Nov. 2018.

[93] W. Jin *et al.*, "Sound Absorption Characteristics of Aluminum Foams Treated by Plasma Electrolytic Oxidation," *Materials (Basel).*, vol. 8, no. 11, pp. 7511–7518, Nov. 2015.

[94] L. Pezzato, M. Dabalà, and K. Brunelli, "Microstructure and Corrosion Properties of PEO Coatings Produced on AM-Aluminum Alloys," *Key Eng. Mater.*, vol. 813, pp. 298–303, Jul. 2019.

[95] Z. Gorgin Karaji, R. Hedayati, B. Pouran, I. Apachitei, and A. A. Zadpoor, "Effects of plasma electrolytic oxidation process on the mechanical properties of additively manufactured porous biomaterials," *Mater. Sci. Eng. C*, vol. 76, pp. 406–416, Jul. 2017.

[96] P. Cerchier *et al.*, "Antibacterial effect of PEO coating with silver on AA7075," *Mater. Sci. Eng. C*, vol. 75, pp. 554–564, Jun. 2017.

[97] L. Yu, J. Li, D. Wang, L. Ouyang, G. Jin, and X. Liu, "Improved antimicrobial activity and bioactivity of porous CaP–TiO_2 coating through surface nanofunctionalisation," *Mater. Technol.*, vol. 30, no. sup6, pp. B109–B114, Aug. 2015.

[98] M. Rizwan, R. Alias, U. Z. Zaidi, R. Mahmoodian, and M. Hamdi, "Surface modification

of valve metals using plasma electrolytic oxidation for antibacterial applications: A review," *J. Biomed. Mater. Res. Part A*, vol. 106, no. 2, pp. 590–605, Feb. 2018.

[99] M. B. Kannan, R. Walter, A. Yamamoto, H. Khakbaz, and C. Blawert, "Electrochemical surface engineering of magnesium metal by plasma electrolytic oxidation and calcium phosphate deposition: biocompatibility and in vitro degradation studies," *RSC Adv.*, vol. 8, no. 51, pp. 29189–29200, 2018.

[100] S. L. Aktuğ, S. Durdu, E. Yalçın, K. Çavuşoğlu, and M. Usta, "Bioactivity and biocompatibility of hydroxyapatite-based bioceramic coatings on zirconium by plasma electrolytic oxidation," *Mater. Sci. Eng. C*, vol. 71, pp. 1020–1027, Feb. 2017.

[101] P.-J. Chu, S.-Y. Wu, K.-C. Chen, J.-L. He, A. Yerokhin, and A. Matthews, "Nano-structured TiO2 films by plasma electrolytic oxidation combined with chemical and thermal post-treatments of titanium, for dye-sensitised solar cell applications," *Thin Solid Films*, vol. 519, no. 5, pp. 1723–1728, Dec. 2010.

[102] G.-W. Lin, J.-S. Chen, W. Tseng, and F.-H. Lu, "Formation of anatase TiO_2 coatings by plasma electrolytic oxidation for photocatalytic applications," *Surf. Coatings Technol.*, vol. 357, pp. 28–35, Jan. 2019.

[103] Y. S. Kim, K. R. Shin, G. W. Kim, Y. G. Ko, and D. H. Shin, "Photocatalytic activity of TiO_2 film containing Fe_2O_3 via plasma electrolytic oxidation," *Surf. Eng.*, vol. 32, no. 6, pp. 443–447, Jun. 2016.

[104] S. Stojadinović, N. Radić, N. Tadić, R. Vasilić, and B. Grbić, "Enhanced ultraviolet light driven photocatalytic activity of ZnO particles incorporated by plasma electrolytic oxidation into Al_2O_3 coatings co-doped with Ce^{3+}," *Opt. Mater. (Amst).*, vol. 101, no. February, 2020.

[105] N. Tadić, S. Stojadinović, N. Radić, B. Grbić, and R. Vasilić, "Characterization and photocatalytic properties of tungsten doped TiO_2 coatings on aluminum obtained by plasma electrolytic oxidation," *Surf. Coatings Technol.*, vol. 305, pp. 192–199, 2016.

[106] A. Ćirić, S. Stojadinović, and M. D. Dramićanin, "Luminescence Intensity Ratio thermometry and Judd-Ofelt analysis of TiO_2:Eu^{3+}," *Opt. Mater. (Amst).*, vol. 85, pp. 261–266, Nov. 2018.

[107] A. Ćirić, S. Stojadinović, and M. D. Dramićanin, "Custom-built thermometry apparatus and luminescence intensity ratio thermometry of ZrO_2:Eu^{3+} and Nb_2O_5:Eu^{3+}," *Meas. Sci. Technol.*, vol. 30, no. 4, p. 045001, Apr. 2019.

[108] A. Zolotarjovs *et al.*, "Thermostimulated luminescence of plasma electrolytic oxidation coatings on 6082 aluminium surface," *Radiat. Meas.*, vol. 124, no. February, pp. 29–34,

2019.

[109] M. Fox, *Optical Properties of Solids*. Oxford University Press, 2001.

[110] G. G. Jayson, B. J. Parsons, and A. J. Swallow, “The mechanism of the fricke dosimeter,” *Int. J. Radiat. Phys. Chem.*, vol. 7, no. 2–3, pp. 363–370, 1975.

[111] Y. Horowitz, L. Oster, and I. Eliyahu, “Review of dose-rate effects in the thermoluminscence of LiF:Mg,Ti (Harshaw),” *Radiat. Prot. Dosimetry*, vol. 179, no. 2, pp. 184–188, Apr. 2018.

[112] S. W. . McKeever, “Thermoluminescence of solids.” .

[113] S. N. Ahmed, *Dosimetry and radiation protection. Physics and Engineering of Radiation Detection*. 2015.

[114] V. I. G. M.S. Akselrod, V.S. Kortov, D.J. Kravetsky, “Highly Sensitive Thermoluminescent Anion-Defective Alpha-Al_2O_3:C Single Crystal Detectors,” *Radiat. Prot. Dosimetry*, Jul. 1990.

[115] M. S. Akselrod and V. S. Kortov, “Thermoluminescent and Exoemission Properties of New High-Sensitivity TLD a-Al_2O_3:C Crystals,” *Radiat. Prot. Dosimetry*, vol. 33, no. 1–4, pp. 123–126, Oct. 1990.

[116] M. S. Akselrod, V. S. Kortov, and E. A. Gorelova, “Preparation and Properties of Alpha-Al_2O_3:C,” *Radiat. Prot. Dosimetry*, vol. 47, no. 1–4, pp. 159–164, May 1993.

[117] M. S. Akselrod and E. A. Gorelova, “Deep traps in highly sensitive α-Al_2O_3:C TLD crystals,” *Nucl. Tracks Radiat. Meas.*, vol. 21, no. 1, pp. 143–146, Jan. 1993.

[118] M. S. Akselrod, S. W. S. McKeever, M. Moscovitch, D. Emfietzoglou, J. S. Durham, and C. G. Soares, “A Thin-Layer Al_2O_3:C Beta TL Detector,” *Radiat. Prot. Dosimetry*, vol. 66, no. 1, pp. 105–110, Jul. 1996.

[119] K. H. Lee and J. H. Crawford, “Luminescence of the F center in sapphire,” *Phys. Rev. B*, vol. 19, no. 6, pp. 3217–3221, Mar. 1979.

[120] B. D. Evans and M. Stapelbroek, “Optical properties of the F+ center in crystalline Al_2O_3,” *Phys. Rev. B*, vol. 18, no. 12, pp. 7089–7098, Dec. 1978.

[121] P. S. Page, B. S. Dhabekar, B. C. Bhatt, A. R. Dhoble, and S. V. Godbole, “Role of Ti4+ in the luminescence process of Al_2O_3:Si,Ti,” *J. Lumin.*, vol. 130, no. 5, pp. 882–887, May 2010.

[122] N. S. Saharin, H. Wagiran, and A. R. Tamuri, “Thermoluminescence Characteristics of Aluminium Oxide Doped Carbon Exposed to Cobalt-60 Gamma Radiation,” *Adv. Mater. Res.*, vol. 1107, pp. 553–558, Jun. 2015.

[123] P. A. Kulis, M. J. Springis, I. A. Tale, V. S. Vainer, and J. A. Valbis, “Impurity-

Associated Colour Centres in Mg- and Ca-Doped Al_2O_3 Single Crystals," *Phys. status solidi*, vol. 104, no. 2, pp. 719–725, Apr. 1981.

[124] P. Pokorny and A. Ibarra, "On the origin of the thermoluminescence of Al_2O_3 :Cr,Ni" *J. Phys. Condens. Matter*, vol. 5, no. 40, pp. 7387–7396, Oct. 1993.

[125] M. N. Konopka *et al.*, "Luminescence dosimetry: Review of methods, detectors and their applications," *Nonlinear Opt. Quantum Opt.*, vol. 48, no. 2, pp. 133–146, 2017.

[126] B. Obryk *et al.*, "The response of different types of TL lithium fluoride detectors to high-energy mixed radiation fields," *Radiat. Meas.*, vol. 43, no. 2–6, pp. 1144–1148, Feb. 2008.

[127] P. Bilski, B. Obryk, P. Olko, E. Mandowska, A. Mandowski, and J. L. Kim, "Characteristics of LiF:Mg,Cu,P thermoluminescence at ultra-high dose range," *Radiat. Meas.*, vol. 43, no. 2–6, pp. 315–318, Feb. 2008.

[128] M. Prokic, "Lithium borate solid TL detectors," *Radiat. Meas.*, vol. 33, no. 4, pp. 393–396, Aug. 2001.

[129] A. Twardak, P. Bilski, B. Marczewska, and W. Gieszczyk, "Analysis of TL and OSL kinetics of lithium aluminate," *Radiat. Meas.*, vol. 71, pp. 143–147, Dec. 2014.

[130] T. Yamashita, N. Nada, H. Onishi, and S. Kitamura, "Calcium Sulfate Activated by Thulium or Dysprosium for Thermoluminescence Dosimetry," *Health Phys.*, vol. 21, no. 2, pp. 295–300, Aug. 1971.

[131] N. Salah, P. D. Sahare, S. P. Lochab, and P. Kumar, "TL and PL studies on : Dy nanoparticles," *Radiat. Meas.*, vol. 41, no. 1, pp. 40–47, Jan. 2006.

[132] K. Watanabe, "Properties of $CaSO_4$: Mn Phosphor under Vacuum Ultraviolet Excitation," *Phys. Rev.*, vol. 83, no. 4, pp. 785–791, Aug. 1951.

[133] M. A. P. Chagas, M. G. Nunes, L. L. Campos, and D. N. Souza, "TL properties of anhydrous $CaSO_4$:Tm improvement," *Radiat. Meas.*, vol. 45, no. 3–6, pp. 550–552, Mar. 2010.

[134] K. G. Vohra, R. C. Bhatt, B. Chandra, A. S. Pradhan, A. R. Lakshmanan, and S. S. Shastry, "A Personnel Dosimeter TLD Badge Based on $CaSO_4$," *Health Phys.*, vol. 38, no. 2, pp. 193–197, Feb. 1980.

[135] T. Kato, G. Okada, and T. Yanagida, "Optical, scintillation and dosimeter properties of MgO transparent ceramic doped with Mn^{2+}," *J. Ceram. Soc. Japan*, vol. 124, no. 5, pp. 559–563, 2016.

[136] P.-S. Weng, P.-C. Hsu, and Y.-H. Chen, "The response of the thermoluminescent dosimeter CaF_2: Tm to protons," *Appl. Radiat. Isot.*, vol. 46, no. 10, pp. 1081–1083, Oct.

1995.

[137] P.-S. Weng, S.-H. Li, P.-C. Hsu, and K.-C. Hsu, “Response of thermoluminescent dosimeter CaF_2:Dy to ionizing and non-ionizing radiations,” *Int. J. Radiat. Appl. Instrumentation. Part A. Appl. Radiat. Isot.*, vol. 43, no. 6, pp. 717–720, Jun. 1992.

[138] K. Sharma, S. Bahl, B. Singh, P. Kumar, S. P. Lochab, and A. Pandey, “$BaSO_4$:Eu as an energy independent thermoluminescent radiation dosimeter for gamma rays and C6+ ion beam,” *Radiat. Phys. Chem.*, vol. 145, pp. 64–73, Apr. 2018.

[139] P. L. Roberson, J. M. Moran, and R. Kulasekere, “Radiographic film dosimetry for IMRT fields in the near-surface buildup region,” *J. Appl. Clin. Med. Phys.*, vol. 9, no. 4, pp. 87–97, Sep. 2008.

[140] S. Alashrah, S. Kandaiya, S. Y. Yong, and S. K. Cheng, “Characterization of a 2D ionization chamber array for IMRT plan verification,” *Nucl. Instruments Methods Phys. Res. Sect. A Accel. Spectrometers, Detect. Assoc. Equip.*, vol. 619, no. 1–3, pp. 181–185, Jul. 2010.

[141] D. Létourneau, M. Gulam, D. Yan, M. Oldham, and J. W. Wong, “Evaluation of a 2D diode array for IMRT quality assurance,” *Radiother. Oncol.*, vol. 70, no. 2, pp. 199–206, Feb. 2004.

[142] M. F. Ahmed *et al.*, “Development of a 2D dosimetry system based on the optically stimulated luminescence of Al_2O_3,” *Radiat. Meas.*, vol. 71, pp. 187–192, Dec. 2014.

[143] P. Olko, B. Marczewska, L. Czopyk, M. A. Czermak, M. Kłosowski, and M. P. R. Waligórski, “New 2-D dosimetric technique for radiotherapy based on planar thermoluminescent detectors,” *Radiat. Prot. Dosimetry*, vol. 118, no. 2, pp. 213–218, May 2006.

[144] S. Ummartyotin and Y. Infahsaeng, “A comprehensive review on ZnS: From synthesis to an approach on solar cell,” *Renew. Sustain. Energy Rev.*, vol. 55, pp. 17–24, Mar. 2016.

[145] W. M. Yen, S. Shionoya, and H. Yamamoto, *Phosphor Handbook*, 2nd ed. CRC Press, 2006.

[146] D. S. Kshatri and A. Khare, “Optical properties of rare earth doped strontium aluminate (SAO) phosphors: A review,” *Opt. Spectrosc.*, vol. 117, no. 5, pp. 769–783, Nov. 2014.

[147] T. Matsuzawa, “A New Long Phosphorescent Phosphor with High Brightness, $SrAl_2O_4$:Eu^{2+},Dy^{3+}” *J. Electrochem. Soc.*, vol. 143, no. 8, p. 2670, 1996.

[148] “List of thermal conductivities.” [Online]. Available: https://en.wikipedia.org/wiki/List_of_thermal_conductivities. [Accessed: 25-May-

2020].

[149] A. Halperin and A. A. Braner, “Evaluation of Thermal Activation Energies from Glow Curves,” *Phys. Rev.*, vol. 117, no. 2, pp. 408–415, Jan. 1960.

[150] D. Ravichandran, S. T. Johnson, S. Erdei, R. Roy, and W. B. White, “Crystal chemistry and luminescence of the Eu^{2+} -activated alkaline earth aluminate phosphors,” *Displays*, vol. 19, no. 4, pp. 197–203, Feb. 1999.

[151] A. L. N. Stevels, “Effect of non-stoichiometry on the luminescence of Eu^{2+}-doped aluminates with the β-alumina-type crystal structure,” *J. Lumin.*, vol. 17, no. 1, pp. 121–133, Jun. 1978.

[152] M. Peng, J. Qiu, L. Yang, and C. Zhao, “Observation of $Eu^{3+}\rightarrow Eu^{2+}$ in barium hexa-aluminates with β′ or β-alumina structures prepared in air,” *Opt. Mater. (Amst).*, vol. 27, no. 3, pp. 591–595, Dec. 2004.

[153] N. Haque, A. Hughes, S. Lim, and C. Vernon, “Rare Earth Elements: Overview of Mining, Mineralogy, Uses, Sustainability and Environmental Impact,” *Resources*, vol. 3, no. 4, pp. 614–635, Oct. 2014.

[154] Y. Yang, H. Wei, L. Zhang, K. Kisslinger, C. L. Melcher, and Y. Wu, “Blue emission of Eu2+-doped translucent alumina,” *J. Lumin.*, vol. 168, pp. 297–303, Dec. 2015.

[155] V. Singh, T. K. Gundu Rao, and J.-J. Zhu, “Synthesis, photoluminescence, thermoluminescence and electron spin resonance investigations of CaAl12O19:Eu phosphor,” *J. Lumin.*, vol. 126, no. 1, pp. 1–6, Sep. 2007.

[156] J. Ueda, T. Shinoda, and S. Tanabe, “Evidence of three different Eu2+ sites and their luminescence quenching processes in $CaAl_2O_4$:Eu^{2+}” *Opt. Mater. (Amst).*, vol. 41, pp. 84–89, Mar. 2015.

[157] J. Sieniawski and M. Wierzbiñska, “Intermetallic phase particles in 6082 aluminium alloy,” *Arch. Mater. Sci. Eng.*, vol. 28, no. 2, pp. 69–76, 2007.

[158] S. Gražulis *et al.*, “Crystallography Open Database – an open-access collection of crystal structures,” *J. Appl. Crystallogr.*, vol. 42, no. 4, pp. 726–729, Aug. 2009.

[159] Y. De Deene, “How important is the dose rate sensitivity of 2D and 3D radiation dosimeters?,” *J. Phys. Conf. Ser.*, vol. 1305, p. 012059, Aug. 2019.

[160] S. Stathakis, P. Myers, C. Esquivel, P. Mavroidis, and N. Papanikolaou, “Characterization of a novel 2D array dosimeter for patient-specific quality assurance with volumetric arc therapy,” *Med. Phys.*, vol. 40, no. 7, p. 071731, Jul. 2013.

[161] H. Chung, J. Li, and S. Samant, “Feasibility of using two-dimensional array dosimeter for in vivo dose reconstruction via transit dosimetry,” *J. Appl. Clin. Med. Phys.*, vol. 12,

no. 3, pp. 90–111, Jun. 2011.

[162] S. J. Davis, Y. Zhao, M. Hinds, T. Moritz, B. W. Pogue, and J. R. Gunn, "A 2D imaging dosimeter for photodynamic therapy," in *Optical Methods for Tumor Treatment and Detection: Mechanisms and Techniques in Photodynamic Therapy XXVIII*, 2019, p. 23.

[163] J. Archer, L. Madden, E. Li, D. Wilkinson, and A. Rosenfeld, "2D photon dosimetry with a scintillation fibre optic dosimeter," *Radiat. Phys. Chem.*, vol. 166, p. 108490, Jan. 2020.

[164] S. Xin, L. Song, R. Zhao, and X. Hu, "Influence of cathodic current on composition, structure and properties of Al_2O_3 coatings on aluminum alloy prepared by micro-arc oxidation process," *Thin Solid Films*, vol. 515, no. 1, pp. 326–332, Sep. 2006.

[165] J. A. Curran and T. W. Clyne, "Porosity in plasma electrolytic oxide coatings," *Acta Mater.*, vol. 54, no. 7, pp. 1985–1993, 2006.

[166] J. M. Kalita and M. L. Chithambo, "Comprehensive kinetic analysis of thermoluminescence peaks of α-Al_2O_3:C,Mg," *J. Lumin.*, vol. 185, pp. 72–82, May 2017.

[167] C. B. Palan, N. S. Bajaj, and S. K. Omanwar, "Luminescence properties of terbium-doped Li_3PO_4 phosphor for radiation dosimetry," *Bull. Mater. Sci.*, vol. 39, no. 7, pp. 1619–1623, Dec. 2016.

[168] I. A. Weinstein, V. E. Pelenyov, and V. S. Kortov, "The Effect of Thermally Stimulated Photoconversion of Oxygen Centres on the Sensitivity of TLD-500 Dosimetric Crystals," *Radiat. Prot. Dosimetry*, vol. 100, no. 1, pp. 159–162, Jul. 2002.

[169] J. M. Kalita and M. L. Chithambo, "On the sensitivity of thermally and optically stimulated luminescence of α-Al_2O_3:C and α-Al_2O_3:C,Mg," *Radiat. Meas.*, vol. 99, pp. 18–24, Apr. 2017.

[170] R. Martínez-Martínez *et al.*, "RBS characterization of Al_2O_3 films doped with Ce and Mn," *Nucl. Instruments Methods Phys. Res. Sect. B Beam Interact. with Mater. Atoms*, vol. 241, no. 1–4, pp. 450–453, Dec. 2005.

[171] G. Salek *et al.*, "Optical properties versus temperature of Cr-doped γ- and α-Al_2O_3: Irreversible thermal sensors application," *J. Lumin.*, vol. 179, pp. 189–196, Nov. 2016.

[172] M. G. Rodriguez, G. Denis, M. S. Akselrod, T. H. Underwood, and E. G. Yukihara, "Thermoluminescence, optically stimulated luminescence and radioluminescence properties of Al_2O_3:C,Mg," *Radiat. Meas.*, vol. 46, no. 12, pp. 1469–1473, Dec. 2011.

[173] A. L. Yerokhin, L. O. Snizhko, N. L. Gurevina, A. Leyland, A. Pilkington, and A. Matthews, "Discharge characterization in plasma," *J. Phys. D Appl. Phys.*, vol. 36, pp. 2110–2120, 2003.

[174] J. Tian, Z. Luo, S. Qi, and X. Sun, “Structure and antiwear behavior of micro-arc oxidized coatings on aluminum alloy,” *Surf. Coatings Technol.*, vol. 154, no. 1, pp. 1–7, 2002.

[175] Oxford Instruments Group, “How to Define the Quantum Efficiency of CCD Cameras.” [Online]. Available: https://andor.oxinst.com/learning/view/article/ccd-spectral-response-(qe). [Accessed: 19-May-2020].

[176] S. Graulis *et al.*, “Crystallography Open Database - An open-access collection of crystal structures,” *J. Appl. Crystallogr.*, vol. 42, no. 4, pp. 726–729, 2009.

[177] N. Doebelin and R. Kleeberg, “computer programs Profex : a graphical user interface for the Rietveld refinement program BGMN,” pp. 1573–1580, 2015.

[178] H. Kong, “Dependence of blue-emitting property on nanopore geometrical structure in Al-based porous anodic alumina membranes,” vol. 1349, pp. 1345–1349, 2005.

[179] S. Li and J. Wang, “Photoluminescence properties of anodic aluminum oxide formed in a mixture of ammonium fluoride and oxalic acid,” vol. 56, no. 6, 2017.

[180] V. Palanza *et al.*, “Luminescence study of transition metal ions in natural magmatic and metamorphic yellow sapphires,” *IOP Conf. Ser. Mater. Sci. Eng.*, vol. 15, p. 012086, Nov. 2010.

[181] J. D. Brewer, B. T. Jeffries, and G. P. Summers, “Low-temperature fluorescence in sapphire,” *Phys. Rev. B*, vol. 22, no. 10, pp. 4900–4906, Nov. 1980.

[182] W. M. de Azevedo, G. B. de Oliveira, E. F. da Silva, H. J. Khoury, and E. F. Oliveira de Jesus, “Highly sensitive thermoluminescent carbon doped nanoporous aluminium oxide detectors,” *Radiat. Prot. Dosimetry*, vol. 119, no. 1–4, pp. 201–205, Sep. 2006.

[183] M. Baronskiy, A. Rastorguev, A. Zhuzhgov, A. Kostyukov, O. Krivoruchko, and V. Snytnikov, “Photoluminescence and Raman spectroscopy studies of low-temperature γ-Al2O3 phases synthesized from different precursors,” *Opt. Mater. (Amst).*, vol. 53, pp. 87–93, 2016.

[184] S. V. Gorbunov, S. O. Cholakh, V. A. Pustovarov, Y. V. Yakovlev, A. F. Zatsepin, and A. I. Kucharenko, “Electronic excitations and intrinsic defects in nanostructural Al 2O3,” *Phys. Status Solidi C Conf.*, vol. 2, no. 1, pp. 351–354, 2005.

[185] M. G. Rodriguez, G. Denis, M. S. Akselrod, T. H. Underwood, and E. G. Yukihara, “Thermoluminescence, optically stimulated luminescence and radioluminescence properties of Al_2O_3:C,Mg,” *Radiat. Meas.*, vol. 46, no. 12, pp. 1469–1473, 2011.

[186] I. V. Berezovskaya, “Oxidation states and microstructure of manganese impurity centers in nanosized Al_2O_3 obtained by combustion method,” *Funct. Mater.*, vol. 25, no. 3, pp.

490–495, Sep. 2018.

[187] A. van Die, A. C. H. I. Leenaers, W. F. van der Weg, and G. Blasse, “A search for luminescence of the trivalent manganese ion in solid aluminates,” *Mater. Res. Bull.*, vol. 22, no. 6, pp. 781–788, Jun. 1987.

[188] A. Kostyukov *et al.*, “Photoluminescence of Cr^{3+} in nanostructured Al_2O_3 synthesized by evaporation using a continuous wave CO 2 laser,” *RSC Adv.*, vol. 6, no. 3, pp. 2072–2078, 2016.

[189] I. Y. D, “Physicochemical properties of corundum doped in supercritical water,” no. February, 2016.

[190] J. T. Randall and M. H. . Wilkins, “The phosphorescence of various solids,” *Proc. R. Soc. London. Ser. A. Math. Phys. Sci.*, vol. 184, no. 999, pp. 347–364, Nov. 1945.

[191] J. T. Randall and M. H. . Wilkins, “Phosphorescence and electron traps - I. The study of trap distributions,” *Proc. R. Soc. London. Ser. A. Math. Phys. Sci.*, vol. 184, no. 999, pp. 365–389, 1945.

[192] J. T. Randall and M. H. F. Wilkins, “Phosphorescence and electron traps II. The interpretation of long-period phosphorescence,” *Proc. R. Soc. London. Ser. A. Math. Phys. Sci.*, vol. 184, no. 999, pp. 390–407, Nov. 1945.

[193] F. Clabau *et al.*, “Mechanism of Phosphorescence Appropriate for the Long-Lasting Phosphors Eu^{2+}-Doped $SrAl_2O_4$ with Codopants Dy^{3+} and B^{3+},” *Chem. Mater.*, vol. 17, pp. 3904–3912, 2005.

[194] H. Chander, D. Haranath, V. Shanker, and P. Sharma, “Synthesis of nanocrystals of long persisting phosphor by modified combustion technique,” *J. Cryst. Growth*, vol. 271, no. 1–2, pp. 307–312, 2004.

[195] R. E. Rojas-Hernandez, F. Rubio-Marcos, A. Serrano, A. Del Campo, and J. F. Fernandez, “Precise Tuning of the Nanostructured Surface leading to the Luminescence Enhancement in SrAl2O4 Based Core/Shell Structure,” *Sci. Rep.*, vol. 7, no. 1, p. 462, 2017.

[196] Z. Pan, Y.-Y. Lu, and F. Liu, “Sunlight-activated long-persistent luminescence in the near-infrared from Cr^{3+}-doped zinc gallogermanates,” *Nat. Mater.*, vol. 11, no. 1, pp. 58–63, 2011.

[197] R. Chen, Y. Wang, Y. Hu, Z. Hu, and C. Liu, “Modification on luminescent properties of $SrAl_2O_4$:Eu^{2+}, Dy^{3+} phosphor by Yb^{3+} ions doping,” *J. Lumin.*, vol. 128, no. 7, pp. 1180–1184, 2008.

[198] V. Liepina, D. Millers, and K. Smits, “Tunneling luminescence in long lasting afterglow

of $SrAl_2O_4$:Eu,Dy," *J. Lumin.*, vol. 185, no. 3, pp. 151–154, 2017.

[199] Z. Xue, S. Deng, Y. Liu, B. Lei, Y. Xiao, and M. Zheng, "Synthesis and luminescence properties of $SrAl_2O_4:Eu^{2+},Dy^{3+}$ hollow microspheres via a solvothermal co-precipitation method," *J. Rare Earths*, vol. 31, no. 3, pp. 241–246, 2013.

[200] A. K. Choubey, N. Brahme, and D. P. Bisen, "Synthesis of $SrAl_2O_4$:Eu phosphor by combustion method and its possible applications for mechanoluminescence dosimetry," *Indian J Pure Appl Phys*, vol. 50, pp. 851–854, 2012.

[201] D. P. Bisen and R. Sharma, "Mechanoluminescence properties of $SrAl_2O_4:Eu^{2+}$ phosphor by combustion synthesis," *Luminescence*, vol. 31, no. 2, pp. 394–400, 2016.

[202] H. Terraschke *et al.*, "$SrAl_2O_4:Eu^{2+},Dy^{3+}$ Nanosized Particles: Synthesis and Interpretation of Temperature-Dependent Optical Properties Huayna," *J. Spectrosc.*, vol. 2015, no. Article ID 541958, p. 12 pages, 2015.

[203] Y. Wu, L. Wang, Y. Qing, N. Yan, C. Tian, and Y. Huang, "A green route to prepare fluorescent and absorbent nano-hybrid hydrogel for water detection," *Sci. Rep.*, vol. 7, no. 1, p. 4380, 2017.

[204] M. P. Anesh, S. K. H. Gulrez, A. Anis, H. Shaikh, M. E. A. Mohsin, and S. M. Al-Zahrani, "Developments in Eu^{+2}-doped strontium aluminate and polymer/strontium aluminate composite," *Adv. Polym. Technol.*, vol. 33, no. S1, pp. 8–11, 2014.

[205] R. E. Rojas-Hernandez, M. a. Rodriguez, and J. F. Fernandez, "Role of the oxidizing agent to complete the synthesis of strontium aluminate based phosphors by the combustion method," *RSC Adv.*, vol. 5, no. 4, pp. 3104–3112, 2015.

[206] T. Katsumata, K. Sasajima, T. Nabae, S. Komuro, and T. Morikawa, "Characteristics of Strontium Aluminate Crystals Used for Long-Duration Phosphors," *J. Am. Ceram. Soc.*, vol. 81, no. 2, pp. 413–416, Jan. 2005.

[207] M. Nazarov, M. G. Brik, D. Spassky, and B. Tsukerblat, "Crystal field splitting of 5d states and luminescence mechanism in $SrAl_2O_4:Eu^{2+}$ phosphor," *J. Lumin.*, vol. 182, pp. 79–86, 2017.

[208] Z. Li and K. Huang, "Blue luminescence in porous anodic alumina films," *J. Phys. Condens. Matter*, vol. 19, no. 21, p. 216203, 2007.

[209] Y. Li, G. H. Li, G. W. Meng, L. D. Zhang, and F. Phillipp, "Photoluminescence and optical absorption caused by the F+ centres in anodic alumina membranes," *J. Phys. Condens. Matter*, vol. 13, no. 13, pp. 2691–2699, 2001.

[210] T. Aitasalo *et al.*, "Effect of temperature on the luminescence processes of $SrAl_2O_4:Eu^{2+}$" *Radiat. Meas.*, vol. 38, no. 4–6, pp. 727–730, 2004.

[211] D. Dutczak, T. Jüstel, C. Ronda, and A. Meijerink, "Eu^{2+} luminescence in strontium aluminates," *Phys. Chem. Chem. Phys.*, vol. 17, no. 23, pp. 15236–15249, 2015.

[212] K. Van den Eeckhout, P. F. Smet, and D. Poelman, "Persistent luminescence in Eu^{2+}-doped compounds: A review," *Materials (Basel).*, vol. 3, no. 4, pp. 2536–2566, 2010.

[213] R. Chen and V. Pagonis, *Thermally and Optically Stimulated Luminescence: A Simulation Approach*. 2011.

[214] R. Chen, "Apparent stretched-exponential luminescence decay in crystalline solids," *J. Lumin.*, vol. 102–103, no. SPEC, pp. 510–518, 2003.

[215] M. N. Berberan-Santos, E. N. Bodunov, and B. Valeur, "Mathematical functions for the analysis of luminescence decays with underlying distributions 1. Kohlrausch decay function (stretched exponential)," *Chem. Phys.*, vol. 315, no. 1–2, pp. 171–182, 2005.